

EVALUATING CHANNEL MIGRATION OF THE LOWER GUADALUPE RIVER:  
SEGUIN, TX, TO THE SAN ANTONIO RIVER CONFLUENCE

Final Report

Contract No. 1548311790

August 2016



John R. Giardino, Ph.D., P.G.  
Department of Geology & Geophysics  
and  
Water Management & Hydrological Science Graduate Program  
Texas A&M University  
College Station, TX 77843

And

Taylor Rowley, M.S.  
Water Management & Hydrological Science Graduate Program  
Texas A&M University  
College Station, TX 77843

Submitted to the Texas Water Development Board

20160814 PM 12:38

EVALUATING CHANNEL MIGRATION OF THE LOWER GUADALUPE RIVER:  
SEGUIN, TX, TO THE SAN ANTONIO RIVER CONFLUENCE

Final Report

**Contract No. 1548311790**

August 2016

John R. Giardino, Ph.D., P.G.  
Department of Geology & Geophysics  
and  
Water Management & Hydrological Science Graduate Program  
Texas A&M University  
College Station, TX 77843

And

Taylor Rowley, M.S.  
Water Management & Hydrological Science Graduate Program  
Texas A&M University  
College Station, TX 77843

Submitted to the Texas Water Development Board

## TABLE OF CONTENTS

	Page
TABLE OF CONTENTS.....	2
LIST OF FIGURES .....	4
LIST OF TABLES.....	10
LIST OF EQUATIONS .....	11
1. INTRODUCTION .....	12
1.1 Project Tasks .....	12
1.2 Context.....	13
2. BACKGROUND .....	15
2.1 River Development and Scale.....	15
2.2 Weather and Climate.....	15
2.3 Dams .....	18
2.4 Geomorphic and Watershed Characteristics .....	18
2.5 Channel Pattern and Geometry .....	19
2.5.1 Radius of Curvature .....	19
3. STUDY AREA .....	22
3.1 Watershed Characteristics and Geomorphology.....	22
3.1.1 Zone 1 – Belmont Fault Zone (BFZ) .....	24
3.1.2 Zone 2 – Upper Coastal Plain (UCP).....	25
3.1.3 Zone 3 – Middle Coastal Plain (MCP) .....	26
3.1.4 Zone 4 – Coastal Plain Transition (CPT).....	28
3.1.5 Zone 5 – Lower Coastal Plain (LCP).....	28
3.1.6 Zone 6 – Upper Delta (UD) .....	29
3.1.7 Zone 7 – Middle Delta (MD).....	30
3.2 Geology and Geomorphology .....	31
3.3 Weather and Climate.....	33
3.4 Land Use .....	34
3.5 Vegetation .....	35
4. METHODS .....	36
4.1 Total Rates of Migration.....	36

4.2 Geomorphic Zones and Specific Meander Bends.....	40
4.2.1 Radius of Curvature .....	41
4.2.3 Vegetation Cover .....	43
4.2.4 Soil Composition .....	43
4.2.5 Discharge – USGS Gauging Stations .....	43
4.3 Statistical Analysis.....	45
5. RESULTS .....	46
5.1 Lateral Channel Migration – 380 km Reach.....	46
5.2 Discharge and Rates of Migration .....	48
5.3 Stream Power and Rates of Migration .....	50
5.4 Lateral Channel Migration for each Reach.....	53
5.5 ANOVA Statistical Analysis .....	64
5.5.1 Vegetation.....	66
5.5.2 Bank Composition .....	66
5.5.3 Type of Bend and Radius of Curvature .....	66
5.6 ANOVA for Reaches .....	68
6. DISCUSSION .....	70
6.1 Lateral Rates of Migration .....	70
6.1.1 Impact of Drought and Changes in Material Cohesion .....	70
6.1.2 Upper Delta and Middle Delta.....	72
6.1.3 Belmont Fault Zone and Upper Coastal Plain .....	73
6.2 Dams .....	75
6.3 Meander Cut-Offs .....	78
6.4 Radius of Curvature .....	79
7. CONCLUSION.....	81
REFERENCES .....	83
APPENDIX A.....	90
A.1 Introduction to Side-Scan Sonar .....	90
A.2 Guidelines for Using Side-Scan Sonar.....	91
A.3 Side-Scan Sonar Work .....	91
A.4 Example from Preliminary Data .....	92
APPENDIX B .....	95
APPENDIX C .....	113

## LIST OF FIGURES

	Page
Figure 1. Guadalupe River Basin with the lower Guadalupe River study area highlighted.....	12
Figure 2. Middle Guadalupe River Basin including Canyon Lake, the Balcones Escarpment and major tributaries to the Lower Guadalupe River. Features are overlain onto a DEM where lighter colors denote a higher elevation, whereas the darker colors denote a lower elevation.....	17
Figure 3. Cross-section of the process of lateral migration in a meander bend (Modified from <a href="http://www.bbc.co.uk">www.bbc.co.uk</a> ). ....	20
Figure 4. Rivers with various radii of curvature and their shape where $R_c$ = radius of curvature and $w$ = channel width (Modified from Briaud et al., 2001.). ....	21
Figure 5. The lower Guadalupe River Basin. ....	22
Figure 6. Map including study reach and associated study sub-reaches by geomorphic zone after Phillips, 2011.....	23
Figure 7. Map of the Belmont Fault Zone geomorphic zone and reach. ....	25
Figure 8. Map of the Upper Coastal Plain geomorphic zone and reach. ....	26
Figure 9. Map of the Middle Coastal Plain geomorphic zone and reach.....	27
Figure 10. Map of the Coastal Plain Transition geomorphic zone and reach.....	28
Figure 11. Map of the Lower Coastal Plain geomorphic zone and reach.....	29
Figure 12. The Upper Delta geomorphic zone and reach. ....	30
Figure 13. The Middle Delta geomorphic zone and reach.....	31
Figure 14. Geology of the lower Guadalupe River Basin.....	32
Figure 15. New Braunfels, TX, Climagraph (USClimate Data, 2016).....	33
Figure 16. Victoria, TX, Climagraph (USClimate Data, 2016).....	34
Figure 17. Change polygons created by subtracting T2 (time) from T1 (time) centerlines to generate a polygon of change for a specific area.....	38

Figure 18. Stacked polygons created from centerline pairs for the study area. ....	39
Figure 19. Geometry of various types of meander bends. Note river flow is from right to left. (Modified from Brice, 1974). ....	41
Figure 20. An example of the determination of radius of curvature. The figure was constructed from the 1960 channel boundary of the Guadalupe River. ....	42
Figure 21. USGS gauging station locations within the lower Guadalupe River study area. ....	44
Figure 22. Boxplots of points of lateral migration for each time period. ....	47
Figure 23. Average monthly discharge for the period 1995-2015 for four gauges within the study reach. (Data obtained from <a href="http://waterdata.usgs.gov">waterdata.usgs.gov</a> , 2016). ...	48
Figure 24. (a) Average monthly discharge and average rates of migration per study time period. (b) Average daily discharge and average rates of migration per study time period. (Data obtained from <a href="http://waterdata.usgs.gov">waterdata.usgs.gov</a> , 2016). ....	49
Figure 25. Longitudinal profile of the lower Guadalupe River study reach with average stream power for each sub-reach reach. ....	52
Figure 26. Lateral rates of migration by geomorphic zone. The x-axis represents each migration polygon; 1 is the uppermost reach, whereas 721 is the downstream end. Geomorphic zone and associated average rate of migration are shown in the red line. ....	53
Figure 27. Average rates of migration by study period for each geomorphic zone. ....	54
Figure 28. Areas of maximum lateral migration, in red, for the study period. ....	55
Figure 29. Rates of migration in the Belmont Fault Zone using a three-class Jenks Natural Break. ....	56
Figure 30. Rates of migration in the Upper Coastal Plain using a three-class Jenks Natural Break. ....	57
Figure 31. Rates of migration in the Middle Coastal Plain using a three-class Jenks Natural Break. The zone was divided into upper (a) and lower (b) as a result of the length. ....	58
Figure 32. Rates of migration in the Coastal Plain Transition zone using a three-class Jenks Natural Break. ....	60

Figure 33. Rates of migration in the Lower Coastal Plain using a three-class Jenks Natural Break. ....	61
Figure 34. Rates of migration in the Upper Delta using a three-class Jenks Natural Break. ....	62
Figure 35. Rates of migration in the Lower Delta using a three-class Jenks Natural Break. ....	63
Figure 36. A map including ten random meander bends per sub-reach used for further analysis. ....	64
Figure 37. Ratio of radius of curvature and width to rate of migration for the Beaton River, Canada, from Nanson and Hickin (1983), and the lower Guadalupe River. ....	67
Figure 38. (a, b) Slumping along an outside bank on the Guadalupe River near Cuero, TX,. (December 5, 2015). ....	71
Figure 39. An example of collapsing banks as a result of undercutting. Photograph taken near Cuero, TX. (December 5, 2015). ....	72
Figure 40. Longitudinal profile showing Post-Vicksburg flexure zone near the end of the reach. ....	73
Figure 41. Rates of migration on the Guadalupe River downstream of Lake Gonzales, TX. Lake Gonzales is a reservoir formed behind one of the dams on the Guadalupe River. ....	75
Figure 42. Rates of migration on the Guadalupe River downstream of Wood Lake, TX. Wood Lake is a reservoir formed behind the second dam within the Upper Coastal Plain reach. ....	76
Figure 43. Hydrograph of USGS gauge 08169792 Guadalupe River at FM 1117 near Seguin, TX showing diurnal flood pulses from releases of upstream dams. (Data from <a href="http://waterdata.usgs.gov">waterdata.usgs.gov</a> , 2016). ....	77
Figure 44. Sonar image examples. The black line in the middle of both images represents the depth of the water column. A wider strip represents a deeper area whereas a narrower strip is more shallow. The lighter pixels typically represent finer materials including sands, silts and clays, whereas the darker pixels relate to denser material including cobbles, boulders and riprap. (Images captured on the Guadalupe River near Cuero, TX.).....	91

Figure 45. (a) Sonar image mosaic. The black box outlines a close-up of sonar waypoints S00167-S00176, and is shown in Figure 44b. ....	93
Figure 46. Map of all photograph locations of meanders during the field survey near Cuero, TX, of a ~50 km reach. ....	95
Figure 47. Map of “A” photograph locations. Rates of migration are included, divided into three classes. ....	96
Figure 48. Map of “B” photograph locations. Rates of migration are included, divided into three classes. ....	97
Figure 49. Location of A1. Photograph taken near Cuero, TX, (December 5, 2016). ....	97
Figure 50. Location of A2. Photograph taken near Cuero, TX, (December 5, 2016). ....	98
Figure 51. Location of A3. Photograph taken near Cuero, TX, (December 5, 2016). ....	98
Figure 52. Location of A4. Photograph taken near Cuero, TX, (December 5, 2016). ....	99
Figure 53. Location of A5. Photograph taken near Cuero, TX, (December 5, 2016). ....	99
Figure 54. Location of A6. Photograph taken near Cuero, TX, (December 5, 2016). ....	100
Figure 55. Location of A7. Photograph taken near Cuero, TX, (December 5, 2016). ....	100
Figure 56. Location of A8. Photograph taken near Cuero, TX, (December 5, 2016). ....	101
Figure 57. Location of A9. Photograph taken near Cuero, TX, (December 5, 2016). ....	101
Figure 58. Location of A10. Photograph taken near Cuero, TX, (December 5, 2016). ....	102
Figure 59. Location of A11. Photograph taken near Cuero, TX, (December 5, 2016). ....	102
Figure 60. Location of A12. Photograph taken near Cuero, TX, (December 5, 2016). ....	103
Figure 61. Location of A13. Photograph taken near Cuero, TX, (December 5, 2016). ....	103

Figure 62. Location of A14. Photograph taken near Cuero, TX, (December 5, 2016).....	104
Figure 63. Location of A15. Photograph taken near Cuero, TX, (December 5, 2016).....	104
Figure 64. Location of B1. Photograph taken near Cuero, TX, (December 6, 2016).....	105
Figure 65. Location of B2. Photograph taken near Cuero, TX, (December 6, 2016).....	105
Figure 66. Location of B3. Photograph taken near Cuero, TX, (December 6, 2016).....	106
Figure 67. Location of B4. Photograph taken near Cuero, TX, (December 6, 2016).....	106
Figure 68. Location of B5. Photograph taken near Cuero, TX, (December 6, 2016).....	107
Figure 69. Location of B6. Photograph taken near Cuero, TX, (December 6, 2016).....	107
Figure 70. Location of B7. Photograph taken near Cuero, TX, (December 6, 2016).....	108
Figure 71. Location of B8. Photograph taken near Cuero, TX, (December 6, 2016).....	108
Figure 72. Location of B9. Photograph taken near Cuero, TX, (December 6, 2016).....	109
Figure 73. Location of B10. Photograph taken near Cuero, TX, (December 6, 2016).....	109
Figure 74. Location of B11. Photograph taken near Cuero, TX, (December 6, 2016).....	110
Figure 75. Location of B12. Photograph taken near Cuero, TX, (December 6, 2016).....	110
Figure 76. Location of B13. Photograph taken near Cuero, TX, (December 6, 2016).....	111

Figure 77. Location of B14. Photograph taken near Cuero, TX, (December 6, 2016).....111

Figure 78. Location of B15. Photograph taken near Cuero, TX, (December 6, 2016).....112

Figure 79. Location of B16. Photograph taken near Cuero, TX, (December 6, 2016).....112

## LIST OF TABLES

	Page
Table 1. Geomorphic zones and associated geographic coordinates using the geographic coordinate system North American Datum 1983. ....	23
Table 2. Characteristics of geomorphic zones adapted from Phillips (2011). ....	24
Table 3. Land use/land cover for 1992 and 2011 and associated changes. ....	35
Table 4. Collected imagery date and spatial resolution. ....	36
Table 5. Study periods. ....	36
Table 6. Number of polygons with a value greater than 6 m total migration. ....	40
Table 7. USGS gauging stations and period of record. ....	44
Table 8. Study time periods for entire study area with associated migration polygons and average rates of migration. ....	46
Table 9. Avulsion occurrence and affected total and rates of lateral migration. ....	47
Table 10. Study period and associated flood stage events. ....	50
Table 11. Stream power for each gauging station. $Q_{\mu}$ = average discharge. ....	51
Table 12. Average rate of migration vs. average stream power. ....	52
Table 13. Average rates of migration in meters per year by geomorphic zone for each study period. ....	54
Table 14. ANOVA comparison of total migration as a function of meander bend characteristics. $R_c/W$ values are averaged for 1960 and 2014, respectively. ....	65
Table 15. ANOVA of average $R_c/W$ values versus type of bend. The $R_c/W$ values below are averaged for 1960 and 2014, respectively. ....	67
Table 16. ANOVA comparison of bend morphology as a function of Geomorphic Zone. Average values for 1960 and 2014 for 70 random meander bends. ...	68

## LIST OF EQUATIONS

	Page
Eq. (1).....	13
Eq. (2).....	39
Eq. (3).....	39
Eq. (4).....	43
Eq. (5).....	45

# 1. INTRODUCTION

## 1.1 Project Tasks

This report presents the results of a study of geomorphic changes on the lower Guadalupe River in Texas from Seguin to the confluence of the San Antonio River. The 380 km reach was assessed at three different scales to include the entire reach, seven sub-reaches, and seventy specific meander bends. The study explains meander migration as a response to geomorphic parameters that occur along the length of the lower Guadalupe River so that river managers and stakeholders can understand the dynamic controls of the river. Documenting evidence of river stability compliments prior work (Holley, 1992; Perkin and Bonner, 2011; Phillips, 2007; 2011; 2012; Phillips and Slattery, 2007), and also provides additional scientific basis for instream flow recommendations for this segment of the river. The Guadalupe River Basin and study area is shown in Figure 1.

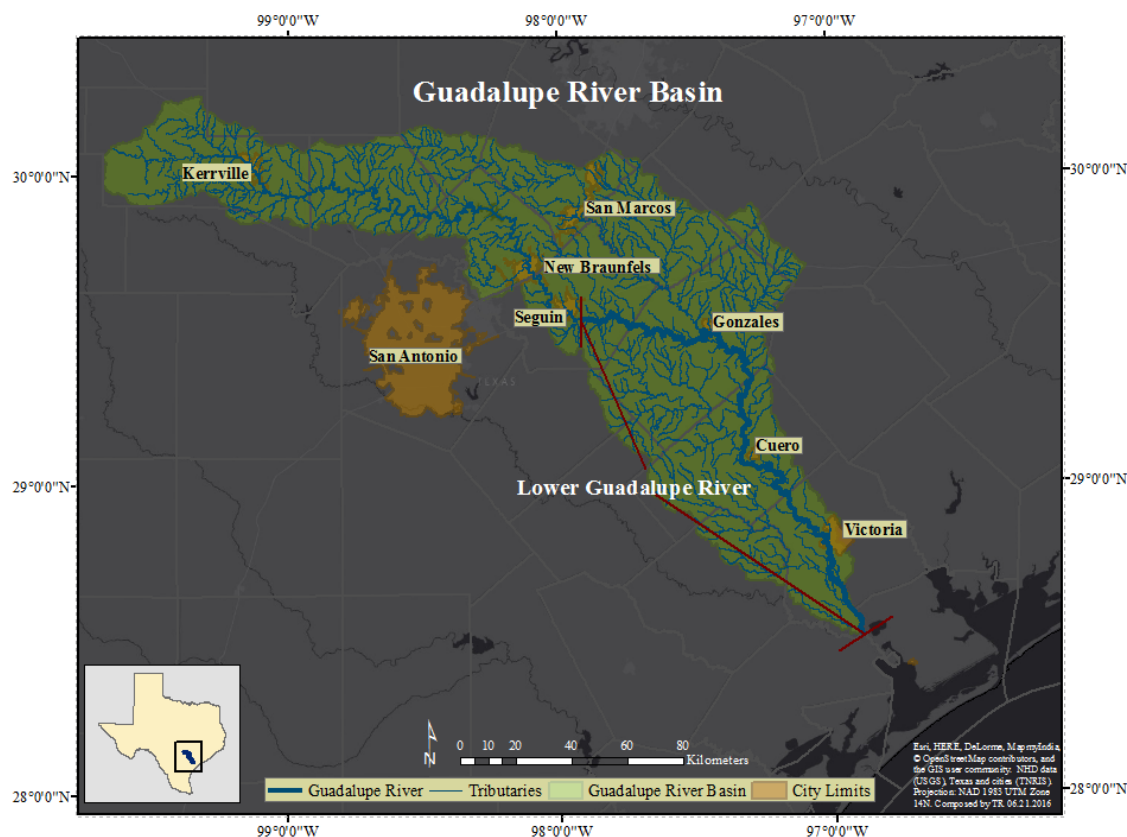


**Figure 1. Guadalupe River Basin with the lower Guadalupe River study area highlighted.**

The specific objectives of the project were to:

- 1.) Calculate rates of meander migration along selected reaches of the Guadalupe River.
- 2.) Determine the driving mechanisms controlling channel migration.

The work of this project was conducted in the context of the Texas Instream Flow Program.

### *1.2 Context*

River meanders are the manifestation of events resulting in instability, which occur along the river-channel boundary. Instability in alluvial streams is the result of two driving aspects of the velocity of water and sediment transport. If both of these are sufficiently robust, sediment transport, along the bottom of the channel, will migrate from the center of the river to one side or the other of the river channel, producing a helical-flow pattern.

A helical-flow pattern increases the deposition along the one side of the channel where water velocities are decreased, whereas faster flows erode the opposite bank. Additionally, the water is deflected through the expanding bend in the direction of the opposite bank of the channel further downstream and triggers the development of a new bend. Through this meander process, sediment-flow instability is sufficiently powerful to form alternate bars in a relatively straight channel. Bank erosion occurs on alternate sides of the channel, which is encouraged by sediment deposits forming bars opposite bank erosion. The result of this alternating pattern of bank erosion and bar deposition is the creation of a meandering river pattern.

One must understand that for a meandering channel to develop, the banks of the stream must be sufficiently cohesive to facilitate maintenance of a reasonably uniform width, as the channel is deformed into a series of bends and reaches. Bank materials consisting of fine silts and clays, as well as the root systems of plants provide the necessary cohesion. If the cohesion is insufficient, however, channel instability can initiate bifurcation of the river into two or into multiple channels.

A river will react to channel instability to achieve a state of dynamic equilibrium where sediment load is balanced with discharge and stream gradient inducing minimal erosion and deposition (Bridge, 2009; Church, 2010). Dynamic equilibrium is a balance within the entire river system. A river is considered to be dynamically stable once the river is in dynamic equilibrium because it has the ability to react to a range of disturbances through self-repair mechanisms (Langbein and Leopold, 1964; Knighton, 2014; WADOE, 2016).

Dynamic equilibrium is a fundamental geomorphic concept (Hack, 1975; Graf, 1977; Cyr and Granger, 2008; Tranmer et al., 2015). River managers, engineers, and geomorphologists base much of their management of rivers on the dynamic equilibrium concept. Although generally accepted in geomorphology, the concept of dynamic equilibrium has been questioned and critiqued for decades (Ahnert, 1994; Bracken and Wainwright, 2006; Lewin, 2016). Phillips (2007) has provided examples of several Texas Coastal Plain rivers that do not follow the concept. Phillips, unfortunately, does not include information on the Guadalupe River, so the equilibrium status of the river is unknown. We assume that the lower Guadalupe River does follow the equilibrium concept because of the shape of the longitudinal channel profile. Phillips (2007) questions the equilibrium of rivers that have a convex profile, but the reach of the lower Guadalupe River approaches a linear profile.

Concave and convex longitudinal profiles are a result of erosion and deposition throughout the channel as a river flows downstream. Sediment exchange is fundamental to river dynamics; however, the amount of exchange of sediment, as well as the length of time, has important implications for the dynamics of a river (TIFP, 2010). Discharge directly affects sediment load and this is often regulated through human intervention (Phillips, 2012). To regulate discharge, structures, such as dams or point-source dischargers, must comply with flow regulations and limitations to minimize disturbance both up and downstream. Regulatory programs, including the Texas Instream Flow Program (TIFP), have been created to establish the ideal rate of discharge to promote ecological health of a river while maintaining beneficial uses for various stakeholders.

## 2. BACKGROUND

### *2.1 River Development and Scale*

River development is dependent on reach and basin scale controls that influence what authors Leopold and Wolman (1957) note about river channel morphology; rivers are straight, meandering, or braided. Rivers migrate across an alluvial floodplain as sediment is eroded from one location and deposited in another. Rivers migrate laterally and vertically. The morphology of a river is primarily dependent on channel slope and discharge relationships. Because other factors play a role in influencing the morphology of a river, numerous classification schemes have been created to explain the additional controls that are operational across multiple scales.

Whereas numerous approaches have been created, we will focus on examples of six different approaches only, as these have the closest fit to the study area. Schumm (1963) relates river adjustment to sediment load and transport mechanisms, as well as to the local geology, rather than specific channel hydraulics. Frissell et al. (1986) view the river in the context of the whole watershed by using a hierarchical framework and systems' approach. Montgomery and Buffington (1997), on the other hand, classify a river in terms of changes in morphology at the reach scale. They use changes in riparian vegetation and hillslope process to determine best-fit reaches. Brierly and Fryirs (2000; 2013) take a completely different perspective by using a bottom-up approach to identify present landforms. They first assess the morphodynamics of the landforms, and then interpret the evolution of the river and its catchment, which are the result from these dynamics. Gurnell (2014) uses the presence of in-stream and riparian vegetation to understand stability, whereas Wohl (2013) uses woody debris to explain controls of geomorphic change.

The six examples explain controls and different ways of understanding geomorphic change; each at different spatial scales. The definition of geomorphic change is dependent on the scale of the questions being asked. As Tobler (1970) said, "Everything is related to everything else, but near things are more related than distant things." The analysis of a river is dependent on scale; hence, the reason why so many classification schemes have been created. Determination of the best approach to use to answer a question being asked is fundamental.

### *2.2 Weather and Climate*

Once a best approach to classify the geomorphology of a river is determined, other factors influencing the evolution of a river must be considered. Weather and climate have a direct impact on the flow regime of a river. Precipitation can lead to runoff, resulting in an increase of discharge to a river. An increase in discharge, increases the stream power, which is the capacity for flowing water to perform geomorphic changes through sediment transport (Phillips and Slattery, 2007; Bizzi and Lerner, 2015). Stream power can be expressed as:

$$\Omega = \gamma Q_{\mu} S \quad \text{Eq. (1)}$$

where,  $\Omega$  is stream power,  $\gamma$  is the specific weight of water ( $9810 \text{ N/m}^3$ ),  $Q_{\mu}$  is the mean daily peak flow, and  $S$  is slope. Increased stream power is a result of higher discharge; thus, an increase in geomorphic work is expected.

Baker (1977) provides an example of this phenomenon on the upper Guadalupe River. He suggests that a threshold must be exceeded by an applied stress for geomorphic work to occur. When stream power increases, thresholds for sediment transport are exceeded. The higher the threshold, the higher the stream power needs to be. Baker observes the result of exceeding a threshold after a flood in 1972 near New Braunfels, TX. He cited as evidence of the flood, large boulders transported downstream, limestone joints plucked from the channel bed, erosion of cut banks, and large scour holes.

Large floods have shaped the upper portion of the river through the Edwards Plateau and the Balcones Escarpment. Limestone and lack of vegetation in this physiographic region, along with the local weather events and climatic influences allow for extreme rates of runoff that increase stream power, which entrain sediments and help carve the channel of the upper Guadalupe River. The middle Guadalupe River Basin, including the New Braunfels area and the Balcones Escarpment, are shown in Figure 2.

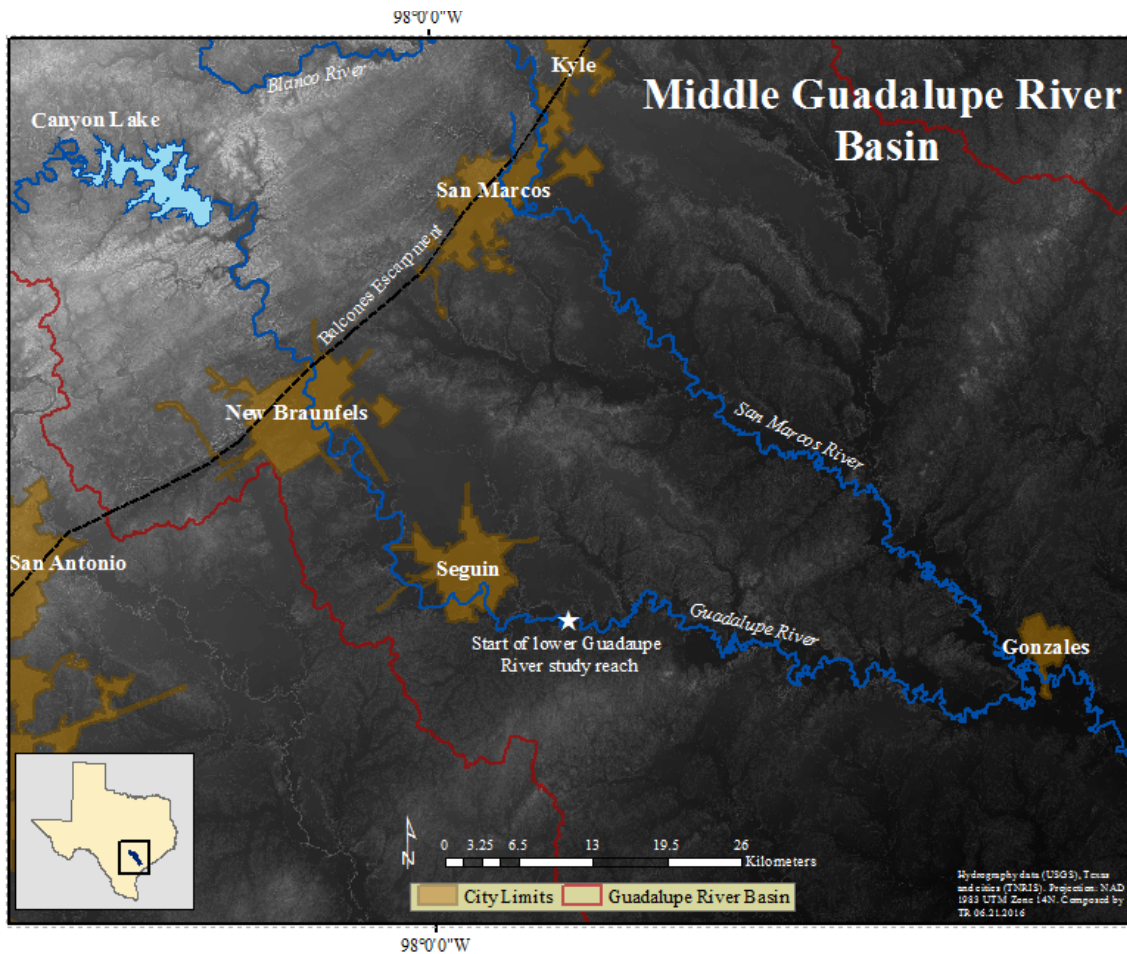


**Figure 2. Middle Guadalupe River Basin including Canyon Lake, the Balcones Escarpment and major tributaries to the Lower Guadalupe River. Features are overlain onto a DEM where lighter colors denote a higher elevation, whereas the darker colors denote a lower elevation.**

Weather in the region is the result of an abrupt topographic change that creates an orographic effect ideal for rapid convective thunderstorm development and torrential rains (Dorroh, 1946). Baker (1975) also notes that storms with a tropical origin can have severe impact when the front reaches the orographic barrier along the escarpment. Longer duration rains persist and create floods resembling the September 1921 storm in which 970 mm of rain fell in 24 hours; one of the greatest magnitude storms in the contiguous U.S. (Baker, 1975). More recently, the region has experienced severe flash flooding, setting record stage heights and discharge volumes in May and October 2015 respectively.

The May and October 2015 storms directly affected the upper Guadalupe River, but the effects were dampened as a result of water retention in Canyon Lake. The lower section of the river was indirectly affected downstream of the confluence of the San Marcos River

near Gonzales, TX. The San Marcos River was affected by the same storm; however, no major dams for flood control exist on the river, only low head dams for flow regulation at lower discharges. Lack of flood control structures enhance the propagation of flood waves to directly affect the Guadalupe River below the confluence. As flood waves propagate downstream, increasing discharge has the potential to reshape the channel of the lower Guadalupe River.

### *2.3 Dams*

Flood waves also propagate downstream as a result of water storage and hydropower generation at Canyon Lake, the largest reservoir on the Guadalupe River. The reservoir is outside of the study area; however, the effects are felt. Two reservoirs, Lake Gonzales and Wood Lake are included in the study area and produce similar, but smaller, effects. Dams regulate flows downstream, especially those used for hydropower. Daily releases made to meet energy needs result in hydropeaking in the hydrograph. These resulting pulses induce irregular flow regimes that raise low flows, and dampen flood peaks (Magilligan and Nislow, 2005; Graf, 2006).

Wolman and Miller (1960) explain that landscapes are modified by frequent moderate flows rather than rare catastrophic floods. The authors observed this in the wet and humid climate of the east coast. Although they did not consider dams to be the cause of a moderate flow regime, their description that this type of flow regime dominates geomorphic changes applies in this regulated reach of the Guadalupe River.

### *2.4 Geomorphic and Watershed Characteristics*

Flow regime, among numerous other factors, control channel changes in the lower Guadalupe River. A Texas Water Development Board study conducted by Phillips (2011) examined geomorphic boundaries and transition zones linked to specific geomorphic controls of the entire length of the Guadalupe River. He outlines seven controls including slope, sinuosity, geology, valley confinement, valley width, floodplain-river connectivity, and flow regime. Each control has its own set of boundary points along the stretch of the river delineated by GIS analysis of DEMs (Digital Elevation Model) and aerial imagery. Visual indicators such as dams, recent avulsions, and oxbow density aided boundary determinations.

We selected geomorphic boundary zones as a way to assess channel migration and mechanisms of change to improve on previous studies. A similar study, examining rates of migration on the lower Brazos River in Texas, was conducted by Giardino and Lee (2011). Their study used counties as boundaries for reach delineation. Counties are not typically determined by Earth-surface properties, thus, boundaries that account for these properties should be used. Another study performed on the Brazos River by Gillespie and

Giardino (1997) used tributary confluences to determine reach boundaries. Richard et al. (2005) also used channel characteristics including confluences, degree of meandering or braiding, presence and manmade controls, and channel confinement to denote reach boundaries for their study of lateral migration downstream of Cochiti Dam, NM.

## *2.5 Channel Pattern and Geometry*

The previous studies used geomorphic-related reach boundaries as well as watershed and channel planform variables to analyze lateral rates of migration. Gillespie and Giardino (1997) and Richard et al. (2005) used variables of radius of curvature, arc length, channel width, amplitude, and sinuosity as indicators of lateral migration. These indicators were analyzed in association with variables including discharge, stream power, sample median grain sizes, and vegetation to identify driving mechanisms of change. Other studies point to a more specific driver of channel change. For example, Nicoll and Hicken (2010) focused on valley confinement as the specific driver of lateral migration in several Canadian Prairie rivers, and Konsoer et al. (2016) used riparian vegetation and bank material heterogeneity as the driving mechanisms for movement of meander bends.

Channel geometry and pattern are variables known to affect and influence lateral movement of meander bends. Channel patterns vary across and within river systems as the channel approaches dynamic equilibrium. As a river adjusts to a specific base level, channel patterns can change (Schumm et al., 2002, Cyr and Granger, 2008).

Channel pattern can be used as a measurement to understand the stability of the river. Sinuosity, or the ratio between channel and valley length, is one characteristic commonly used. Schumm (1963) relates sinuosity to river patterns, and he classified these into five categories: straight (1-1.3), transitional (1.3-1.7), regular (1.7-1.8), irregular (1.8-2.3), and torturous (>2.3).

Channel geometries also vary. The quantification of various geometries can serve as additional indicators of the stability of the river. In a meandering system, distinct relationships are present between channel planform characteristics including width, wavelength, and radius of curvature of meanders. The wavelength between two meanders averages eleven times the average width of the channel, and the radius of curvature is generally one fifth of the wavelength (Leopold, 1994).

### **2.5.1 Radius of Curvature**

Radius of curvature is an important parameter used when analyzing lateral migration; the result of shear stress acting on the outside bank of a meander bend. Figure 3 illustrates the mechanics of lateral migration in a meander bend.

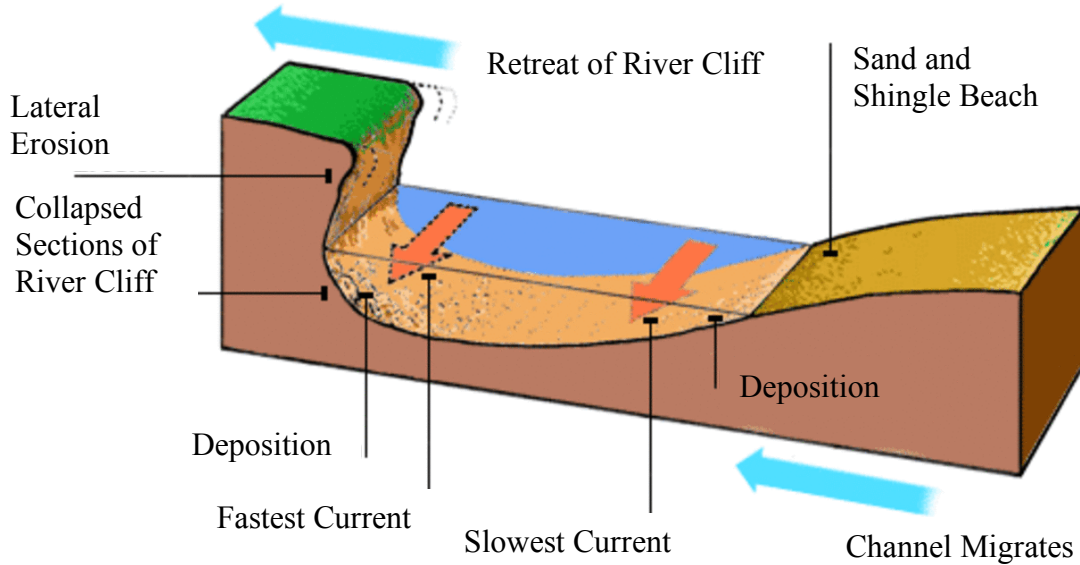


**Figure 3. Cross-section of the process of lateral migration in a meander bend (Modified from [www.bbc.co.uk](http://www.bbc.co.uk)).**

During high discharges, meander bends can migrate laterally as the bend is eroded by increased shear stresses that destabilize the bank (Briaud, 2001; Darby et al. 2002, Wallick et al., 2006). Shear stress is controlled by flow velocities in the channel as well as the channel geometry and bank material. Leopold and Wolman (1957) suggest that radius of curvature, or tightness of a bend, relates to lateral migration. To scale the radius to channel size, a ratio of radius and average channel width is often used.

The tightness of the bend relates to the resistance of the outside bank to erosion. Bagnold (1960) suggests that resistance is lowest at a ratio of  $\sim 2$ . When values are less than two, the flow loses force and does not directly impact the outside bend. At values greater than two, the bend is less “tight” and results in a higher resistance on the outside bend. The difference in channel pattern for a variety of ratio values is displayed in Figure 4.

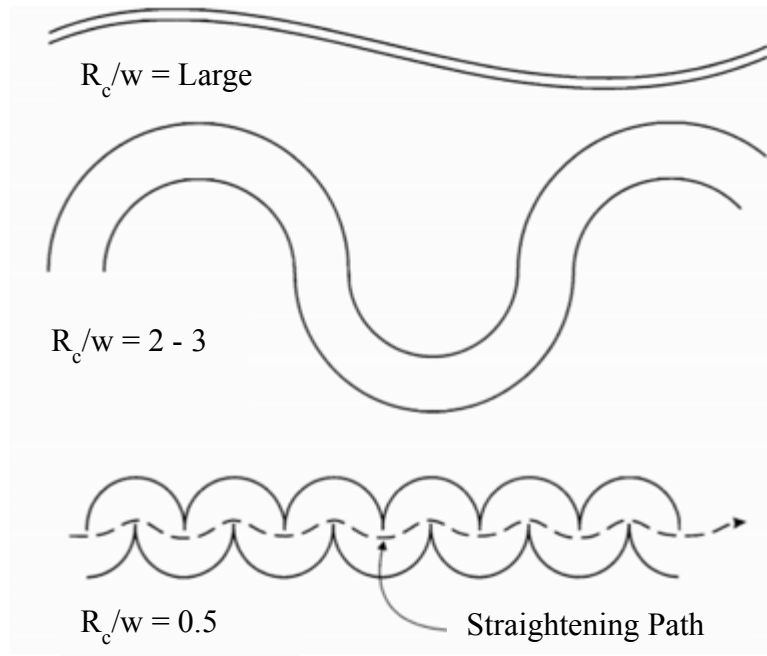


**Figure 4. Rivers with various radii of curvature and their shape where  $R_c$  = radius of curvature and  $w$  = channel width (Modified from Briaud et al., 2001.).**

Nanson and Hickin (1983; 1984; 1986) test Bagnold’s theory in a field setting on several rivers of the Canadian Prairie in British Columbia. They compare rates of lateral migration to values of the ratio of radius of curvature and channel width. They find a strong relationship exists between the highest rates of lateral migration in the dataset and ratio values between two and three. Values less than two and greater than three relate to lower rates of migration. Therefore, the authors determine the ratio of radius of curvature and channel width can be used as an indicator of meander stability. Unfortunately, the rivers of the Canadian Prairie are not applicable to the rivers in Texas. To determine if Texas rivers also follow the same trends as the rivers of the Canadian Prairie, our study attempted to understand if the ratio holds true for rivers of Texas.

### 3. STUDY AREA

#### 3.1 Watershed Characteristics and Geomorphology

The headwaters of the Guadalupe River are located near Kerrville, TX, in Kerr County, Texas, where the river forms from groundwater springs and flows east on the Edwards Plateau before dropping through the Balcones Escarpment and turning southeast, where it flows toward the San Marcos River confluence near Gonzales, TX. At Gonzales it flows south for 280 km through the Gulf Coastal Prairie before draining into Guadalupe Bay in the Gulf of Mexico. The Guadalupe River drainage area is ~15,418 km<sup>2</sup> and has a river length of ~ 658 km (TSHA, 2010). Our study evaluates a ~380 km section from the USGS gauge at US HWY 1117 in Seguin, TX, to the confluence of the San Antonio River, 11 km before the Gulf of Mexico. A map of the lower Guadalupe River Basin is shown in Figure 5.

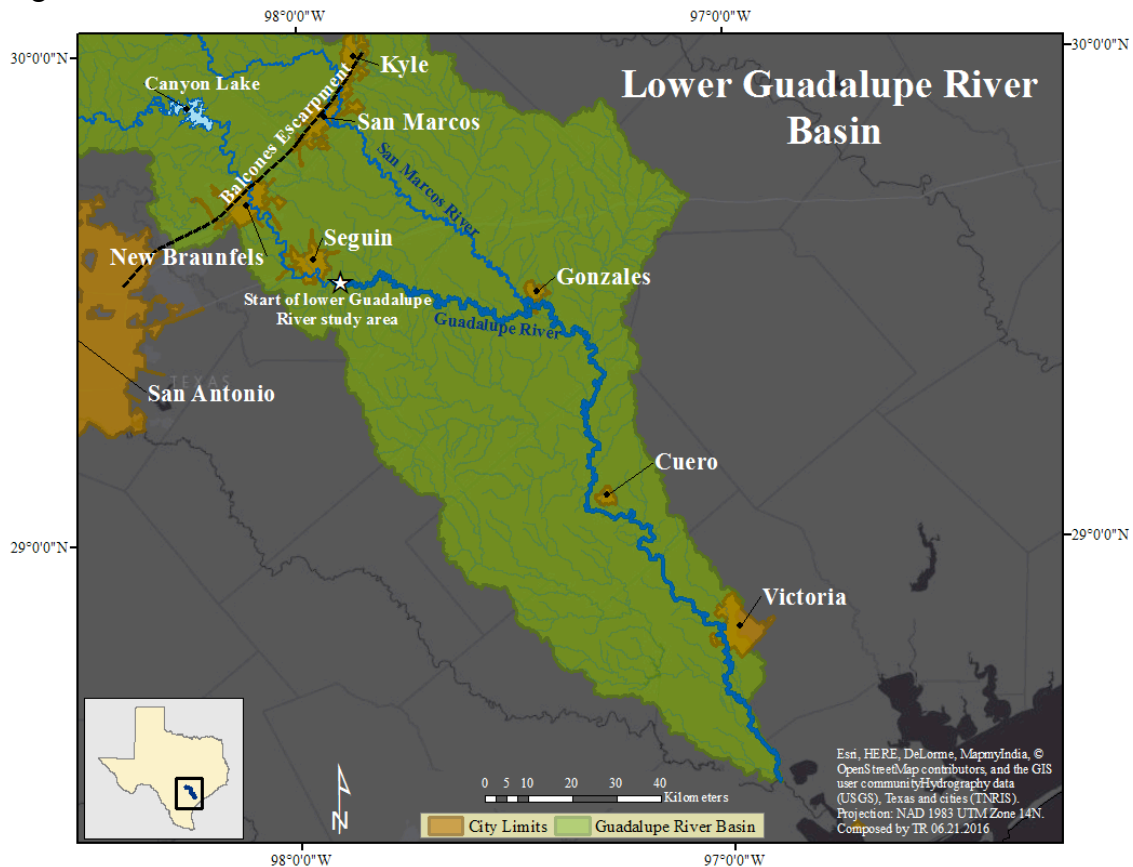


**Figure 5. The lower Guadalupe River Basin.**

As previously mentioned, Phillips (2011) designated geomorphic boundary thresholds along the Guadalupe River. Based on the thresholds, seven zones occur within the lower Guadalupe River study area. Figure 6 shows the seven delineated geomorphic zones,

Table 1 includes the zones and the associated coordinates, and Table 2 provides characteristics of each zone.

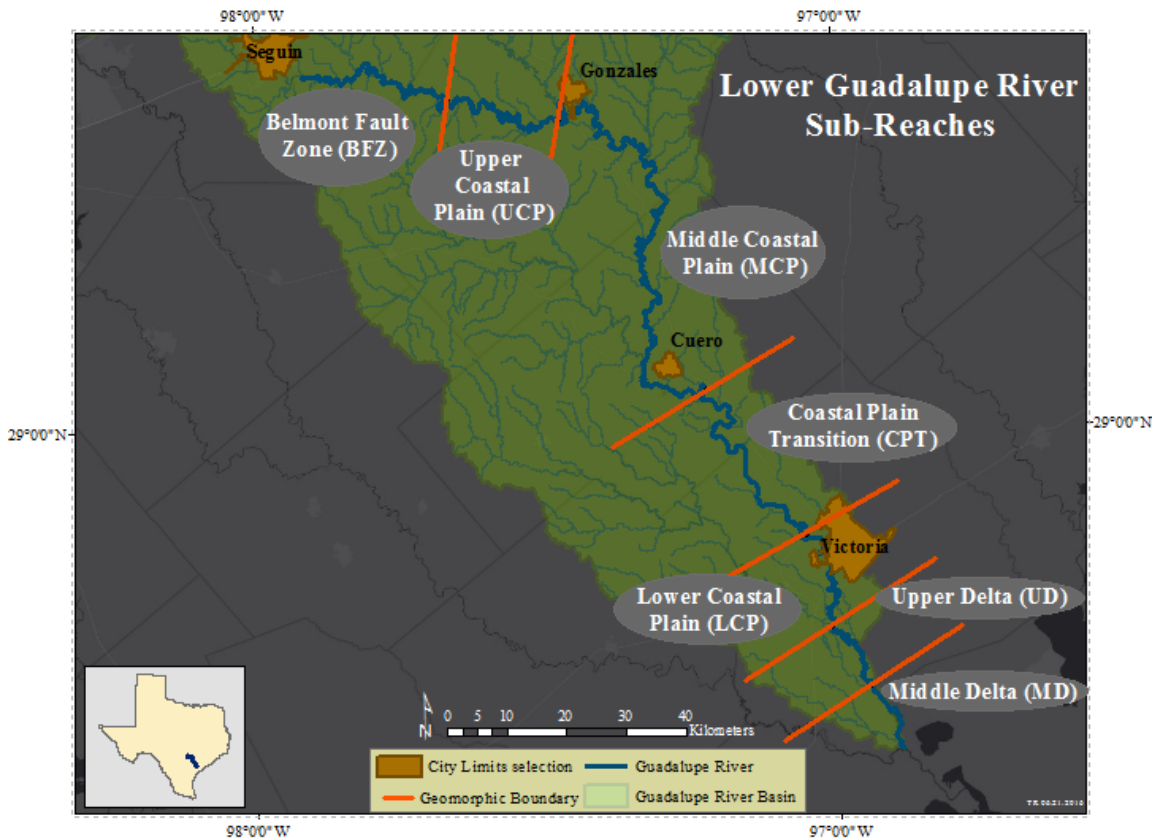


Figure 6. Map including study reach and associated study sub-reaches by geomorphic zone after Phillips, 2011.

Table 1. Geomorphic zones and associated geographic coordinates using the geographic coordinate system North American Datum 1983.

Geomorphic Zone	Distance from Gulf (km)	Reach Distance (km)	Latitude	Longitude
Belmont Fault Zone	376	79	29.503	-97.663
Upper Coastal Plain	327	35	29.469	-97.472
Middle Coastal Plain	287	40	29.058	-97.222
Coastal Plain Transition	130	157	28.836	-97.054
Lower Coastal Plain	78	52	28.698	-97.013
Upper Delta	40	38	28.608	-96.946
Middle Delta	11	29	28.506	-96.84

**Table 2. Characteristics of geomorphic zones adapted from Phillips (2011).**

<b>Geomorphic Zone</b>	<b>Slope (Gradient in degrees)</b>	<b>Sinuosity</b>	<b>Valley Width (km)</b>	<b>Valley Confinement</b>	<b>CFC</b>	<b>Geology</b>
<b>Belmont Fault Zone</b>	$6.5 \times 10^{-4}$ (0.04°)	3.07	0.8-2.1	Partially Confined	Moderate	Eocene; Carrizo Sand and Recklaw
<b>Upper Coastal Plain</b>	$6.1 \times 10^{-4}$ (0.03°)	2.38	0.9-3.5	Partially Confined	Moderate	Eocene; Carrizo Sand
<b>Middle Coastal Plain</b>	$2.7 \times 10^{-4}$ (0.02°)	2.87	0.8-7.1	Partially Confined	Moderate	Eocene
<b>Coastal Plain Transition</b>	$3.7 \times 10^{-4}$ (0.02°)	1.73	1-2.8	Partially Confined	High	Miocene, Pliocene
<b>Lower Coastal Plain</b>	$3.3 \times 10^{-4}$ (0.02°)	2.49	4.5-5.5	Unconfined	High	Qt Lissie and Beaumont
<b>Upper Delta</b>	$5.9 \times 10^{-5}$ (~0.00°)	2.13	5.0-6.0	Unconfined	Very High	Holocene Delta, Qt Beaumont
<b>Middle Delta</b>	$1.9 \times 10^{-4}$ (0.01°)	1.39	6.0-7.0	Unconfined	Very High	Holocene Delta, Qt Beaumont

Lateral rates of migration were assessed for the entire reach as well as in each sub-reach. A description of each zone, upstream to downstream, is provided in the following sections. The descriptions have been slightly altered from Phillips (2011) original discussion.

### **3.1.1 Zone 1 – Belmont Fault Zone (BFZ)**

The reach begins at the FM 1117 bridge, east of Seguin, TX, and extends 55 km to the upper end of Zone 2. This zone has tortuous meanders and straight segments, often parallel with mapped faults near Belmont. Geologic changes constrain the river in this reach. The valley widens where the Carrizo Sand Formation outcrops, whereas the more resistant Recklaw formation confines the lower valley. Regular dam releases from Canyon Lake dominate the flow through this reach. The Belmont Fault Zone sub-reach is shown in Figure 7.

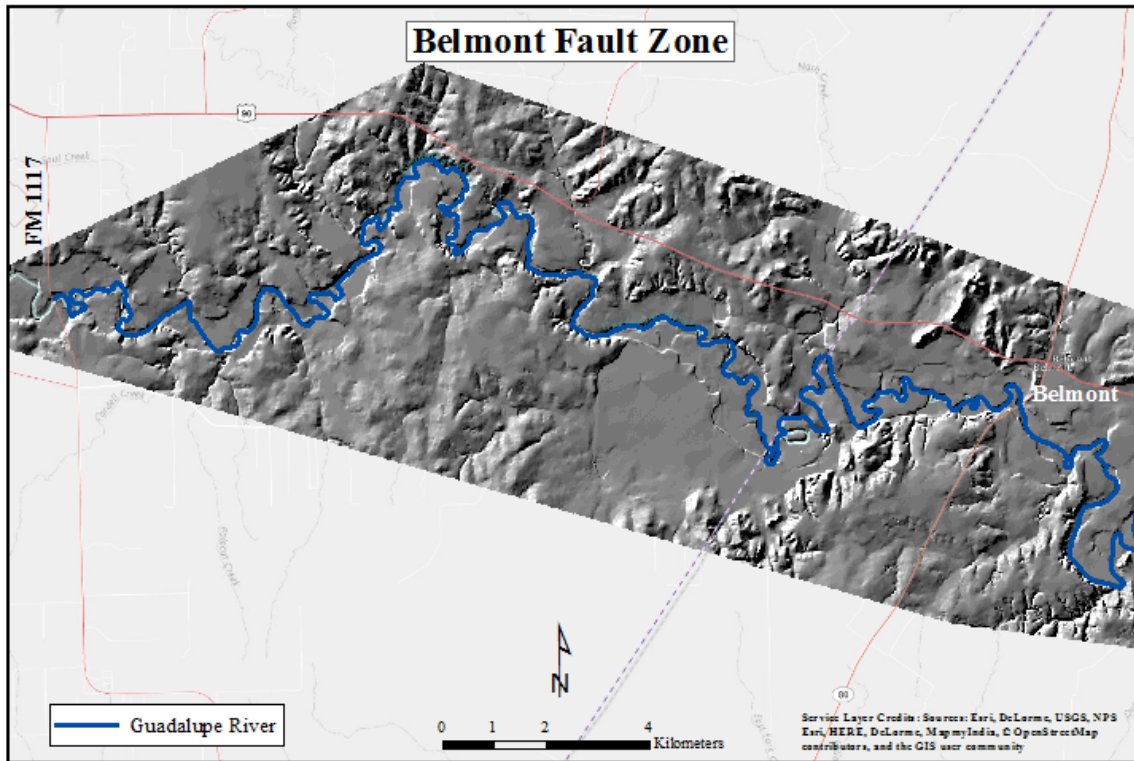


**Figure 7. Map of the Belmont Fault Zone geomorphic zone and reach.**

### **3.1.2 Zone 2 – Upper Coastal Plain (UCP)**

The upper coastal plain starts near Belmont, TX, and extends 44 km to the San Marcos River confluence. The reach has the highest sinuosity and slope of all zones within the study area. The valley is partially confined and less variable than in Zone 1. Zone 2 has several small hydroelectric dams that control flow, but the river is highly influenced by Canyon Lake reservoir, as well as the Comal and San Marcos Rivers. The reach includes two reservoirs, Lake Gonzales and Wood Lake. Zone 2 is shown on the map in Figure 8.

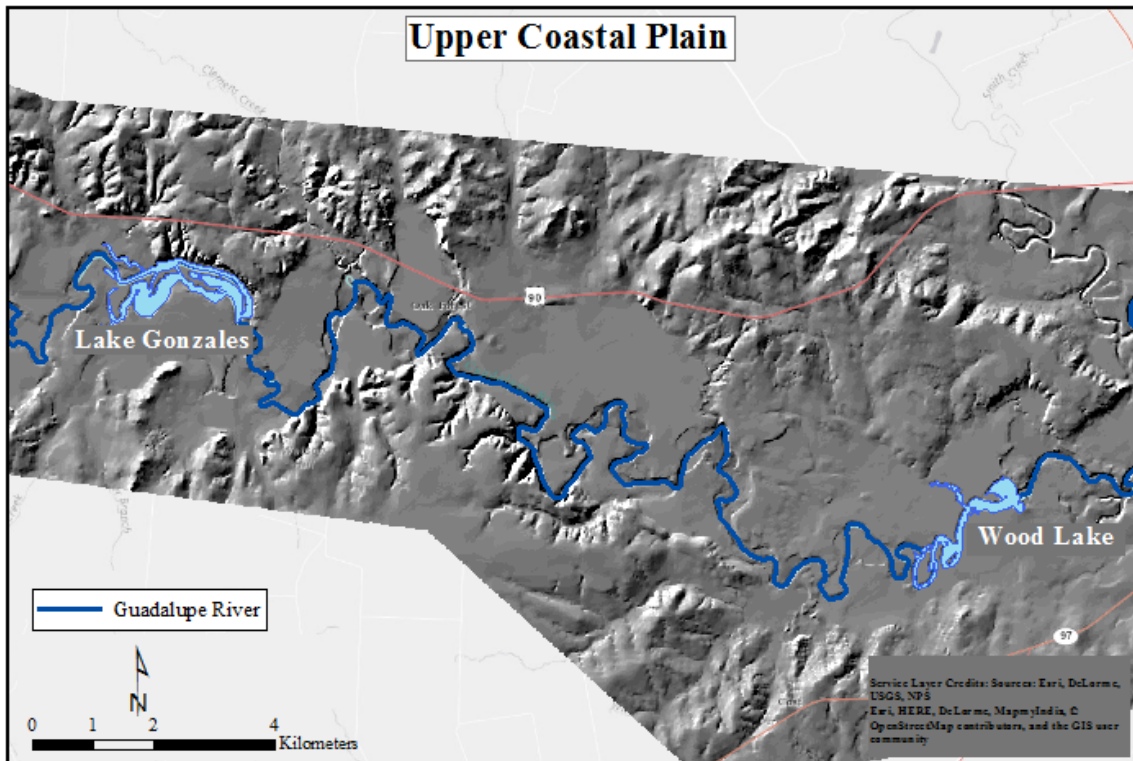


**Figure 8. Map of the Upper Coastal Plain geomorphic zone and reach.**

### **3.1.3 Zone 3 – Middle Coastal Plain (MCP)**

Zone 3 is the longest reach in which the river flows 147 km from its confluence with the San Marcos River to just downstream of Cuero, TX. The reach is partially confined with variable valley widths. Sinuosity is lower than the surrounding up and downstream reaches. Again, the Carrizo Sand Formation dominates the wider valley sections, whereas more narrow sections are confined by minor, less resistant, Eocene-aged formations. High channel-floodplain connectivity (CFC) is characteristic of this zone as a result of several paleo-channels. The channels indicate movement within the valley; more than in other zones. The following map in Figure 9 shows the arcing path of the river from the beginning of the zone to the end.

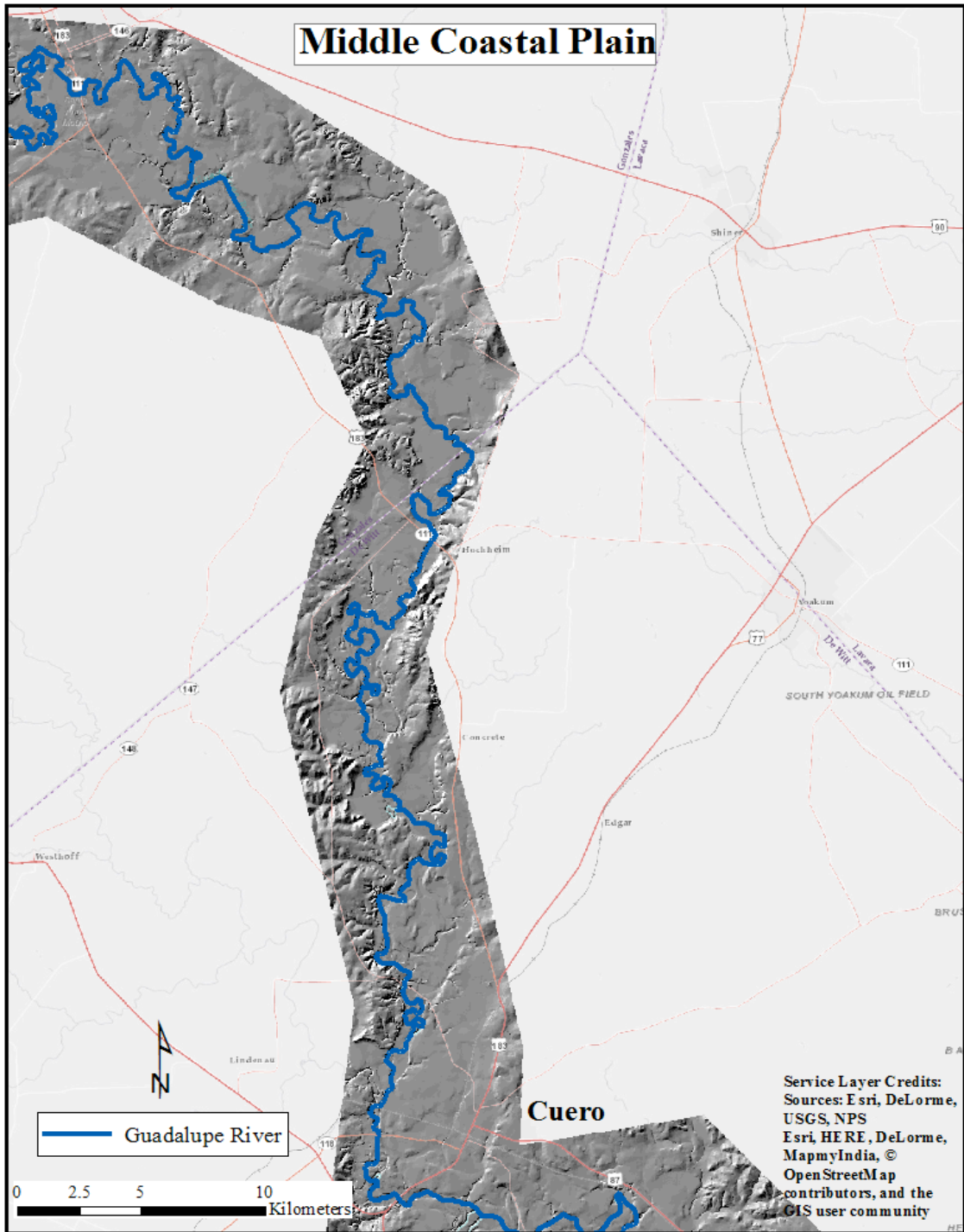


Figure 9. Map of the Middle Coastal Plain geomorphic zone and reach.

### 3.1.4 Zone 4 – Coastal Plain Transition (CPT)

Zone 4 transitions from Miocene-aged valley walls near Cuero, TX, to Pliocene-aged deposits upstream of Victoria, TX. The 51 km reach decreases in sinuosity and has a gentle slope. The path of the river as it flows through Zone 4 is shown in Figure 10.

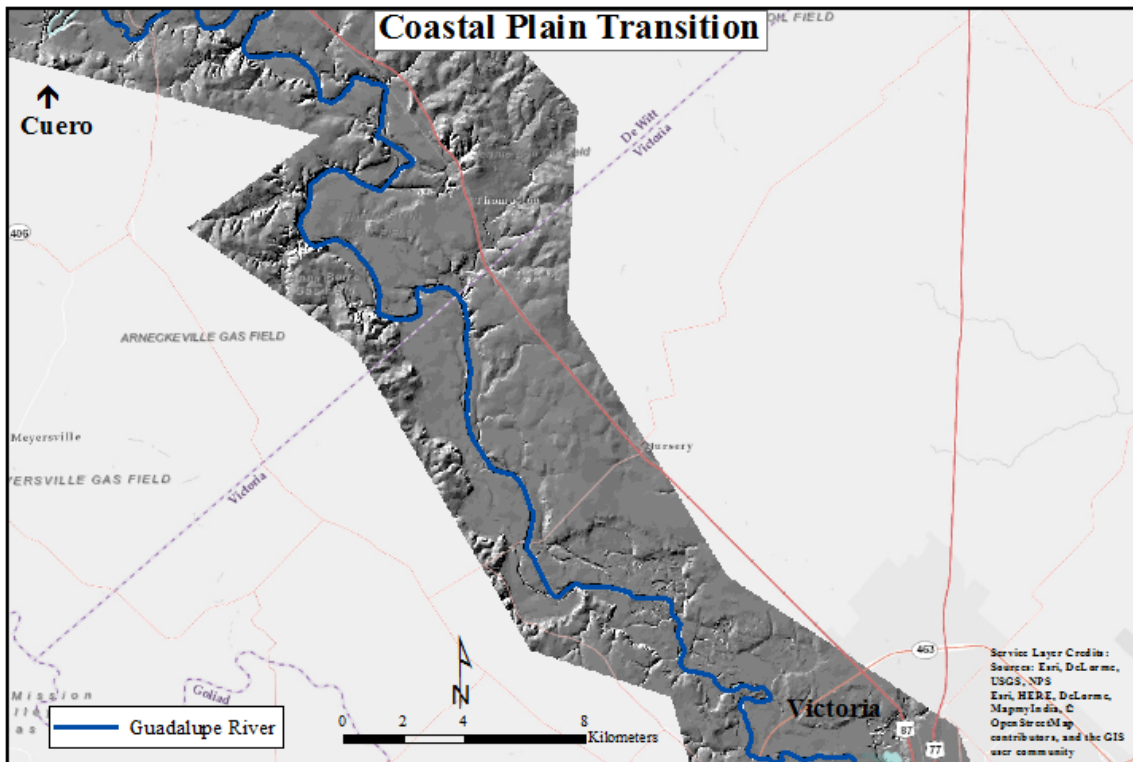
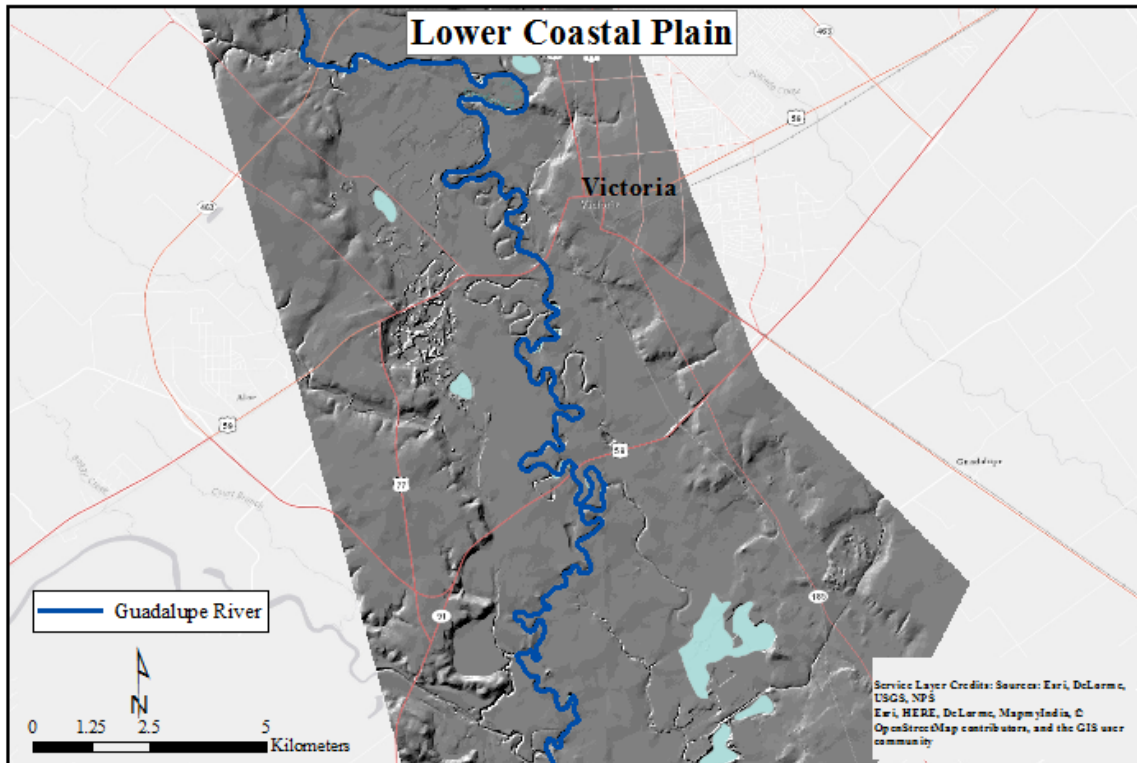


Figure 10. Map of the Coastal Plain Transition geomorphic zone and reach.

### 3.1.5 Zone 5 – Lower Coastal Plain (LCP)

The lower coastal plain extends 39 km from upstream of Victoria, TX, to Zone 6. The reach has a low gradient of 0.02°; however, is sinuous with a sinuosity greater than two. Zone 5 has high CFC as a result of low banks allowing for common overbank flow. The extent of Zone 5 is shown in Figure 11.



**Figure 11. Map of the Lower Coastal Plain geomorphic zone and reach.**

### **3.1.6 Zone 6 – Upper Delta (UD)**

The upper delta is a 25 km reach extending from the confluence with Coleta Creek to Zone 7. Characteristic of a deltaic area, slope and sinuosity are low. The zone is sufficiently far enough upstream from Guadalupe Bay, so is not affected by tides or backwater effects. An unconfined valley and low banks allow for very high CFC in this reach. Although unconfined, cohesive Beaumont clays exhibit some control on channel morphology. The extent of Zone 6 is shown in Figure 12.

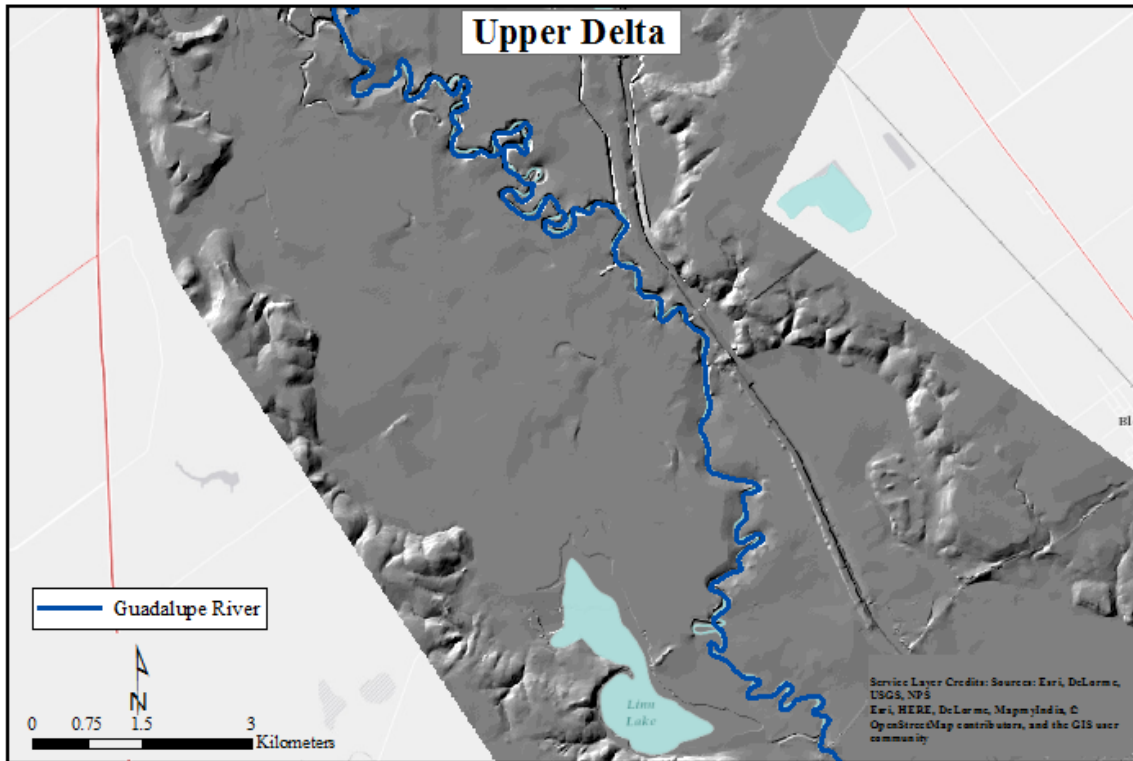


**Figure 12. The Upper Delta geomorphic zone and reach.**

**3.1.7 Zone 7 – Middle Delta (MD)**

The middle delta is a 23 km reach near Bloomington to just south of the confluence with the San Antonio River. The zone is similar to the upper delta, but it is more influenced by Guadalupe Bay. A saltwater barrier at Tivoli limits the amount of tidal and saltwater influences in the zone, but it is present. The Middle Delta is shown in Figure 13.

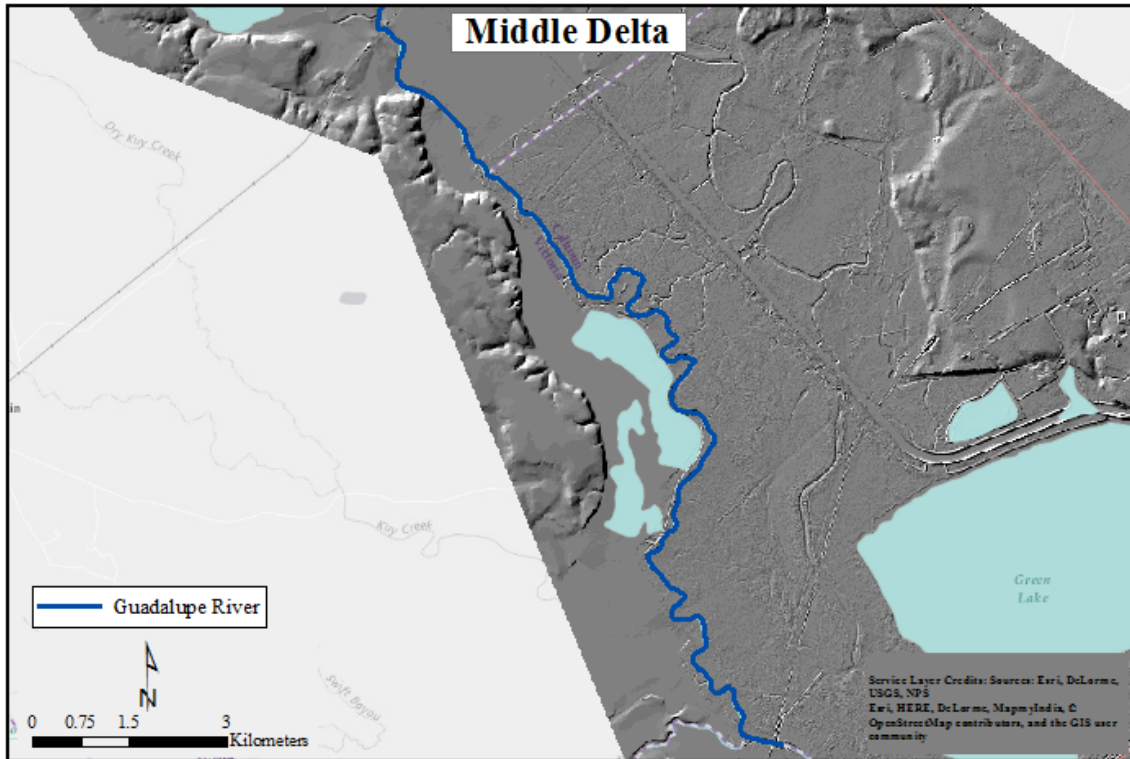


**Figure 13. The Middle Delta geomorphic zone and reach.**

In summary, the Belmont Fault Zone has the highest slope with a gradient of  $0.04^\circ$ , whereas the Upper Delta has the lowest slope with a gradient of  $\sim 0.0^\circ$ . The Belmont Fault Zone has the highest sinuosity of 3.07, whereas the Middle Delta has the lowest of 1.39. The four upper reaches have partially confined valleys as a result of local alluvial terraces, Eocene-aged outcropping in the Belmont Fault Zone, and Miocene-aged outcropping in the Middle Coastal Plain. The lower three reaches have unconfined valleys, flowing through Quaternary alluvial deposits. The valley is narrowest in the Belmont Fault Zone and widest in the Middle Delta.

### 3.2 Geology and Geomorphology

The Balcones Escarpment fault zone lies within the Guadalupe River Basin, and it served as the divide between the uplifted Edwards Plateau and the Gulf Coastal Plain (Baker, 1976). The escarpment is a natural divide between the contrasting upper and lower Guadalupe River. In the upper reach, the Edwards Plateau is a karst-dominated region consisting of limestone, dolomite, and marl. Numerous confined, incised channels dissect the Plateau before flowing down the escarpment to the alluvial plain toward the lower reach. Here, the Gulf Coastal Plain is dominated by sand, silt and clay. The lower river reach, of which this present study encompasses, meanders across the largely unconfined alluvium toward the Gulf of Mexico.

Roughly 200 million years ago, the Guadalupe River Basin and much of Texas was covered by seas. Beds are situated parallel to the current Gulf Coast as a result of sea regression, shown in Figure 14.

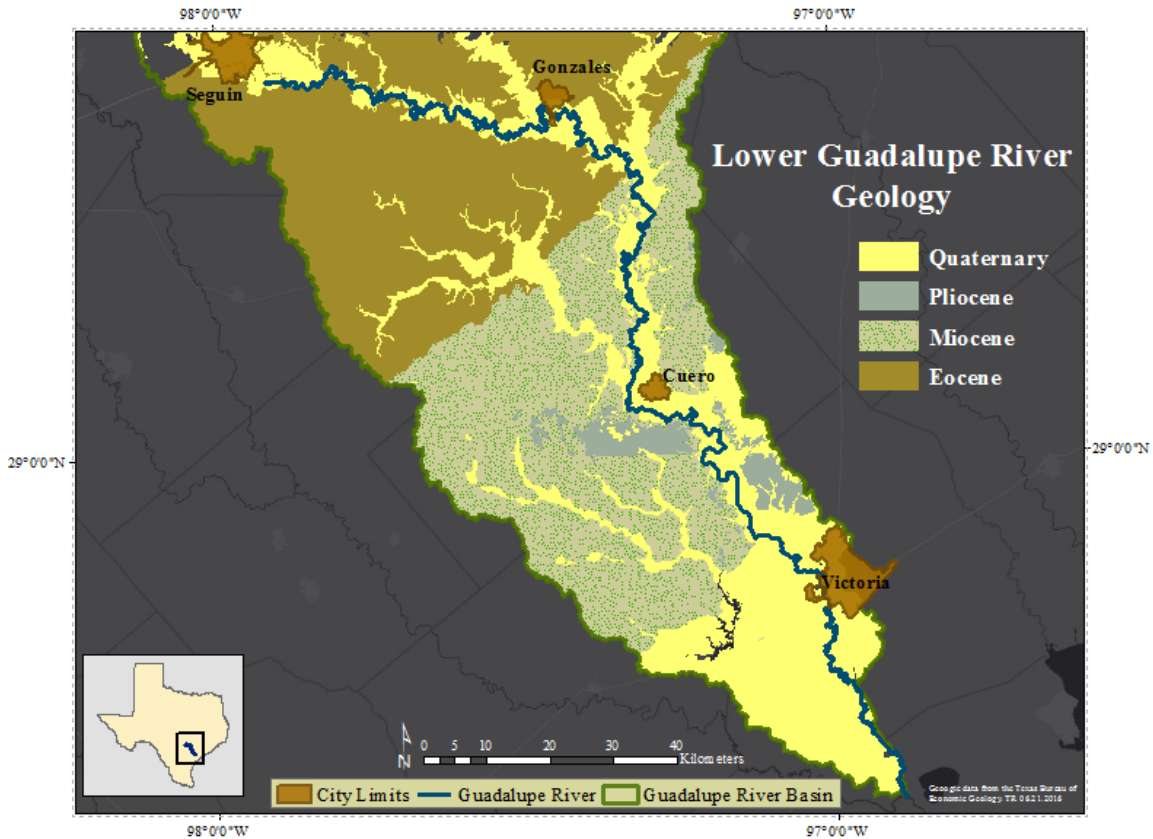


**Figure 14. Geology of the lower Guadalupe River Basin.**

Seguin to just east of Gonzales consists of the Eocene-aged Wilcox Group, Recklaw, Yegua, and Manning Formations; all sand dominated. East of Gonzales, the Miocene-aged Catahoula and Fleming Formations are dominant until Cuero where the Pliocene clay and mud-dominated sandstone of the Goliad and Willis Formations cut into the sand and mudstone Miocene formations. North of Victoria, the Pleistocene-aged Lissie Formation dominates the western side of the river valley, whereas the Beaumont Formation dominates the east side. The Lissie Formation is sand-silt dominated, whereas the Beaumont Formation is predominately clay. Quaternary alluvium and terrace deposits dominate the valley from this location to the Gulf of Mexico (Deussen, 1924; Solis and Raul, 1981).

### 3.3 Weather and Climate

The climate of this region is considered subtropical humid, characterized by warm summers, and mild, dry winters. The average annual temperature is 19°C at the northern part of the study area near New Braunfels, 22 km northwest of Seguin. The hottest month occurs in August where the average high is 35°C and low is 22°C. January is the coolest month where the average high is 16 °C and the low is 3°C. At the southern end of the study area, the mean annual temperature in Victoria is 21°C. The hottest month occurs in August with an average high temperature of 35°C and low of 23°C, respectively. The coldest month occurs in January with an average high temperature of 18°C and a low temperature of 6°C (USClimate Data, 2016). Climagraphs for New Braunfels, TX, and Victoria, TX, are shown in Figures 15 and 16, respectively.

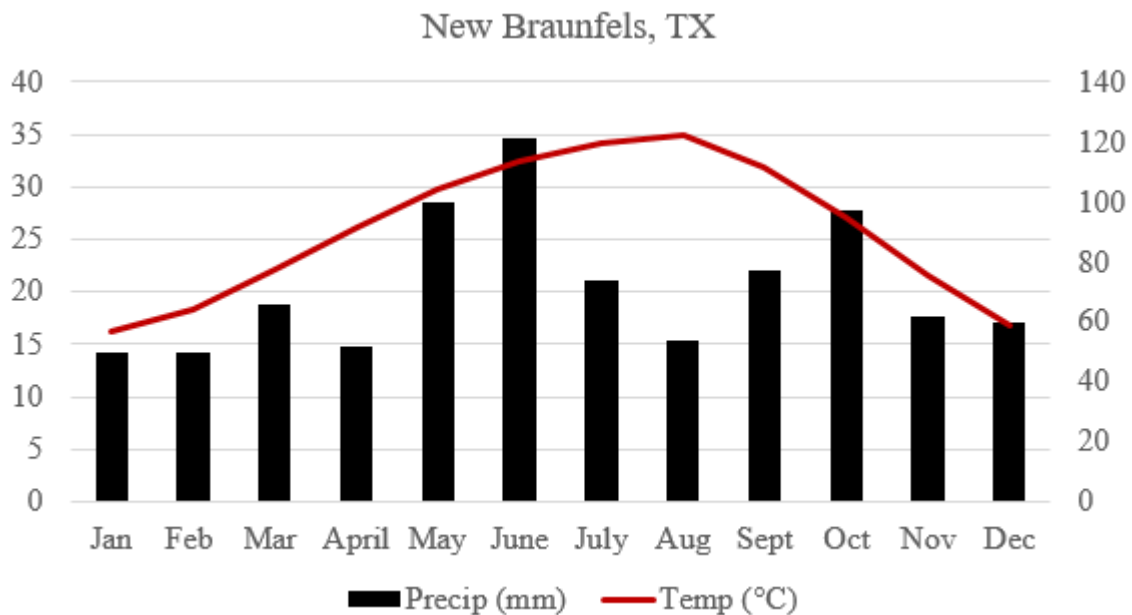
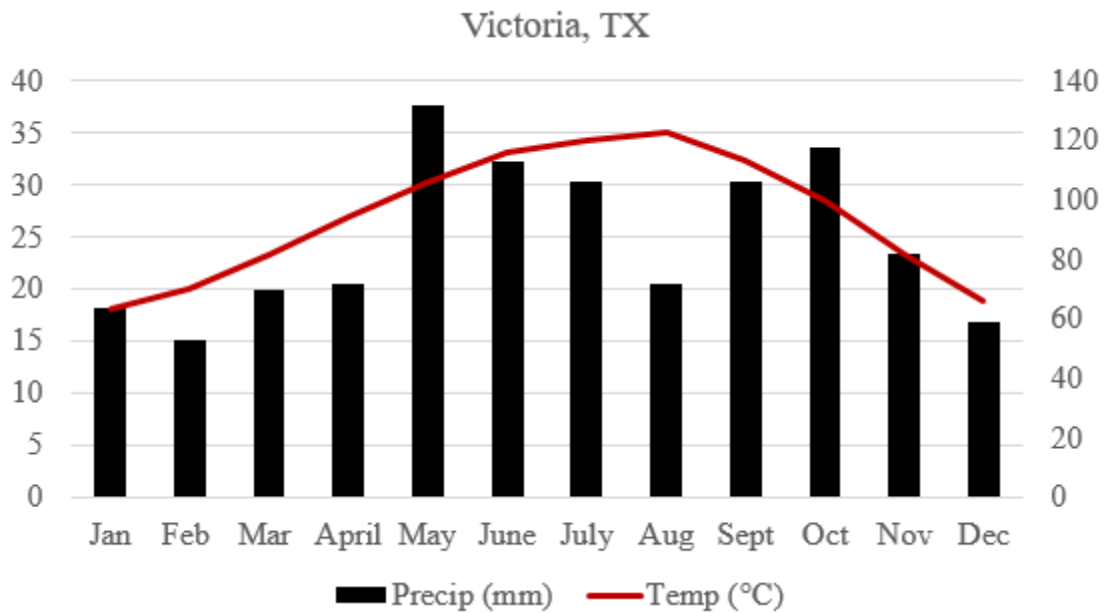


Figure 15. New Braunfels, TX, Climagraph (US Climate Data, 2016).



**Figure 16. Victoria, TX, Climograph (US Climate Data, 2016).**

Annual precipitation averages from 863 mm to 1,047 mm in New Braunfels and Victoria, respectively. The majority of the precipitation falls as rain, and is heaviest in the spring, early summer, and fall. This region is unique because it experiences a variety of types of storms capable of catastrophic rainfall. In the spring and early summer, cold fronts from the northwest meet moist air masses originating from the Gulf of Mexico to create squall lines of thunderstorms that produce the majority of the rainfall. In the fall, tropical disturbances and remnant storms will move landward, stalling out over the escarpment region with the potential to produce large amounts of rainfall.

### 3.4 Land Use

Land use for the Guadalupe River watershed for 1992 and 2011, respectively, is shown in Table 3. Percent change that has occurred over 19 years is also shown.

**Table 3. Land use/land cover for 1992 and 2011 and associated changes.**

<b>Land Unit</b>	<b>1992 Land Cover Percentage</b>	<b>2011 Land Cover Percentage</b>	<b>Percent Change (1992-2011)</b>
Open Water	<1%	<1%	<1%
Urban	1.8%	8.6%	6.8%
Barren Land	<1%	<1%	<1%
Deciduous Forest	15.1%	7.0%	-8.1%
Evergreen Forest	20.2%	10.5%	-9.7%
Mixed Forest	<1%	<1%	<1%
Shrub/Scrub	16.7%	36.3%	19.6%
Grassland/Herbaceous	22.6%	8.2%	-14.4%
Pasture/Hay	15.9%	18.6%	2.7%
Cultivated Crops	5.6%	6.2%	0.6%
Woody Wetlands	<1%	2.4%	2.1%
Emergent Herbaceous Wetlands	<1%	<1%	<1%

Overall, the Guadalupe River Basin is predominantly shrub/scrub-brush and pasture, which accounts for ~55% of the land cover. Land cover in the region has shifted from grasslands to more pasture and scrub. Forested areas are scattered throughout the basin, but they are dominant along riparian areas. Urban presence and growth is minimal with two main centers in the study area: Seguin and Victoria. Victoria is the larger urban area inside the basin with a population of ~66,000 whereas Seguin has a population ~ 26,500 (Census.gov, 2014).

### *3.5 Vegetation*

The Guadalupe River flows through four distinct vegetation regions. These four vegetation regions are: Blackland Prairie, Oak-Hickory, Fayette and Coastal Prairie. The Blackland Prairie consists of abundant scrub-brush and cultivated plots. The Oak-Hickory consists of grasslands and stands of timber, whereas the Fayette and Coastal Prairie host a majority of grasslands (Hatch et al., 1990).

Riparian cover changes throughout the watershed. The uppermost reaches of the Guadalupe River Basin are dominated by deciduous forest and cropland. Deciduous plants found in this area include Cypress, Oak, and Cottonwood. As one moves down the basin deciduous and croplands are interspersed between the dominant grasslands.

## 4. METHODS

### 4.1 Total Rates of Migration

The various methods and data sources used to collect and prove data for this study are described in the following section. These methods and data include: interpretation of topographic maps and satellite imagery; GIS analysis, digitization of temporally sequential river locations, polygon construction, classification of meander type, radius of curvature, slope, sinuosity, and vegetation cover.

To accomplish the objective of determining lateral rates of migration, a GIS was used. Imagery and historical maps were collected, georeferenced, and digitized for the years 1951-1964 (as one group denoted as 1960 in the GIS), 1995, 2004, 2010, and 2014. Images for the period 1951-1964 are grouped as a result of various dates for USGS topographic maps. The images for 1960 were georeferenced to the 2004 imagery because it was pre-referenced and provided the highest quality resolution. All images and data were referenced using the projected coordinate system NAD 1983: UTM Zone 14 N. Table 4 shows the years and sources of imagery because each were acquired from various sources and have different spatial resolutions. Table 5 includes each study period and span of years for the period. The base-year of 1960 was selected, as that showed the best resolution for the earlier time period.

**Table 4. Collected imagery date and spatial resolution.**

<b>Study Period</b>	<b>Imagery Source (resolution)</b>
<b>1960</b>	USGS Topographic Maps (~2.5m)
<b>1995</b>	Digital Ortho Quadrangles (~1m)
<b>2004</b>	National Agriculture Imagery Program (NAIP) (~1m)
<b>2010</b>	NAIP (~1m)
<b>2014</b>	NAIP (~1m)

**Table 5. Study periods.**

<b>Study Years</b>	<b>Time Interval (Years)</b>
<b>1960-1995</b>	35
<b>1995-2004</b>	9
<b>2004-2010</b>	6
<b>2010-2014</b>	4

Each acquired image for a particular study year was combined into a mosaic in ArcGIS® and included the entire reach in the study period. River position was digitized at a scale

of 1: 4,000 for all images. Spatial resolution ranged from 1-2 m for all images, so a scale of 1: 4,000 was determined acceptable for the range of resolutions. This scale was used for all images to minimize error and subjectivity resulting from the bias of one digitizer.

Other rules for digitization were also established to streamline the process and reduce error. The rules were:

- Use the edge of vegetation on an exposed channel bank as a boundary (Richard et al., 2005).
- Use line of established vegetation for exposed point bars.
- Where the channel boundary is not exposed, digitize the bank through the canopy center of the tree closest to the water (Winterbottom, 2000).

From the digitized left and right banks of the river, a centerline was created using the “collapse dual lines to centerline” tool in ArcGIS®. It is important to understand that the centerline does not represent the thalweg, but rather the exact center between the bank lines. A central line provides a clear representation of lateral rates of migration, and minimizes error from digitization. The use of a center line also eliminates bias of thalweg position not necessarily changing when channel boundaries do.

Centerlines for the respective time periods are compared using the “feature to polygon” tool in ArcGIS®. Polygons are created between centerlines time 1 and time 2. Figure 17 displays the single polygons that were created.

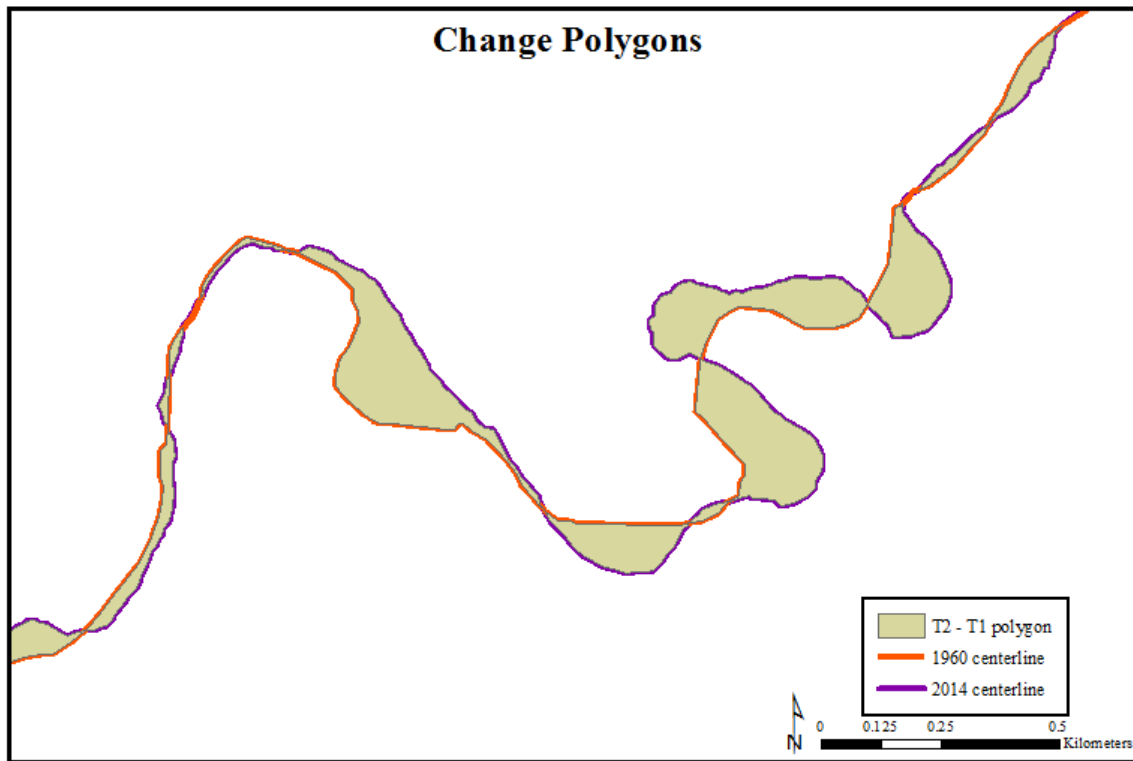


**Figure 17. Change polygons created by subtracting T2 (time) from T1 (time) centerlines to generate a polygon of change for a specific area.**

An example of consecutive meander bends with stacked polygons for each interval is shown in Figure 18. The stacked polygons display the progression of lateral migration over the study time period.

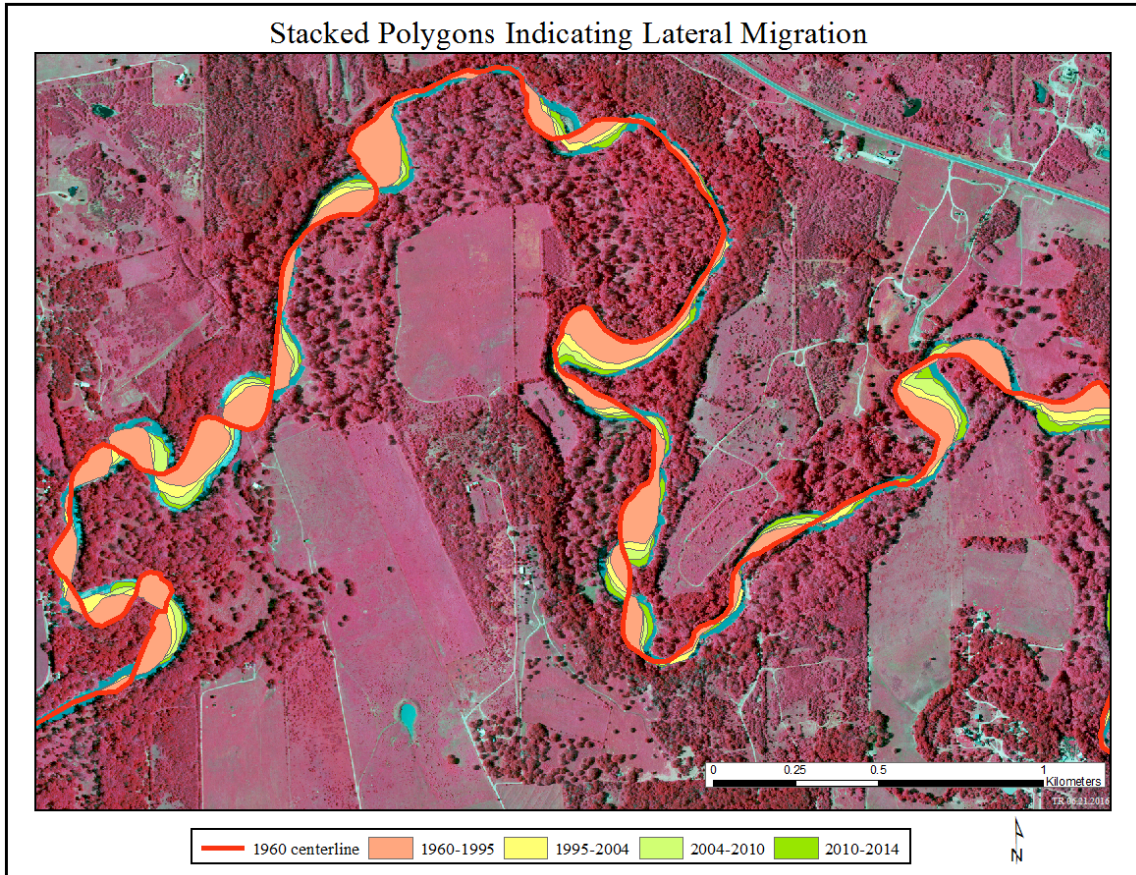


**Figure 18. Stacked polygons created from centerline pairs for the study area.**

The total amounts of migration between time intervals can be calculated from the polygons. Total migration is calculated as follows:

$$M_n = \frac{A}{\frac{1}{2}P} \quad \text{Eq. (2)}$$

where,  $M_n$  is the total rate of migration,  $A$  is the area of the polygon, and  $P$  is the perimeter of the polygon. Yearly rates of migration from the total amount, are calculated as follows:

$$R_y = \frac{M_n}{N} \quad \text{Eq. (3)}$$

where,  $R_y$  is the yearly rate,  $M_n$  is the total rate of migration, and  $N$  is the number of years in the study period. We took steps to minimize spatial error associated with digitizing and using imagery of various resolutions. Thus, total migration values less than 6 m were

eliminated. Whereas this step eliminated several meanders from consideration, it did ensure the fidelity of our measured rates of migration. The number of polygons created for each time interval are shown in Table 6.

**Table 6. Number of polygons with a value greater than 6 m total migration.**

Study Years	Number of Polygons
1960-1995	651
1995-2004	411
2004-2010	247
2010-2014	251
1960-2014	745

In this study, no attempt was made to separate positive change polygon from negative change polygon migration. This step was done because any movement, positive (erosion) or negative (aggradation) is a result of instability. The purpose of this study is to determine the stability of the lower Guadalupe River, so instability of any kind is used as an indicator.

#### *4.2 Geomorphic Zones and Specific Meander Bends*

To determine the driving mechanisms associated with lateral migration, an analysis was completed separating the study area into the seven sub-reaches based on geomorphic zones. The zonal boundaries, were imported into ArcGIS®. (Based on the work of Phillips (2011)). The upper and lower zones are adjusted to encompass the top and bottom ends of the study area. Polygons calculated for the entire study area were sectioned and divided into the seven reaches.

To gain additional understanding, meander bends from each reach were chosen at random for further analysis. Not all meander bends in a study reach were assessed as a result of the high number of bends. The “create random points” tool was used to generate ten points per reach. A 2 km buffer was used to eliminate potential clustering in one bend. If a point was generated between two bends, the closer bend was chosen for analysis. The total time period 1960 – 2014 was used for analysis. Initially, each time period, four in total, were assessed for the first and fourth reaches. No significant change in radius of curvature measurements were detected. Thus, it was assumed that total time period would be sufficient for analysis. A total of seventy meander bends were analyzed for the time period for a total of 140 points.

Channel characteristics, including type of bend (i.e., compound or simple), radius of curvature, channel width, slope, and sinuosity, were calculated for each point. Drainage basin characteristics, including riparian presence, density, and bank composition, were also collected.

### 4.2.1 Radius of Curvature

To determine radius of curvature for selected meanders, we used a method adapted from Nanson and Hickin (1983) by Geist (2005). This technique entails fitting two separate circles to a meander bend where the radii from the two circles are averaged, and the result is the radius of curvature. To determine the best fit for two circles, the point of maximum curvature of a specific bend was determined from the original channel placement. Two years, 1960 and 2014, were used in the analysis, and the 1960 outer channel boundary was used as the reference.

The Guadalupe River has a series of compound bends, or bends embedded within a larger bend, thus, it is challenging to distinguish which bend and associated point of maximum curvature to use. Figure 19, from Brice (1974), displays a variety of shapes of meander bends and served as a reference for determination of the appropriate bend and maximum point of curvature.

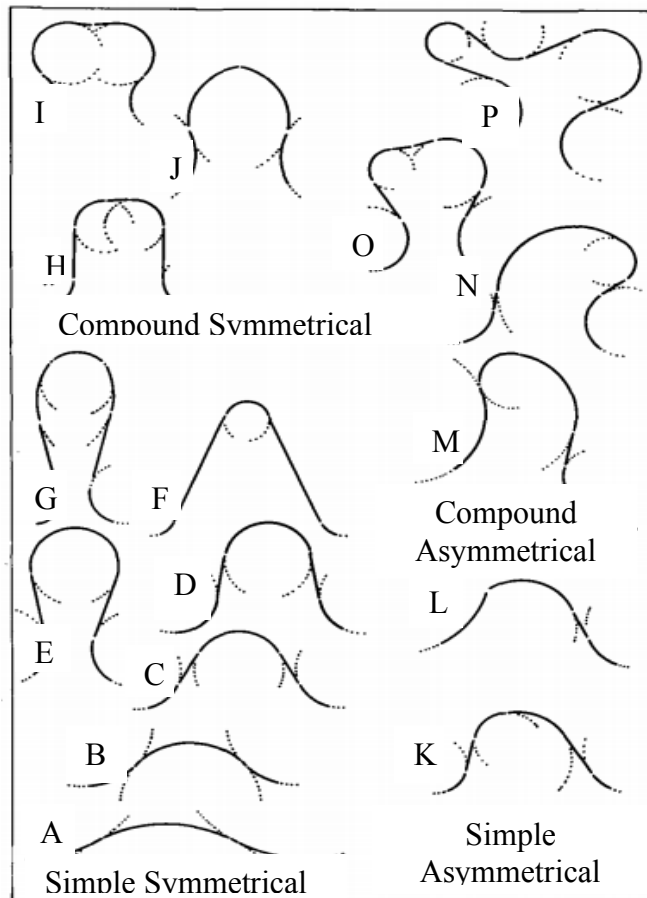


**Figure 19. Geometry of various types of meander bends. Note river flow is from right to left. (Modified from Brice, 1974).**

Once the appropriate bend and maximum point of curvature are determined, five points of channel width are measured within the meander bend. Between both points of inflection, an average width is determined. Points of inflection determine one meander bend from another, so it is important to log measurements between these two points, respectively. The average width is then used as the arc length spacing to establish two points on either side of the maximum point of curvature. The procedure is straightforward where the first circle is fit to the three innermost points, and the outer circle is fit to the middle point and two outer points. An example of a measurement of the radius of curvature in meander bend for 1960 is shown in Figure 20.

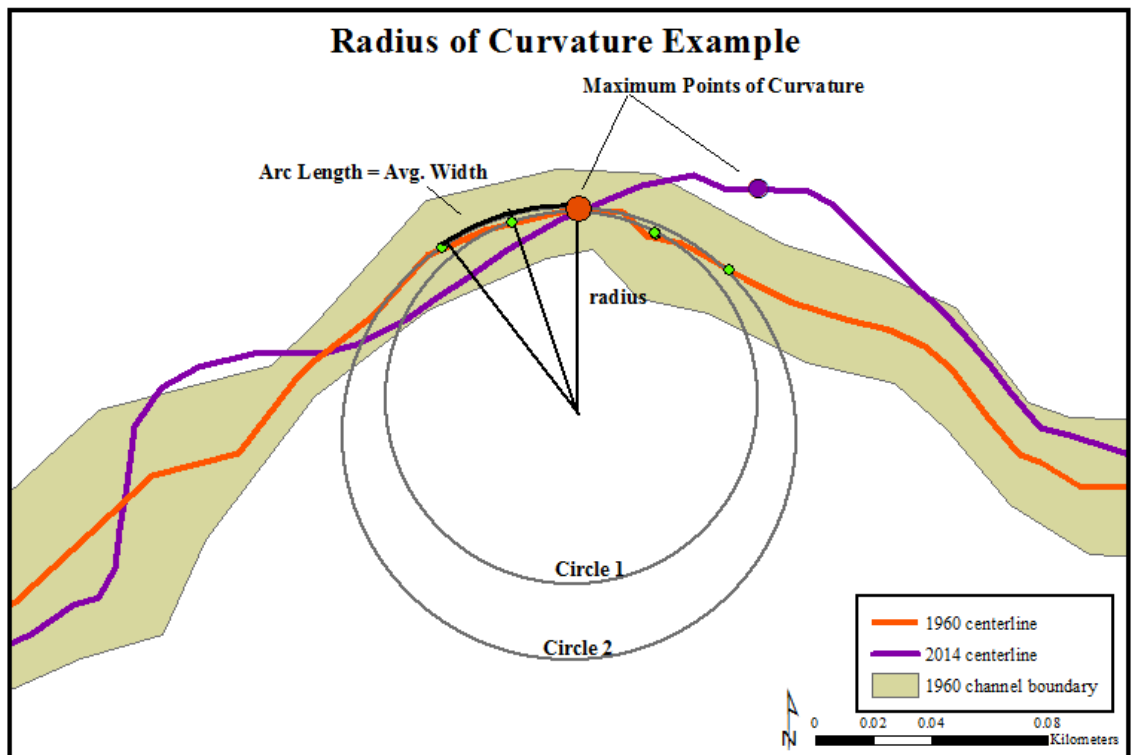


**Figure 20. An example of the determination of radius of curvature. The figure was constructed from the 1960 channel boundary of the Guadalupe River.**

#### 4.2.2 Slope and Sinuosity

For meanders that we measure the radius of curvature, local slope was established for each bend using a 2014 10 m digital elevation model (DEM). As much of the Gulf Coastal Plain and adjacent areas have been stable during the Holocene, slope was assumed temporally constant. Points of measurement were established at 1 km intervals for the study area. Slope was determined using the elevational difference between points that were 2 km apart to encompass the entire bend.

Local sinuosity was also measured using the same points defined above for consistency. The sinuosity of each 2 km length was determined using the following equation:

$$S_R = \frac{C_L}{V_L} \quad \text{Eq. (4)}$$

where,  $S_R$  is the sinuosity of the 2 km length,  $C_L$  is the length of the channel, and  $V_L$  is the length of the valley.

#### **4.2.3 Vegetation Cover**

Vegetation cover was one of the channel planform variables measured for each reach. The presence or absence of vegetation was determined from 2014 imagery for each bend on both the inside and outside boundaries. A 500 m buffer was used on both banks to ensure the entire floodplain was captured. The buffer was also used for land use/land cover categories. Land cover was mapped on both sides of the channel for each bend as forest (tree vegetation), barren (scrub, grasslands, cropland, road), or wetlands.

#### **4.2.4 Soil Composition**

The material make-up of the banks and deposits of the Guadalupe River are an important factor of stability. Soil composition of inside and outside channel banks was mapped using from the Natural Resources Conservation Service (NRCS) shapefiles of county soil surveys. A shapefile and associated database were used in a GIS to map bank composition. We assumed that vertical composition of cut banks along the outside bend are homogenous. A 500 m buffer was also used to map dominant soil type, silt-clay percentage, and soil hydrologic unit.

#### **4.2.5 Discharge – USGS Gauging Stations**

To establish mechanisms of lateral migration, the dynamics of discharge were assessed for the study area also. United States Geological Survey (USGS) gauging stations provide consecutive and continuous measurements of discharge at four sites within the study area. The locations of the four gauging stations within the study area are shown in Figure 21, and the variability of each station's period of record is presented in downstream order in Table 7.

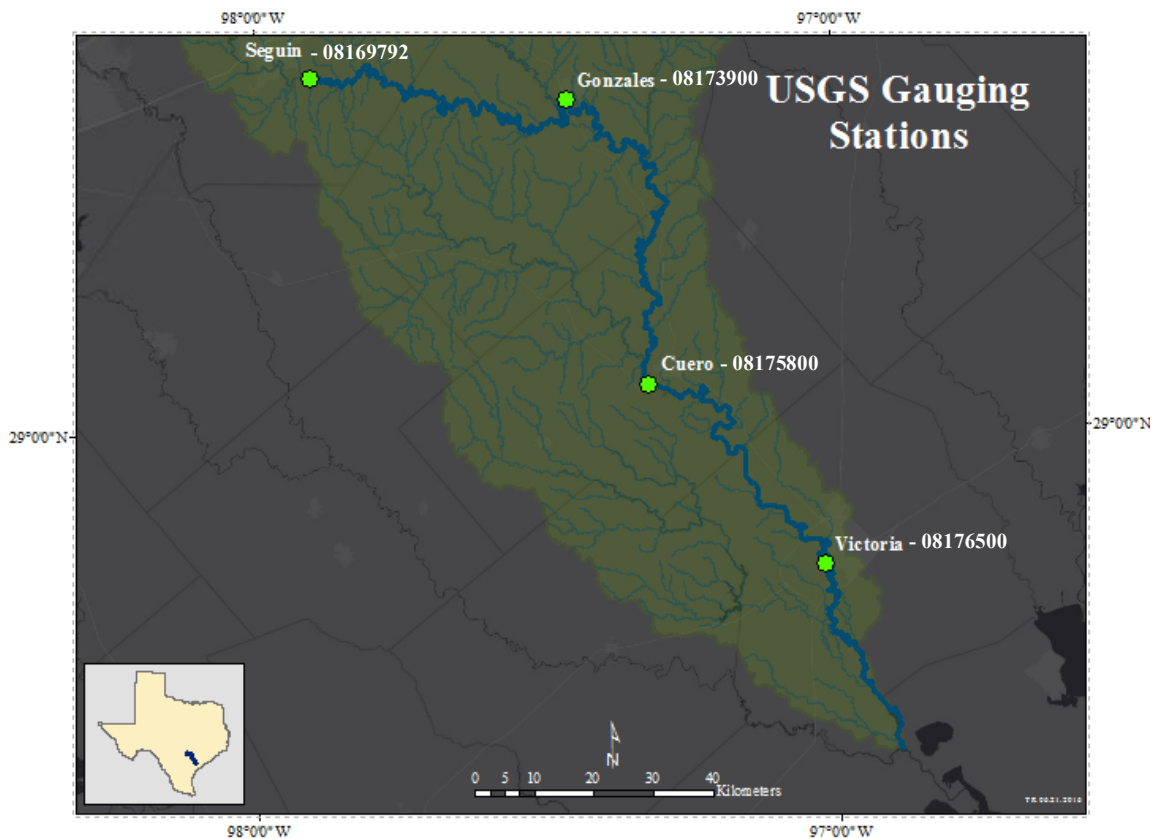


**Figure 21. USGS gauging station locations within the lower Guadalupe River study area.**

**Table 7. USGS gauging stations and period of record.**

<b>Guadalupe River near</b>	<b>Gauge ID</b>	<b>Gauge Discharge Record Start</b>	<b>Drainage Area (km<sup>2</sup>)</b>	<b>Distance from Gulf (km)</b>
<b>Seguin</b>	08169792	3/15/2005	5069	399
<b>Gonzales</b>	08173900	10/12/1996	5617	282
<b>Cuero</b>	08175800	1/1/1964	7941	165
<b>Victoria</b>	08176500	11/4/1934	13463	68

A single gauging station near Victoria, TX, was chosen for detailed analysis based on its geographic location at the southern end of the study area and the sufficient distance from tidal influence of the Gulf of Mexico. The station also has the longest period of record of 81 years. Average monthly and annual discharges were calculated and used in the analysis for each of the study periods.

Gauging stations also provide a means to obtain a rough estimate of stream power using Eq. (1). Each station was analyzed to find a five consecutive-day time period with minimal variability of discharge between both stations. Stage height, at the established time period, was added to the surveyed elevations of the gauges. To obtain a value for slope of the water surface, the following equation was used:

$$S_W = \frac{((E_U + H_S) - (E_D + H_S))}{C_L} \quad \text{Eq. (5)}$$

where,  $S_W$  is slope of the water surface,  $E_U$  is the elevation of the upstream gauge,  $E_D$  is the elevation of the downstream gauge,  $H_S$  is the stage height at a particular gauging station, and  $C_L$  is the length of the channel between two gauging stations. We make the assumption that slope is constant between gauging stations.

To determine average stream power for the reach, average daily discharge was calculated for each station. Bankfull stream power was also calculated using the stage and associated discharge when the river reaches bankfull, or minor flood stage as defined by the USGS and National Weather Service (NWS). Initial reaches used to calculate stream power are defined by gauging-station location and not the geomorphic boundary reach to produce a more accurate value. Reaches were analyzed separately using the slope determined from the 10 m DEM and average discharge of the nearest gauging station.

### 4.3 Statistical Analysis

Once all variables are collected, analysis of variance (ANOVA) tests were used to identify statistically possible mechanisms of lateral migration. All statistical analyses were performed with JMP<sup>®</sup> software. The dependent variable, total migration, was analyzed against collected independent variables for the entire study area and reaches of the Guadalupe River. For this analysis, it is assumed that all variables are independent of each other. Resulting F-statistic and p-values, indicating level of confidence, guided the analysis toward controlling variables.

## 5. RESULTS

### 5.1 Lateral Channel Migration – 380 km Reach

An overview of each time period for the entire study reach is shown in Table 8. The table shows the five time periods as well as the total time period.

**Table 8. Study time periods for entire study area with associated migration polygons and average rates of migration.**

<b>Study Years (Span)</b>	<b>Number of Polygons</b>	<b>Minimum Migration (m)</b>	<b>Maximum Migration (m)</b>	<b>Average Total Migration (m)</b>	<b>Average Rate of Migration (m/yr)</b>
<b>1960-1995 (35)</b>	651	6.00	87.11	15.1	0.43
<b>1995-2004 (9)</b>	411	6.00	201.83	10.27	1.14
<b>2004-2010 (6)</b>	247	6.00	133.74	10.58	1.06
<b>2010-2014 (4)</b>	251	6.00	178.79	9.86	2.47
<b>1960-2014 (54)</b>	745	6.00	221.47	19.5	0.36

Although each time period has a different time span, rates of migration were normalized using Eq. (3). This allows rates of migration to be compared with each other in each study period without bias.

Avulsions have the potential to skew the data toward larger rates of migration; thus, it was important to identify avulsions and account for them in the analysis. Results in Table 8 include avulsions. To further remove bias, the inclusion of avulsions, or meander cut-offs, in the analysis was investigated by analyzing rates of migration with and without avulsions. The number of avulsions in each time period, and the associated difference in migration and rate of migration with and without avulsions is shown in Table 9.

**Table 9. Avulsion occurrence and affected total and rates of lateral migration.**

Study Period	Number of avulsions	Average Rate of migration w/o avulsions (m/yr)	Average Rate of migration with avulsions (m/yr)	Average Total migration w/o avulsions (m)	Average Total migration with avulsions (m)
1960-1995	1	0.43	0.43	14.93	15.10
1995-2004	4	1.01	1.14	9.13	10.27
2004-2010	2	0.95	1.06	9.47	10.58
2010-2014	0	2.30	2.47	9.19	9.86
1960-2014	7	0.34	0.36	18.15	19.50

Comparison of total migration and rates of migration with and without avulsions as shown in the dataset, suggest minimal change. Although change is minimal, analysis proceeded without avulsions. This step provided a less skewed average when smaller reach datasets were analyzed.

Visual results of the analysis of the entire study area is shown in Figure 22 as a boxplot of lateral rates of migration for each time period. Each point represents a migration polygon with total migration of 6 m or greater. Total migration is used as a general indicator, but rates of migration are used to normalize the data and compare across study time periods as rates are per year.

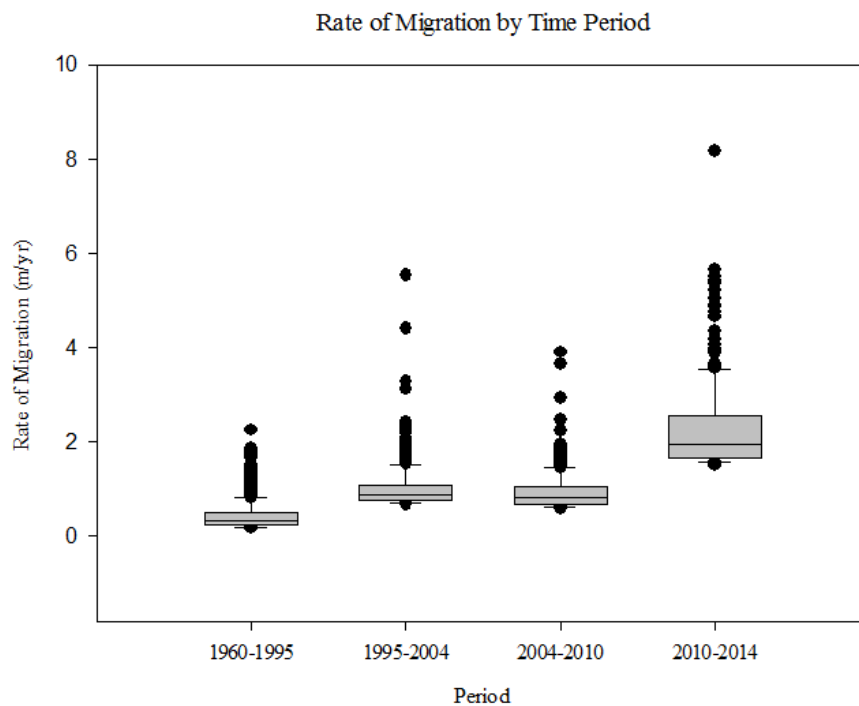


**Figure 22. Boxplots of points of lateral migration for each time period.**

Analysis of the results show that variability in rates of migration increased from 1960 to 2014. The period 2010-2014 stands out as having the highest median rate of migration, whereas is also has the highest minimum and maximum rates for all time periods.

## 5.2 Discharge and Rates of Migration

To understand the mechanisms controlling the variability of rates of migration for the study periods, discharge was related to rates of migration. Past studies have established lateral migration as a function of discharge (Gillespie and Giardino, 1997; Briaud, 2001; Hooke, 2003; Phillips, 2012). Discharge can be the main influence on lateral migration, but it is often coupled with, or driving, other processes closely related to lateral migration. Therefore, the dynamics of the river and lateral rates of migration need to be understood in the context of discharge variability.

The USGS gauge near Victoria, TX, (08176500) was used in the analysis because of its geographic location and length of record. Because of minimal variance between the gauges within the study reach, we accepted the gauge at Victoria as an appropriate analog for discharge variability along the lower Guadalupe River. The average monthly discharge for the period 1995-2015 encompasses the period of record for all gauges and is shown in Figure 23.

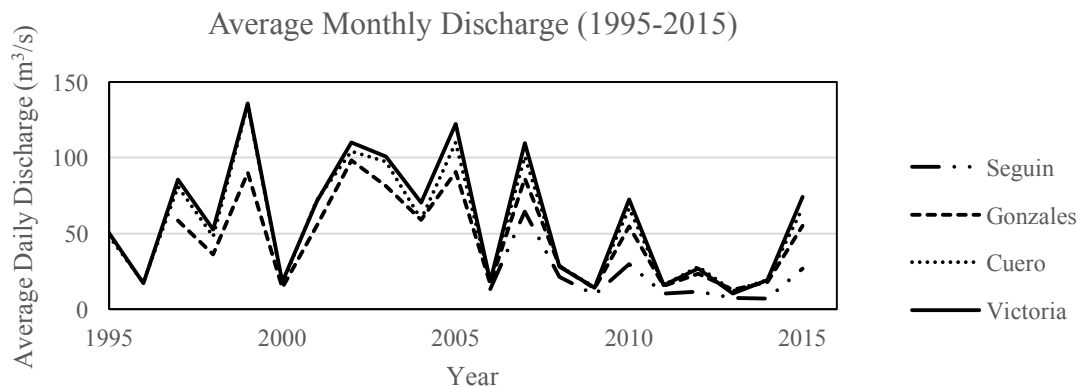
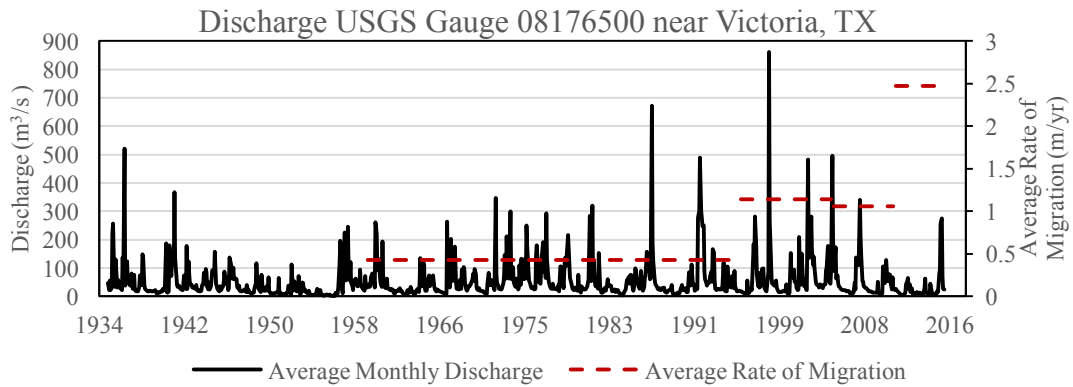


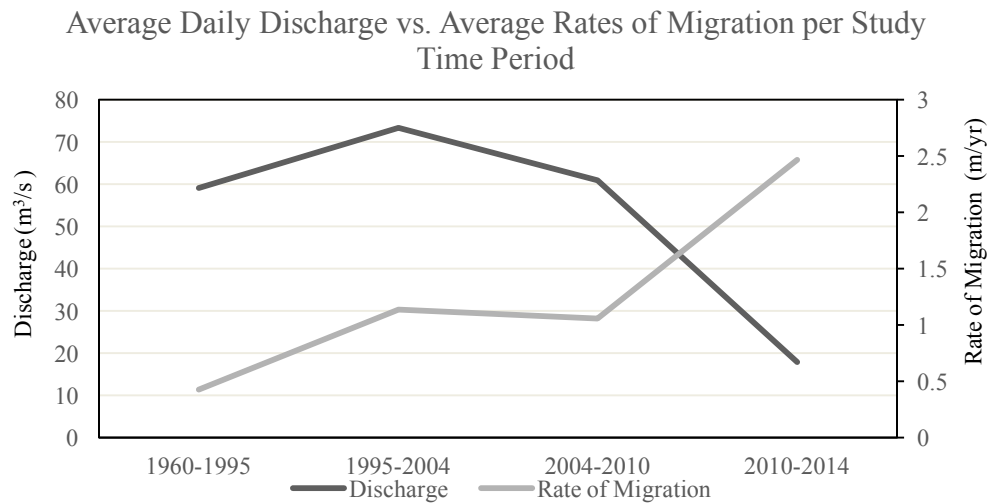
**Figure 23. Average monthly discharge for the period 1995-2015 for four gauges within the study reach. (Data obtained from [waterdata.usgs.gov](http://waterdata.usgs.gov), 2016).**

Discharge increases in the downstream direction, and no major tributary inputs occur downstream of the San Marcos River confluence in Gonzales until the San Antonio River confluence below Victoria. As a result, discharge at the Cuero gauge is aligned closely to the gauge at Victoria. Throughout the period of record for the Cuero gauge, the largest difference in monthly average discharge between the two gauges is 97.69 m<sup>3</sup>/s, which

occurred in November 2004. Discrepancies arise during precipitation events because runoff into the river is dependent on location, landcover, speed and direction of, and movement of the precipitation events. The spatial variability of precipitation events can affect discharge at one gauge and not another. Overall the variance is minimal, and thus, we used the Victoria gauge for analysis. The average monthly discharge for the period of record at the Victoria gauge (08176500) with associated average rates of migration for each study period are shown in Figure 24a. The average daily discharge and associated average rate of migration for each time period is shown in Figure 24b.



(a)



(b)

**Figure 24. (a) Average monthly discharge and average rates of migration per study time period. (b) Average daily discharge and average rates of migration per study time period. (Data obtained from [waterdata.usgs.gov](http://waterdata.usgs.gov), 2016).**

Analysis of the data suggest that the rate of migration and discharge both follow a similar trend for the first three study periods, but have opposite trends for the last period of 2010-2014. The lowest discharge has the highest average rate of migration. Observing the variability in flow regime as shown in Figure 24a suggests that no high-discharge months occurred during the time period as compared to the other time periods.

To gain a better understanding of the variance in flow regime for high-discharge months, daily average discharge was analyzed for each study period to pinpoint the times of floods. It is known that one event can significantly alter a channel, however, this does not seem to be the case for the lower Guadalupe River. The study period and associated number of events at flood stage are shown in Table 10. Moderate flood stage at the USGS gauge near Victoria (08176500) was used. Moderate flood stage is 9m and discharge is  $\sim 990 \text{ m}^3/\text{s}$  (Nws.gov, 2016).

**Table 10. Study period and associated flood stage events.**

<b>Study period</b>	<b>Number of flood-stage events</b>
<b>1960-1995</b>	10
<b>1995-2004</b>	4
<b>2004-2010</b>	1
<b>2010-2014</b>	0

Ten major floods occurred during the 1960-1995 period, and the period of 1995-2004 had floods every other year, including two record-setting events in 1998 and 2002. Rates of migration, however, are lower than the 2010-2014 period which had no major flood events. The period 2010-2014 experienced a major drought that may have impacted rates of migration for that time period.

### *5.3 Stream Power and Rates of Migration*

Flooding, high stream power, and rates of migration appear to have minimal association. Nevertheless, the relationship between stream power and rates of migration was investigated. Stream power was calculated for four reaches within the study reach as a result of gauge-station locations. Average stream power and average bankfull stream power for each reach are shown in Table 11. Bankfull stream power is based on the discharge at minor flood stage for each gauge. Values were calculated based on the assumption that slope and average discharge are constant throughout a reach and through time. Stream power is presented in watts per meter.

**Table 11. Stream power for each gauging station.  $Q_{\mu}$  = average discharge.**

<b>USGS Gauging Station</b>	<b>Study Period</b>	<b>Slope</b>	<b><math>Q_{\mu}</math> (m<sup>3</sup>/s)</b>	<b>Stream Power (<math>Q_{\mu}</math>) (W/m)</b>	<b>Bankfull Stream Power (<math>Q_{\mu}</math>) (W/m)</b>
<b>Seguin</b>	1960-1995	0.000443	-	-	-
	1995-2004		-	-	-
	2004-2010		27.96	121.53	2400.34
	2010-2014		9.13	39.71	2400.34
<b>Gonzales</b>	1960-1995	0.000297	-	-	-
	1995-2004		61.77	180.20	1163.93
	2004-2010		48.43	141.30	1163.93
	2010-2014		17.49	51.04	1163.93
<b>Cuero</b>	1960-1995	0.000344	55.92	188.62	1331.78
	1995-2004		70.03	236.23	1331.78
	2004-2010		62.94	212.33	1331.78
	2010-2014		22.29	75.18	1331.78
<b>Victoria</b>	1960-1995	0.000148	58.85	85.48	374.73
	1995-2004		73.47	106.73	374.73
	2004-2010		60.85	88.39	374.73
	2010-2014		18.18	26.40	374.73

Average stream power is compared using the data from 2004-2010. Other time periods were not used in the calculation because of a lack of continuous data for all gauging stations and the 2011-2012 drought. The reach between Cuero and Victoria had the highest value at 212.33 W/m, whereas the reach from Seguin to Gonzales had the highest average bankfull stream power value at 2400.34 W/m.

To further understand the differences in stream power, stream power was calculated using slopes established from a 10 m DEM for each of the seven reaches. The gauging station closest to the reach is used for the average daily discharge. Average stream power is compared to the longitudinal river profile in Figure 25.

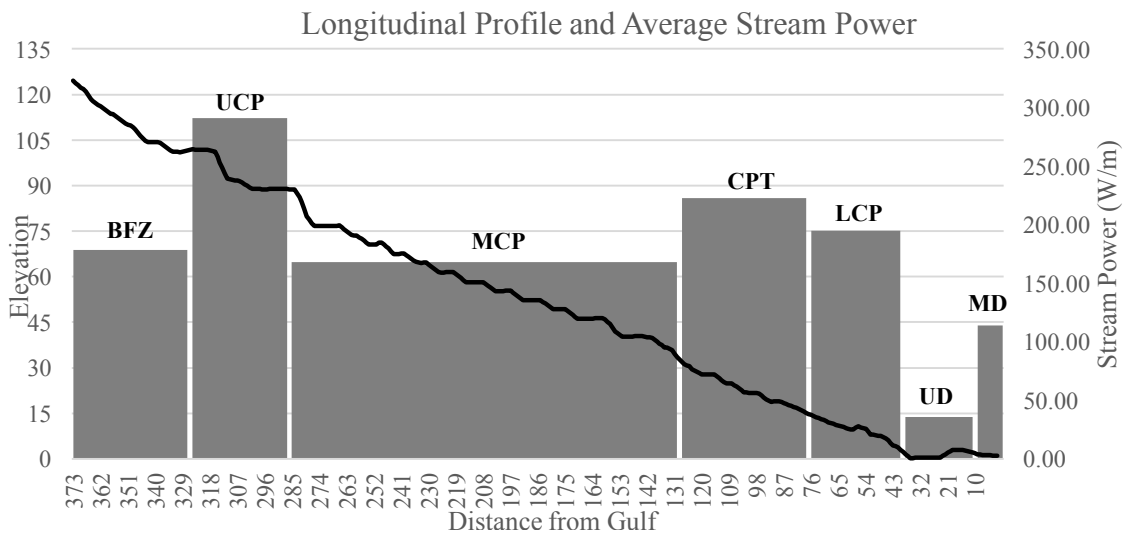


**Figure 25. Longitudinal profile of the lower Guadalupe River study reach with average stream power for each sub-reach reach.**

Figure 25 provides an excellent visual interpretation of stream power for the entire study area. Close examination of this figure provides some interpretation insights. The UCP reach has the highest average stream power at 290.67 W/m. The reach includes a knickpoint, or sudden change in slope, as a result of the dam that exaggerates values for slope and stream power. The CPT has the second highest average stream power at 222.78 W/m. The lowest average stream power of 35.7 W/m is in the UD reach where subsidence is occurring.

The question then becomes: Is there a relationship between stream power and rate of migration? The relationship between stream power and average rate of migration is shown in Table 12 for the 2004-2010 study period.

**Table 12. Average rate of migration vs. average stream power.**

Geomorphic Zone	Average Rate of Migration (2004-2010) (m/yr)	Average Stream Power (2004-2010) (W/m)
<b>Belmont Fault Zone</b>	1.05	178.31
<b>Upper Coastal Plain</b>	0.93	290.67
<b>Middle Coastal Plain</b>	0.89	167.89
<b>Coastal Plain Transition</b>	0.96	222.78
<b>Lower Coastal Plain</b>	0.96	194.84
<b>Upper Delta</b>	0.83	35.70
<b>Middle Delta</b>	0.65	113.96

No relationship is apparent between average rates of migration and average stream power for each reach. This lack of relationship may be the result of significantly generalizing the values of stream power. We suggest one reason that might account for the lack of a relationship might be related to the fact that channel roughness and width-depth ratio, as well as the influence of sediment are not considered. A more in-depth analysis of stream power for each reach is needed. This might yield a more distinct relationship between the two variables.

#### 5.4 Lateral Channel Migration for each Reach

Lateral rates of migration were analyzed at a reach scale to gain a clear understanding of lateral migration along the lower Guadalupe River, as well as to better determine the mechanisms influencing channel migration. Rates of migration were calculated for each study period within each reach. The trend of rates of migration by reach is shown in Figure 26.

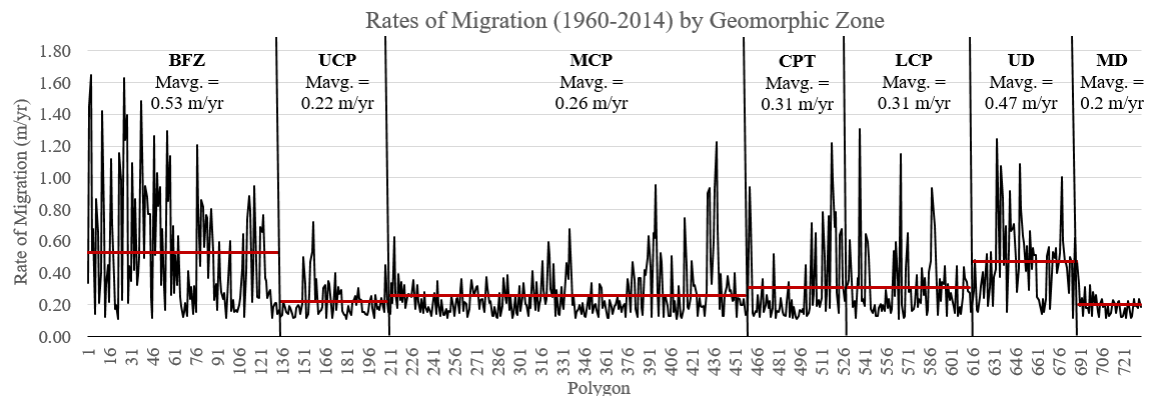


**Figure 26. Lateral rates of migration by geomorphic zone. The x-axis represents each migration polygon; 1 is the uppermost reach, whereas 721 is the downstream end. Geomorphic zone and associated average rate of migration are shown in the red line**

Reach rates of migration were also analyzed for each time period. The average rates of migration for each time period are shown in Table 13 and Figure 27.

**Table 13. Average rates of migration in meters per year by geomorphic zone for each study period.**

Study Period	Average Rates of Migration (m/yr) by Geomorphic Zone						
	BFZ	UCP	MCP	CPT	LCP	UD	MD
1960-1995	0.61	0.35	0.34	0.34	0.36	0.67	0.25
1995-2004	1.22	0.92	0.98	1.03	1	0.83	0.74
2004-2010	1.05	0.93	0.89	0.96	0.96	0.83	0.65
2010-2014	2.51	2.49	2.05	2.34	2.19	1.77	1.54
1960-2014	0.53	0.22	0.26	0.31	0.31	0.47	0.20



**Figure 27. Average rates of migration by study period for each geomorphic zone.**

Variability is seen between and within each zone for the full time period, as well as the individual study periods. To obtain a better understanding of the variability and where migration is occurring, rates of migration were classified into three groups: low, medium, and high rates. Classes were designated using a natural-breaks Jenks classification in ArcGIS®. Natural breaks were based on results of the variability within each study period

and a highly right-skewed dataset for each time period. Jenks' natural breaks partitions data by a goodness of variance of fit measure. This method has been widely used for highly skewed data (Brewer and Pickle, 2002; Baz et al., 2009; Jiang, 2013).

Areas of highest rates of migration were calculated for each time period for the entire study reach. Maximum points of migration along the 380 km reach are shown in Figure 28.

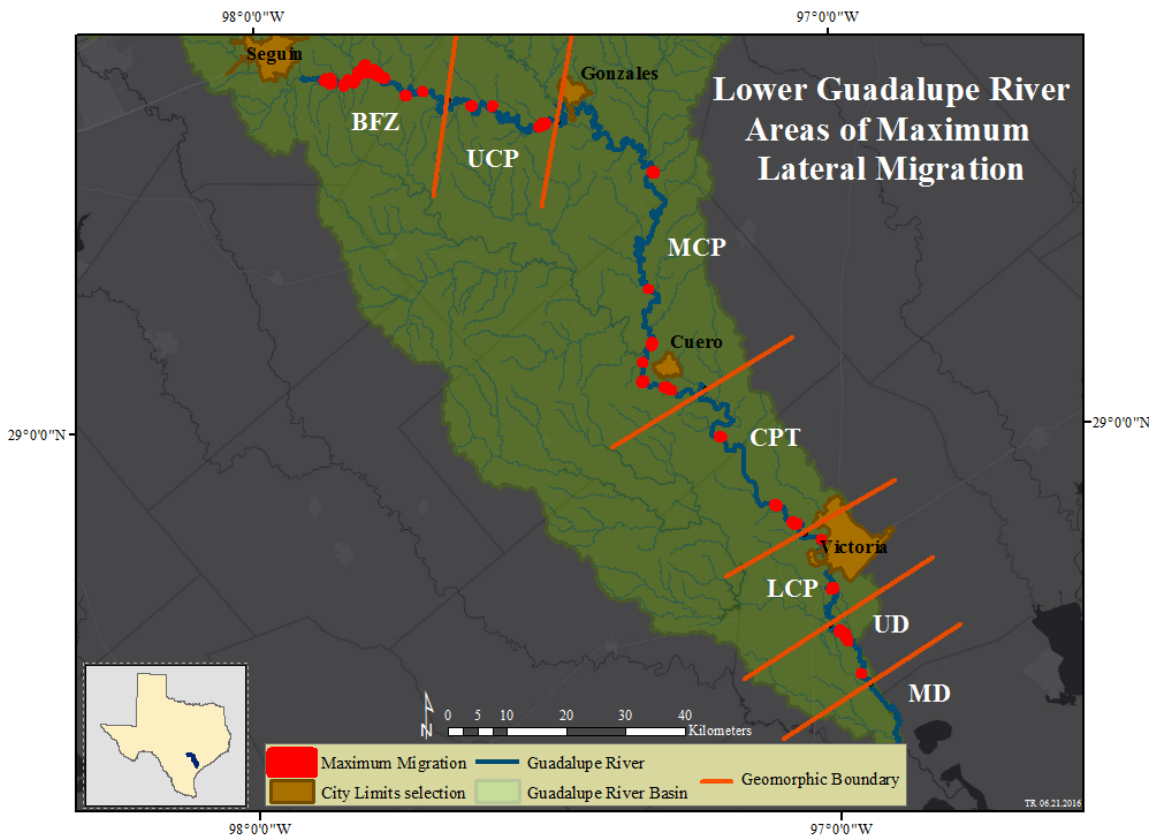


**Figure 28. Areas of maximum lateral migration, in red, for the study period.**

Each sub-reach has several areas of maximum rates of migration, except for the lowest reach. As previous figures have shown, the BFZ has the highest occurrence of maximum rates of migration. Figures 29 through 35 provide details of the rates of migration for each sub-reach. The river is overlain onto the cropped 10 m DEM to provide a visualization of the river valley and surrounding area.

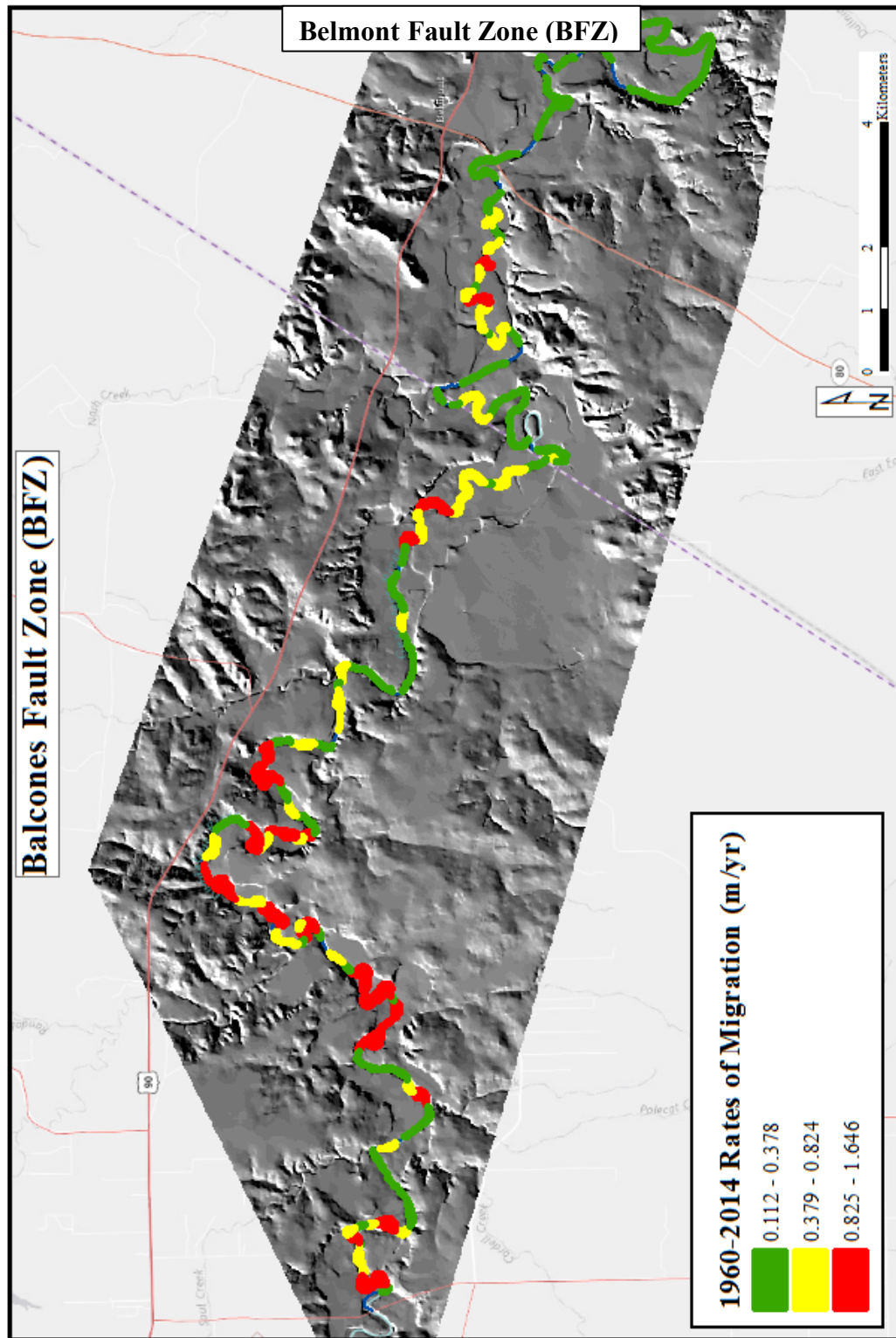


Figure 29. Rates of migration in the Belmont Fault Zone using a three-class Jenks Natural Break.

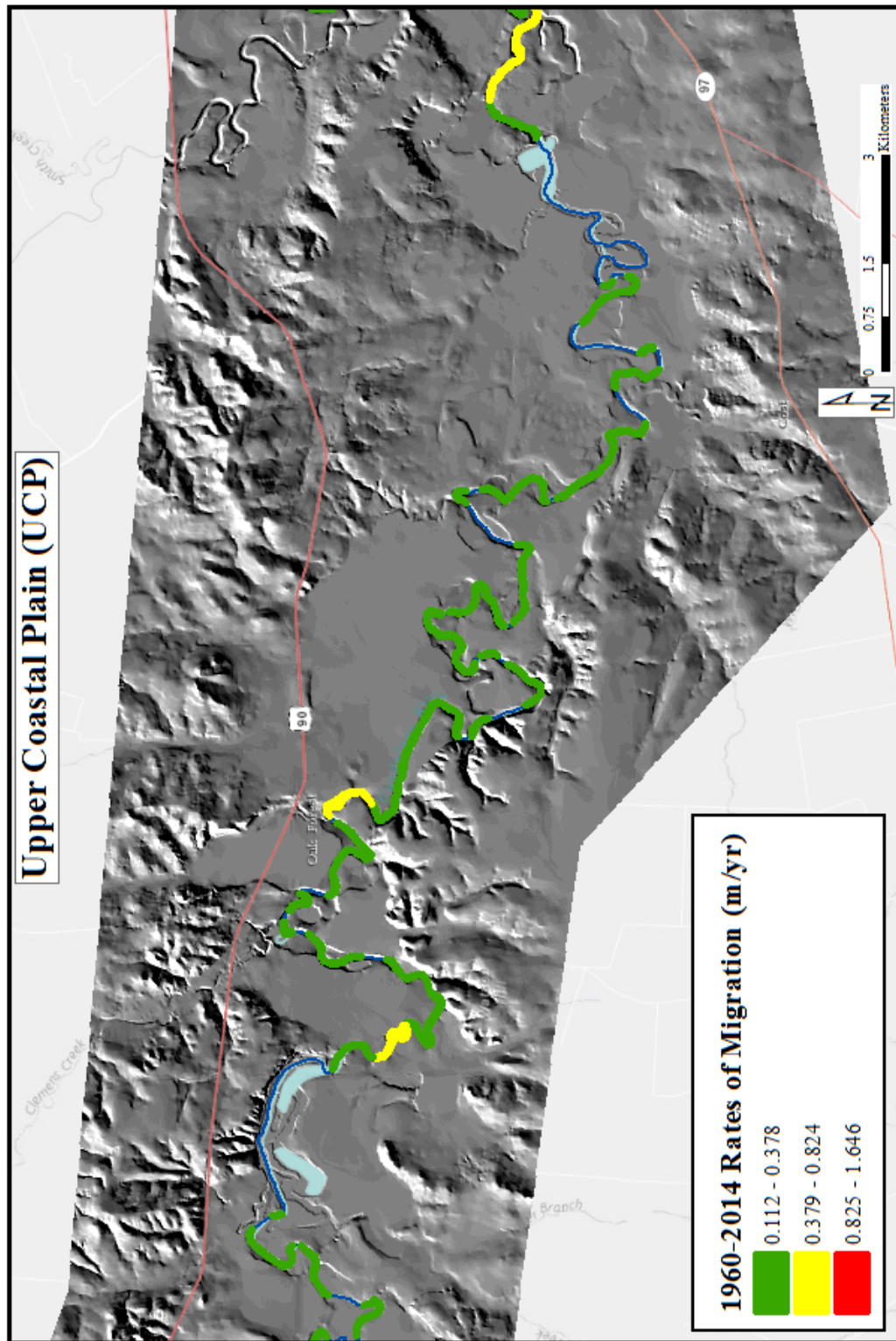
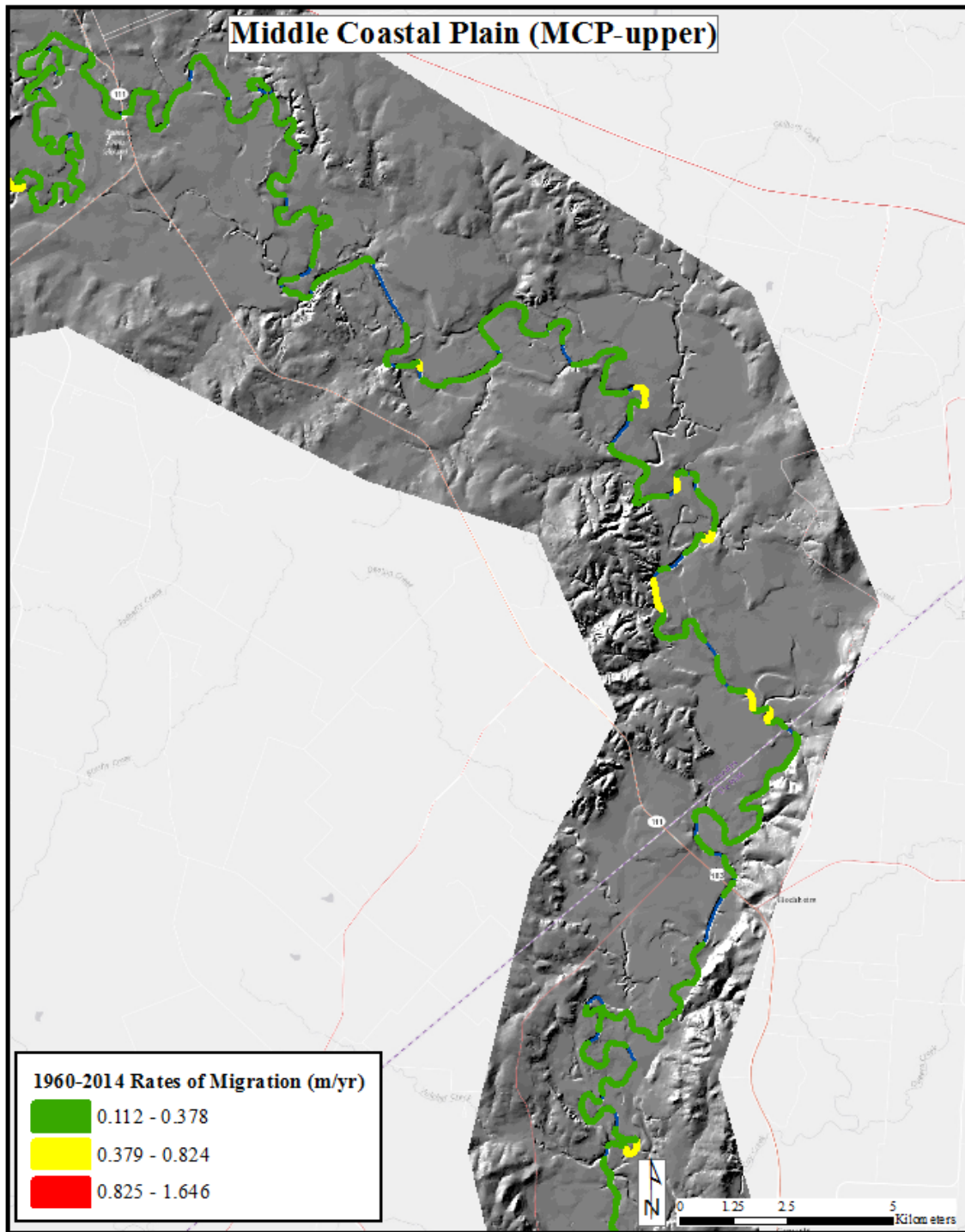
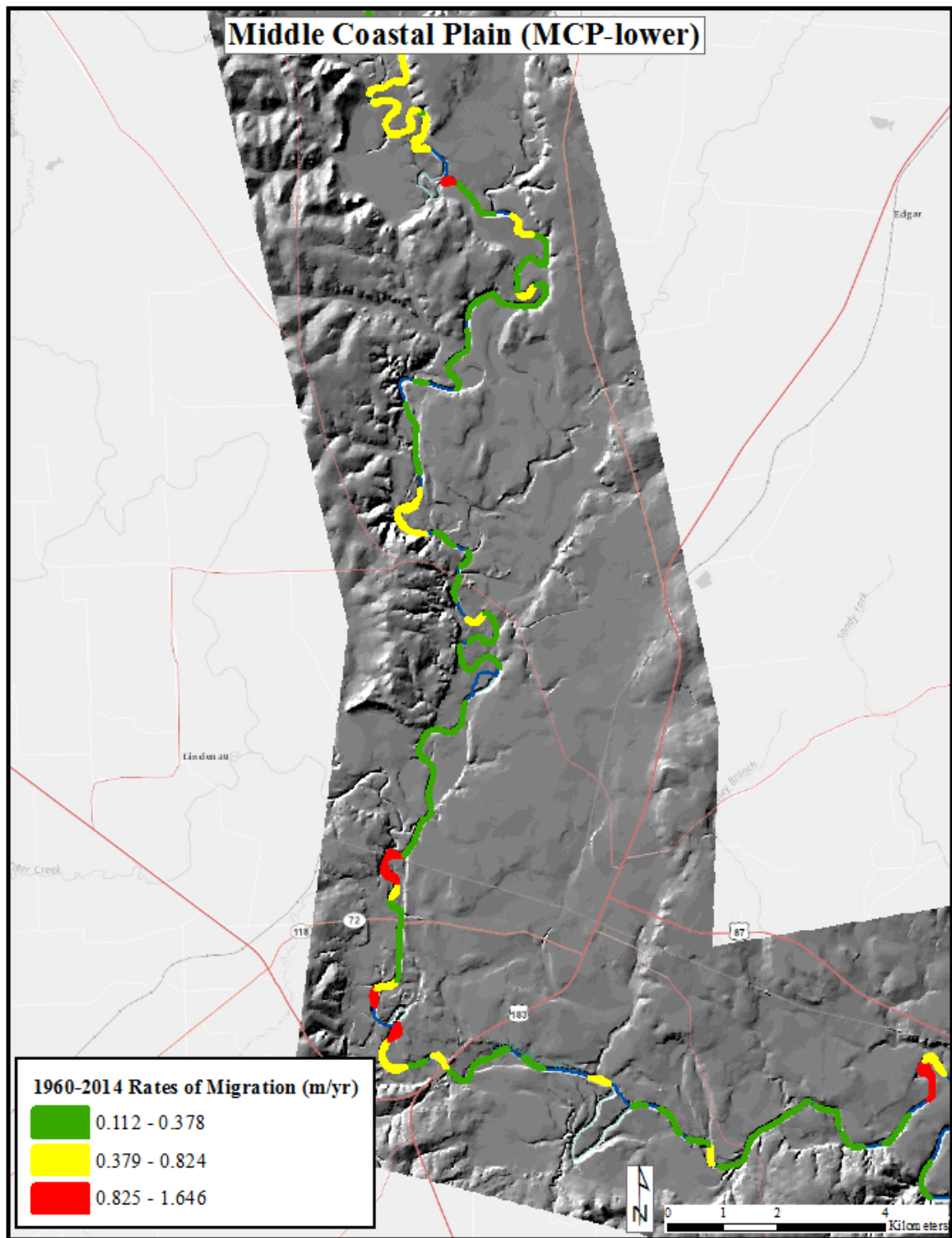


Figure 30. Rates of migration in the Upper Coastal Plain using a three-class Jenks Natural Break.



(a)

Figure 31. Rates of migration in the Middle Coastal Plain using a three-class Jenks Natural Break. The zone was divided into upper (a) and lower (b) as a result of the length.



(b)

Figure 31. Continued.

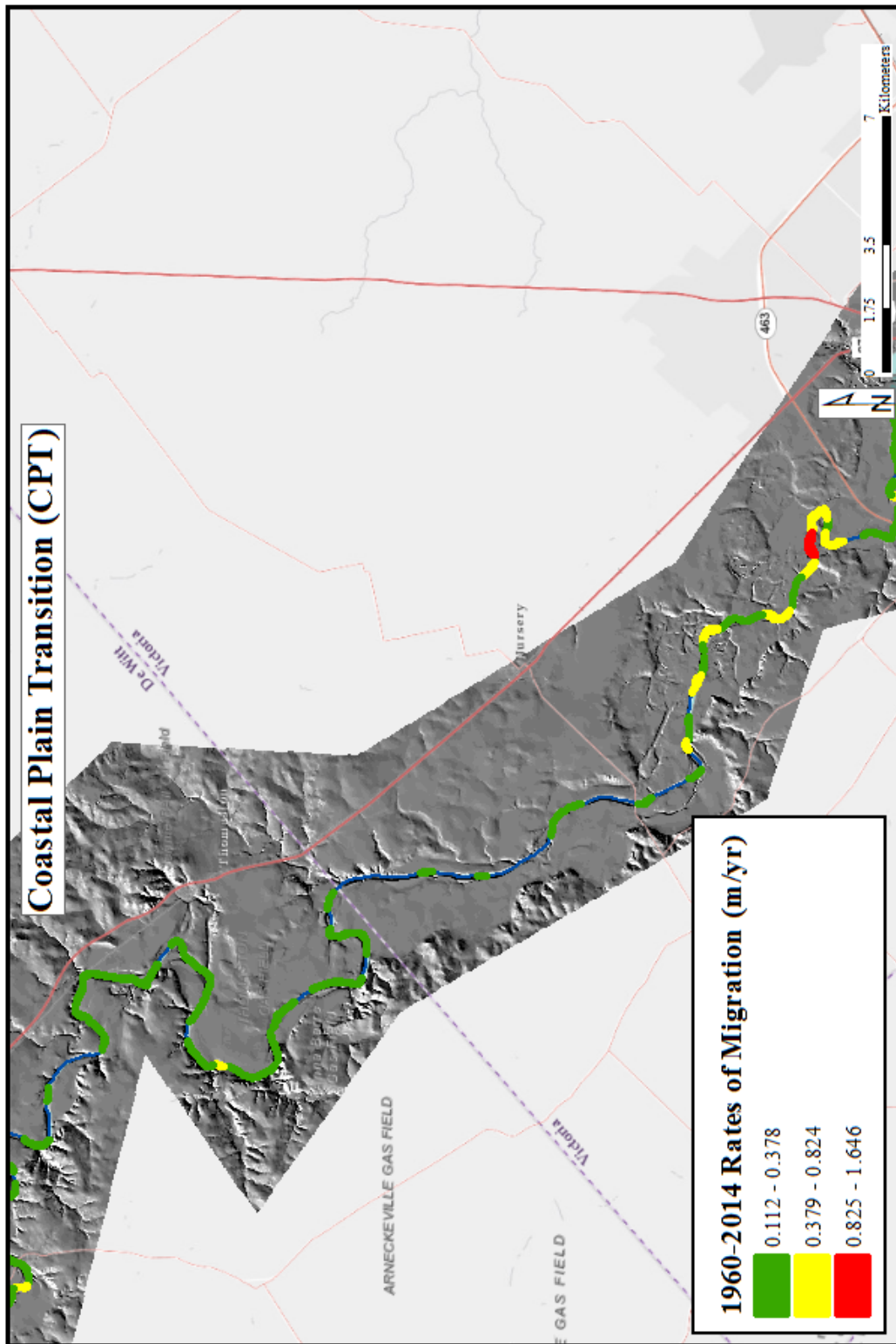


Figure 32. Rates of migration in the Coastal Plain Transition zone using a three-class Jenks Natural Break.

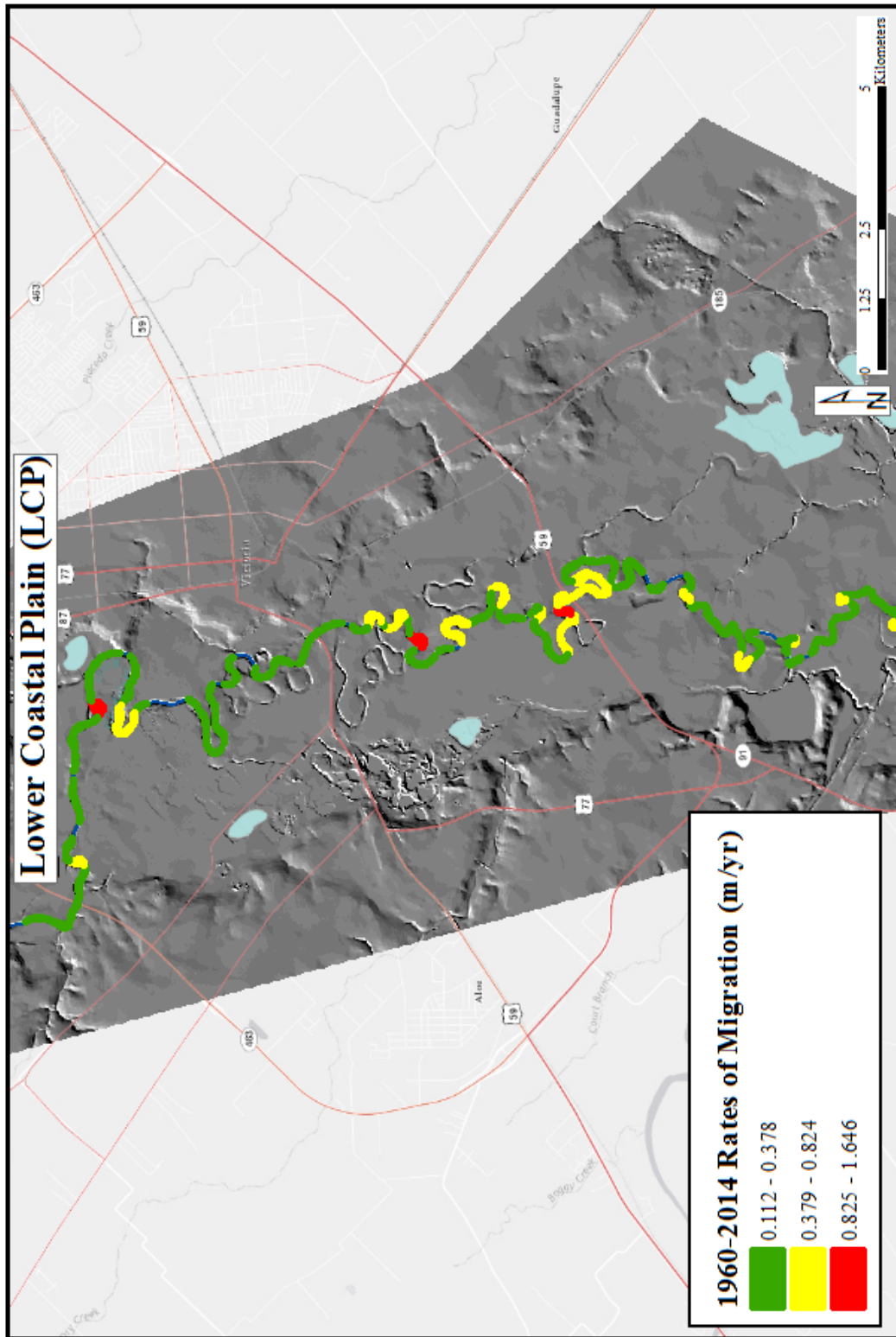


Figure 33. Rates of migration in the Lower Coastal Plain using a three-class Jenks Natural Break.

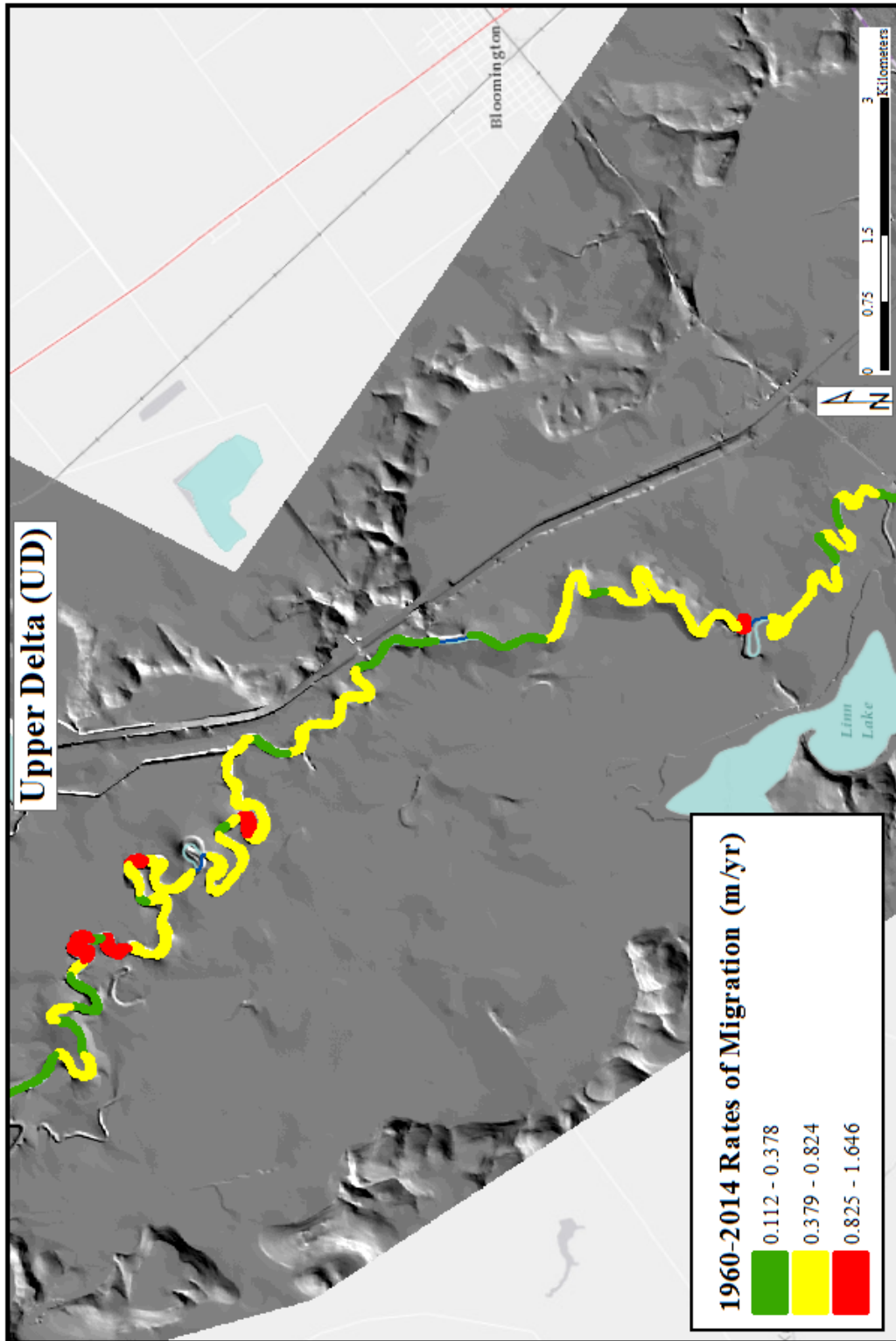


Figure 34. Rates of migration in the Upper Delta using a three-class Jenks Natural Break.

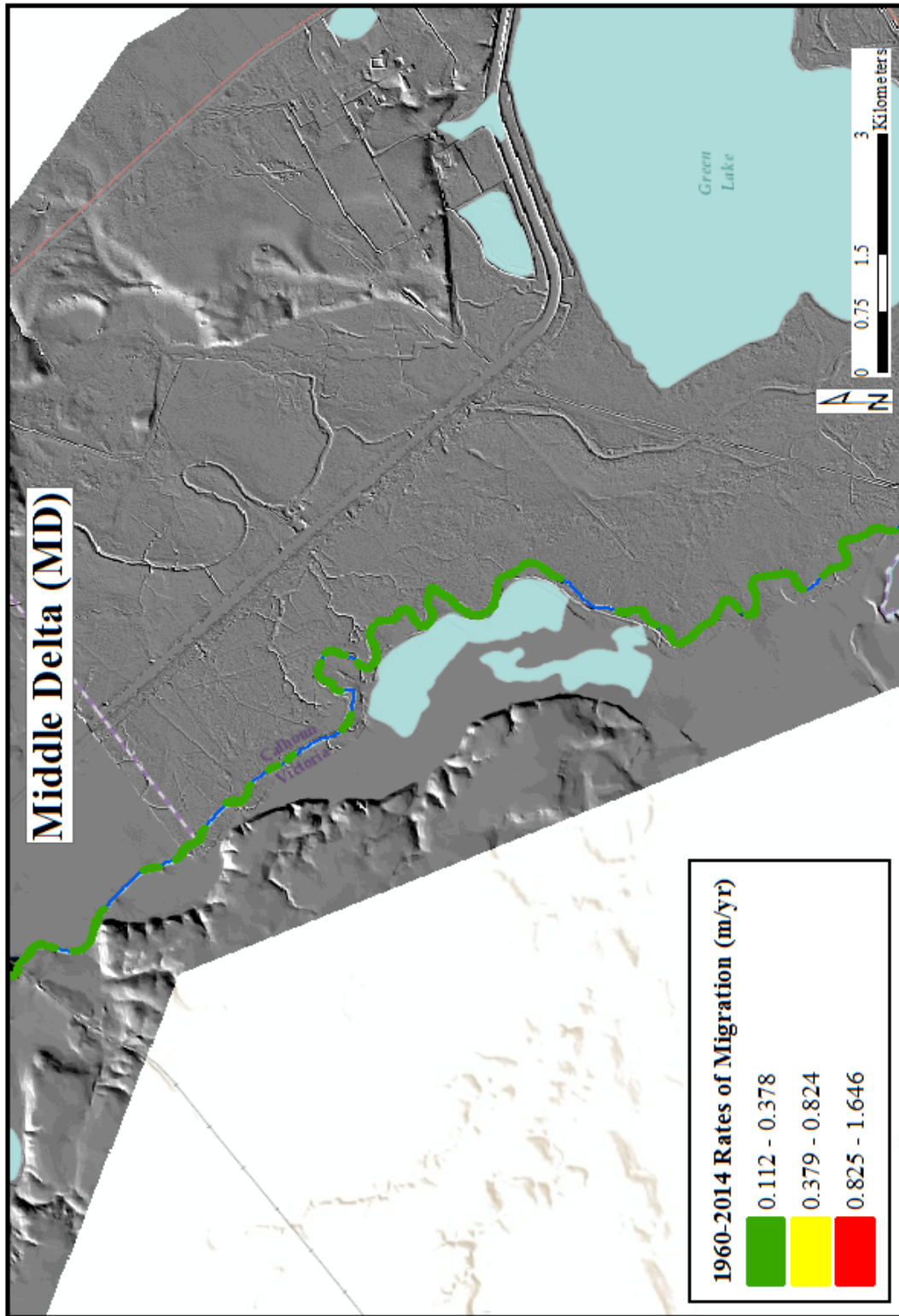
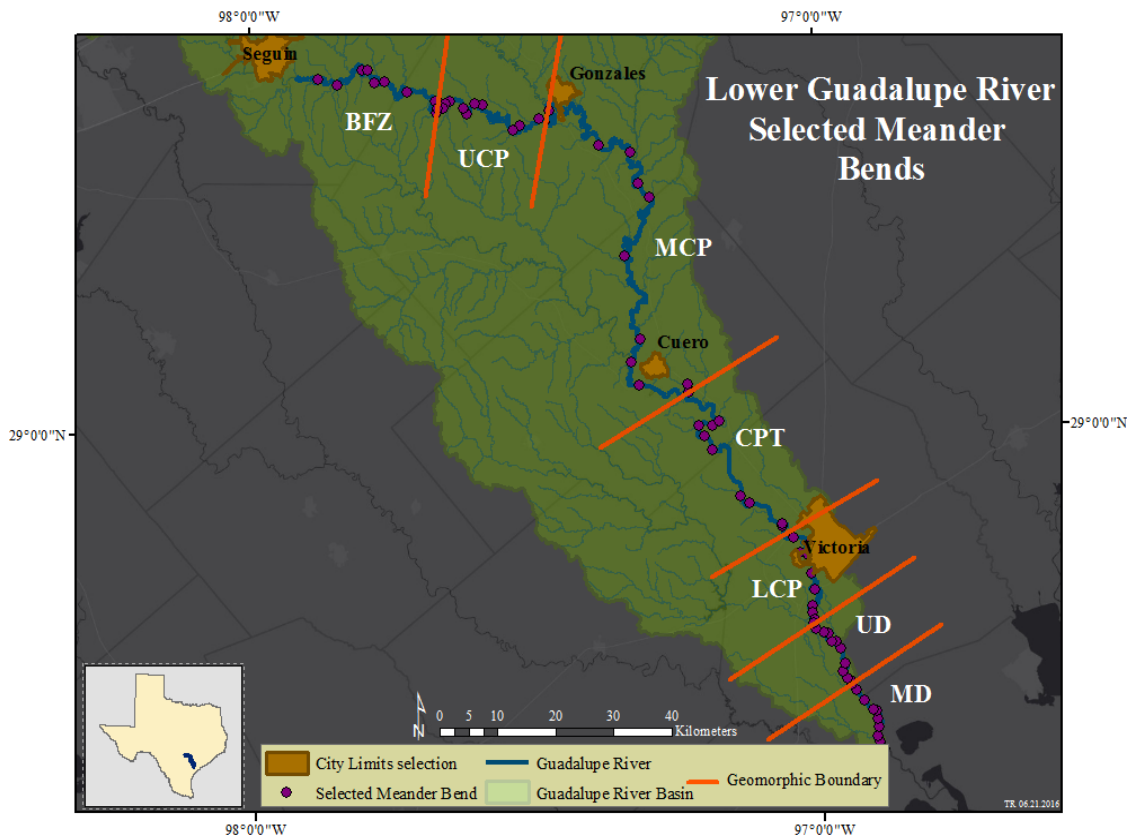


Figure 35. Rates of migration in the Lower Delta using a three-class Jenks Natural Break.

Study of areas of migration overlain on a DEM shows the valley confinement present in the BFZ. Analysis of this scene suggest confinement and channel constriction influence channel adjustment in this reach. The other reach that is significant is the UD where the valley is wide, but the channel has several areas of maximum migration. A zone of subsidence drives channel adjustment in this area and is discussed in detail in the discussion.

### 5.5 ANOVA Statistical Analysis

To gain a better understanding of possible mechanisms of lateral migration, ten meander bends were designated per reach at random. A GIS was used to aid in further analysis of place. The reference line for random-point generation was the 2014 channel line. The channel line was chosen rather than migration polygons to eliminate bias of analyzing only meanders that have experienced lateral migration. The locations of random meander bend points within each sub-reach are shown in Figure 36.



**Figure 36. A map including ten random meander bends per sub-reach used for further analysis.**

Each meander bend was analyzed for various parameters. The parameters were: the ratio of radius of curvature to width, type of meander bend, vegetation presence, and soil composition. An analysis of the relationship between rate of migration and characteristics of the meander bend are shown in Table 14.

**Table 14. ANOVA comparison of total migration as a function of meander bend characteristics. Rc/W values are averaged for 1960 and 2014, respectively.**

<u>Variable</u>	<u>Rc/W</u>	<u>n</u>	<u>Mean</u>	<u>F-Statistic</u>	<u>P-Value</u>	
<u>Rate of Migration (m/yr)</u>	<2	31	0.502	3.8112	0.0271	
	2-3	16	0.319			
	>3	23	0.29			
<u>Rate of Migration (m/yr)</u>	<u>Bend Type</u>			3.1998	0.0781	
	Simple	34	0.32			
<u>Rate of Migration (m/yr)</u>	Compound		36	0.46		
	<u>Rate of Migration (m/yr)</u>	<u>Outside Bank (OB) Vegetation</u>			8.6219	0.0045
Yes		58	0.343			
No		12	0.621			
<u>Rate of Migration (m/yr)</u>	<u>(OB) Silt-Clay Content (%)</u>			4.857	0.0107	
	33-50%	5	0.168			
	51-70%	11	0.62			
<u>Rate of Migration (m/yr)</u>	71-93%		45	0.364		
	<u>Rate of Migration (m/yr)</u>	<u>(OB) Silt Content (%)</u>			4.7698	0.0116
		15-35%	25	0.304		
35-50%		13	0.614			
<u>Rate of Migration (m/yr)</u>	50-70%		32	0.367		
	<u>Rate of Migration (m/yr)</u>	<u>(OB) Clay Content (%)</u>			2.4332	0.0727
		15-25%	11	0.532		
25-35%		37	0.366			
35-50%		13	0.246			
<u>Rate of Migration (m/yr)</u>	50-70%		9	0.527		

### **5.5.1 Vegetation**

ANOVA analysis of vegetation cover shows the presence of vegetation on the outside bank has the highest p-value, or confidence level. It is known that lateral migration often occurs by eroding the outside bank, so characteristics of the outside bend were analyzed. Vegetation was defined as any vegetation taller than a short grass that would be found in a grazing or crop field. From our analysis, we can say that when vegetation is present, rates of migration are lower because the associated root system provides stability along an outside bank. Different species of vegetation provide more or less stability depending on size, canopy cover, and the root system. Our analysis only took into account presence or absence. We did not consider species type.

### **5.5.2 Bank Composition**

The composition of the soil of the outside banks was measured as a percentage of silt-clay in the soil. The soil composition-migration relationship has the second most significant relationship of all the characteristics. The percentages were grouped into three classes. We found that a 51-70% silt-clay composition has the highest rates of migration. Clays are cohesive and can resist high shear stresses because of inherent geotechnical properties. Silts are cohesive as well, but to a lesser degree than clay. The remaining percentage bank composition was classified as sand, which is non-cohesive. We made the assumption that sand plays a minimal role in bank stability for the chosen meanders, thus, only silt and clay were analyzed.

To determine which fraction, silt or clay, has a greater influence, the two fractions were analyzed separately. A 35-50% silt composition is associated with higher rates of migration, whereas 15-25% and 50-75% clay compositions are associated with higher rates of migration. Separately analyzing the two fractions confirms that the presence of both fractions strengthens a bank. None of the banks we mapped in the study area had a homogenous silt or clay content, so the relationship of silt or clay alone to lateral rates of migration is unknown. This is a question that needs to be studied in the future.

### **5.5.3 Type of Bend and Radius of Curvature**

The results from the ANOVA analysis suggest that radius and curvature and type of bend have significant relationships with lateral rates of migration. Simple and compound types of bends have significantly different mean rates of migration (Table 14). Compound bends have higher rates of migration, which might be related to dynamic shear stresses because flows do not follow a typical sinuous curve. Compound versus simple bends are related to the size and tightness of the bend, so type of bend and  $R_c/W$  measurements were compared in Table 15.

**Table 15. ANOVA of average Rc/W values versus type of bend. The Rc/W values below are averaged for 1960 and 2014, respectively.**

	Type of Bend	n	Mean	F-Statistic	P-Value
Average Rc/W	Simple	34	2.31	0.2870	0.5939
	Compound	36	2.45		

The results from the ANOVA analysis show no significant difference in the means of Rc/W when grouped by simple versus compound bends. The average Rc/W value is 2.38, which is in the generally accepted range for maximum migration (Hickin and Nanson, 1984). However, maximum migration occurs closer to 2 for the lower Guadalupe River.

Rc/W is grouped according to the findings of Hickin and Nanson (1984) where a ratio of 2-3 has the highest rates of migration. The results suggest that a ratio closer to two has higher rates of migration. The relationship between Rc/W and rate of migration data from Nanson and Hickin (1986) to the lower Guadalupe River data are shown in Figure 37.

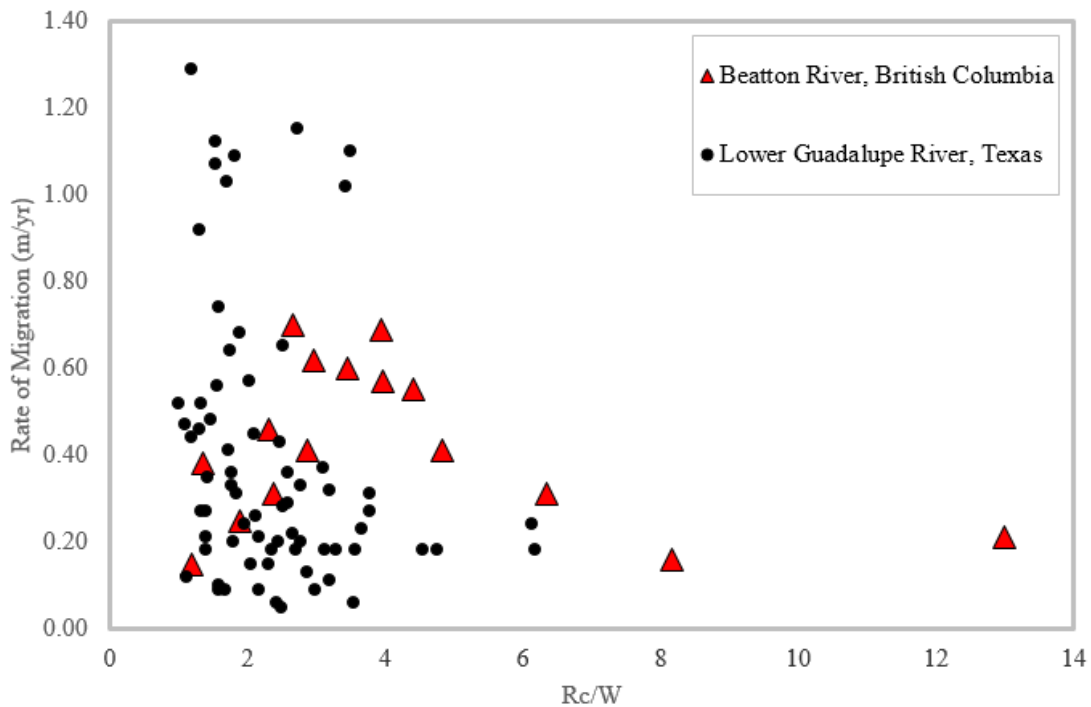


**Figure 37. Ratio of radius of curvature and width to rate of migration for the Beatton River, Canada, from Nanson and Hickin (1983), and the lower Guadalupe River.**

Although the maximum rates of migration occur at values closer to two for the lower Guadalupe River, the scatterplot plots within the same ranges as data on the Beaton River. Our data have several values for lower rates of migration, where Nanson and Hickin do not. This difference can be attributed to different sample sizes, as well as different river systems.

### 5.6 ANOVA for Reaches

An ANOVA analysis was run to determine differences in geomorphic variable per each reach. The ANOVA analysis supports that a significant difference in rates of migration exist between reaches. The results of the ANOVA analysis are shown in Table 16

**Table 16. ANOVA comparison of bend morphology as a function of Geomorphic Zone. Average values for 1960 and 2014 for 70 random meander bends.**

<u>Variable</u>	<u>Reach</u>	<u>n</u>	<u>Mean</u>	<u>F-Statistic</u>	<u>P-Value</u>
<u>Rate of Migration (m/yr)</u>	BFZ	10	0.596	4.4151	0.0009
	UCP	10	0.221		
	MCP	10	0.391		
	CPT	10	0.324		
	LCP	10	0.382		
	UD	10	0.661		
	MD	10	0.16		
<u>Average Rc/W</u>	BFZ	10	2.42	2.285	0.0465
	UCP	10	2.04		
	MCP	10	2.36		
	CPT	10	2.62		
	LCP	10	2.6		
	UD	10	1.54		
	MD	10	3.09		

---

**Table 16. Continued.**

<u>Variable</u>	<u>Reach</u>	<u>n</u>	<u>Mean</u>	<u>F-Statistic</u>	<u>P-Value</u>
<u>Sinuosity</u>	BFZ	10	1.507	0.8624	0.528
	UCP	10	1.508		
	MCP	10	1.369		
	CPT	10	1.199		
	LCP	10	1.339		
	UD	10	1.368		
	MD	10	1.234		
<u>Slope (m/m)</u>	BFZ	10	0.097	0.942	0.4714
	UCP	10	0.98		
	MCP	10	0.057		
	CPT	10	0.153		
	LCP	10	0.482		
	UD	10	0.021		
	MD	10	0.017		
<u>Average channel width (m)</u>	BFZ	10	36.02	5.098	0.0003
	UCP	10	45.15		
	MCP	10	45.19		
	CPT	10	53.68		
	LCP	10	41.83		
	UD	10	41.9		
	MD	10	36.89		

Two important findings can be stated: average Rc/W and average channel width are significantly different between sub-reaches, whereas sinuosity and slope are not. Because significant differences occur in rates of migration between reaches, we feel confident in stating that sinuosity and slope, alone, are not mechanisms related to rates of migration, whereas Rc/W and average channel width are.

## 6. DISCUSSION

This discussion section is organized to provide a discussion of the various factors that came into play during the study period. These factors include drought, which resulted in change in cohesion of bank materials, and the influence of dams in the study area. In addition, the various measures and resulting data and conclusion are also discussed.

### *6.1 Lateral Rates of Migration*

#### **6.1.1 Impact of Drought and Changes in Material Cohesion**

Discharge and rates of migration throughout the study period have a relationship, which trend in a similar direction. It is important to note that the study period 2010-2014 had a very low average discharge and the highest rates of migration for the study periods. A major drought occurred across Texas during 2011 and 2012. Reduced rates of precipitation result in water scarcity and reduced discharges in rivers. All this results in lower flows in rivers across the affected area. Lower flows result in lower river stages, and a lower stage results in banks that are normally wet or submerged are now dry.

Water, at a specific velocity, helps stabilize a river bank by ensuring increased pore-water pressure in the bank soils. A drought can cause banks that had increased pore-water pressures to rely solely on cohesion. One must appreciate the fact that although cohesive, slip faces increase as fractures occur from a lack of water to bind the cohesive materials. Thus, increased fractures result in bank instability. When unstable, failure of river banks can occur in the form of slumping as seen in Figure 38 (a) and (b). This failure can result in increased sediment transport in the river and result in both accelerated bank erosion as well as downstream deposition.



(a)



(b)

**Figure 38. (a, b) Slumping along an outside bank on the Guadalupe River near Cuero, TX. (December 5, 2015).**

Undercutting of banks is another type of bank failure that can occur resulting from drought-related reduced discharge. A cut-bank typically has high angle slopes exposed, and a submerged toe slump that is a result of previous erosion. As river levels drop, the river will begin to erode the toe slump, destabilizing the lower part of the cut-bank, which eventually results in collapses. Collapsing banks can produce exaggerated rates of migration because the process is immediate rather than a gradual erosion of the bank over the course of several years. An example of undercut banks near Cuero, TX, is shown in Figure 39.



**Figure 39. An example of collapsing banks as a result of undercutting. Photograph taken near Cuero, TX. (December 5, 2015).**

### **6.1.2 Upper Delta and Middle Delta**

To identify other mechanisms controlling lateral migration, we examined adjacent reaches; the Upper Delta and Middle Delta. The Upper Delta has the second highest rates of migration, and the Middle Delta has the lowest rates of migration. The low rate of migration in the Middle Delta reach is the result of the relatively close proximity to the Gulf of Mexico, which serves as the base-level. Low rates of migration occur in the Middle Delta are the result of tidal fluctuation influences on the river. Because tides limit downstream flow, they can cause flow reversal that results in standing water. Standing water lacks energy to promote lateral migration; thus, aggradation dominates and rates of migration are significantly lower in this area. The rise of sea level also causes aggradation

into the delta, inhibiting incision of the river (Donaldson et al., 1970 ; Blum and Aslan, 2006).

The relationship between the river and the Gulf is not the only explanation of rates of migration in these reaches. Another reason for the contrast in rates of migration between the two reaches is a result of a zone of subsidence. Ouchi (1985) investigated the influence of the Post-Vicksburg flexure zone located near the confluence of Coletto Creek, 32 km above the mouth of the river in the Upper Delta reach. He found a steepened channel just upstream of the flexure and an increase in sinuosity within the flexure zone. The flexure is clearly seen in Figure 40 as a small concave zone near the end of the reach.

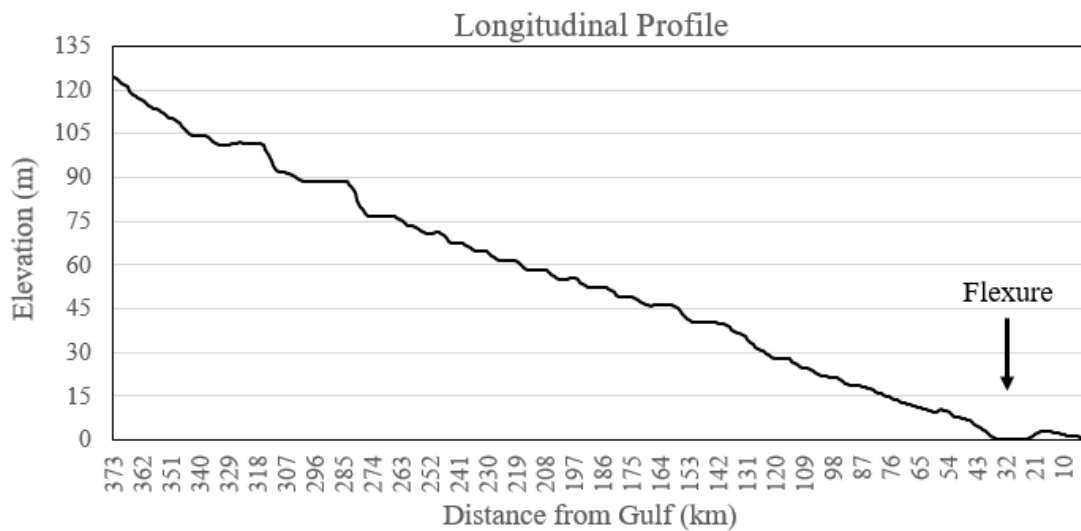


**Figure 40. Longitudinal profile showing Post-Vicksburg flexure zone near the end of the reach.**

Upstream of the flexure, a higher valley slope of the Guadalupe River increases the sinuosity in the reach of the part of the river because it is in a state of equilibrium adjustment. This adjustment results in higher rates of migration in the Upper Delta. Just below the flexure in the Middle Delta, the slope is nearly flat, and the river approaches a relatively straight course where aggradation dominates, limiting the rates of migration. Base level in the Middle Delta is the Gulf of Mexico, thus river adjustment is much less here because elevation approaches sea-level.

### 6.1.3 Belmont Fault Zone and Upper Coastal Plain

At the northern part of the study area, channel adjustment occurs in the Belmont Fault Zone and Upper Coastal Plain. The Belmont Fault Zone has the highest rates of migration and the Upper Coastal Plain has the second lowest rates of migration of all the geomorphic zones. The Belmont Fault Zone has a very confined valley compared to other reaches,

which contributes to high rates of migration. Confined valleys restrict meander formation and movement because of more resistant valley walls.

Properties of the geology are another factor that can restrict movement. In the Belmont Fault Zone, alluvial terraces dominate the valley walls. Although the walls are erodible, they are less erodible than the alluvium in which the channel resides. In the lower Belmont Fault Zone, the valley constricts the channel and causes increased rates of migration upstream. A point of constriction will result in the development of a straighter segment of river through the constriction and widening of the channel above and below the constriction. This constriction on the Guadalupe River is associated with Eocene-aged sediments that are less erodible than the alluvial terraces and fill, which were deposited during the Quaternary.

An additional possible influence on the high rates of migration of the river is the construction of the FM 1117 bridge. The bridge was constructed in 1984. Some of the highest amounts of migration are directly downstream of the bridge. Based on our fieldwork, it is unclear if the high rates of migration are the direct result of the bridge, or if other factors within the zone are the cause.

Geographic location of the Belmont Fault Zone is an additional factor affecting the reach. The Belmont Fault Zone is located ~22 km below the Balcones Escarpment. The Guadalupe River flows off of the steep-sloped escarpment onto the flat coastal plain where excess energy is dissipated. This dissipation of energy results in both aggradation and erosion. We think this process is responsible for some of the migration in this area. However, a stark change occurs in the adjacent reach relative to the upstream reach. Although the escarpment is a factor, the active fault zone within the reach has a greater impact on the zone. Movement produced by the fault can affect the channel in both up and downstream directions; upstream is more active in the study area. The effects of the fault downstream may be dampened as a result of proximity to the dam.

Following the concept of dynamic equilibrium, the high rates of migration in the Belmont Fault Zone can also be attributed to dams up and downstream from the zone. The construction of a dam changed the base level that the reach of river was flowing to prior to construction. A change in base level will cause aggradation upstream of the impoundment and erosion downstream. Adjustment can occur for decades after construction; however, rapid change typically occurs shortly after construction because the channel begins to immediately adjust to a new flow regime and sediment load. Six dams, four upstream of the Belmont Fault Zone and two within the Upper Coastal Plain affect these reaches. The dams were all built between 1928 and 1931, so adjustment should be less significant than after the initial construction. We think this might be the reason for low rates of migration in the Upper Coastal Plain, where it appears the two dams are in equilibrium with each other and the river channel.

## 6.2 Dams

Because we are using data that is thirty years after the construction of the two dams, we, unfortunately, cannot establish how much adjustment occurred in the river channel after the construction of the dams in the Upper Coastal Plain reach. The rates of migration for the 1960-2014 time period below both dams is shown in Figures 41 and 42. Nevertheless, we can quantify lateral adjustment, but we cannot account for any vertical adjustments of the river channel.

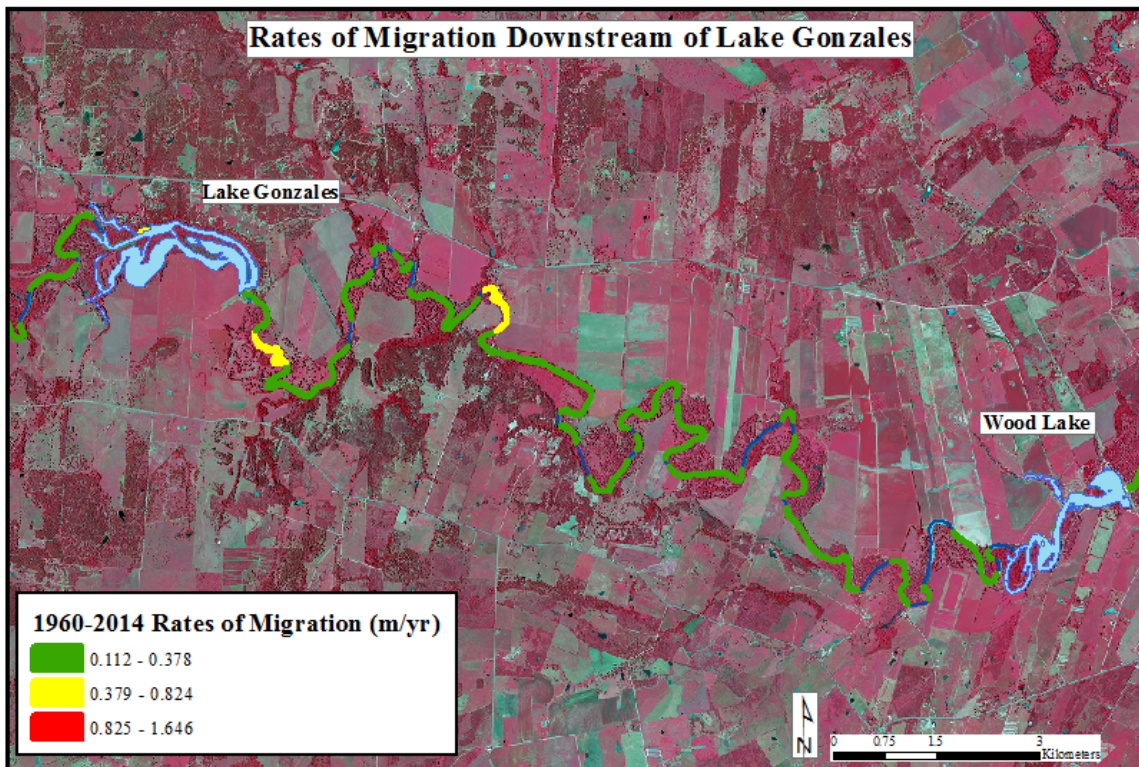


**Figure 41. Rates of migration on the Guadalupe River downstream of Lake Gonzales, TX. Lake Gonzales is a reservoir formed behind one of the dams on the Guadalupe River.**

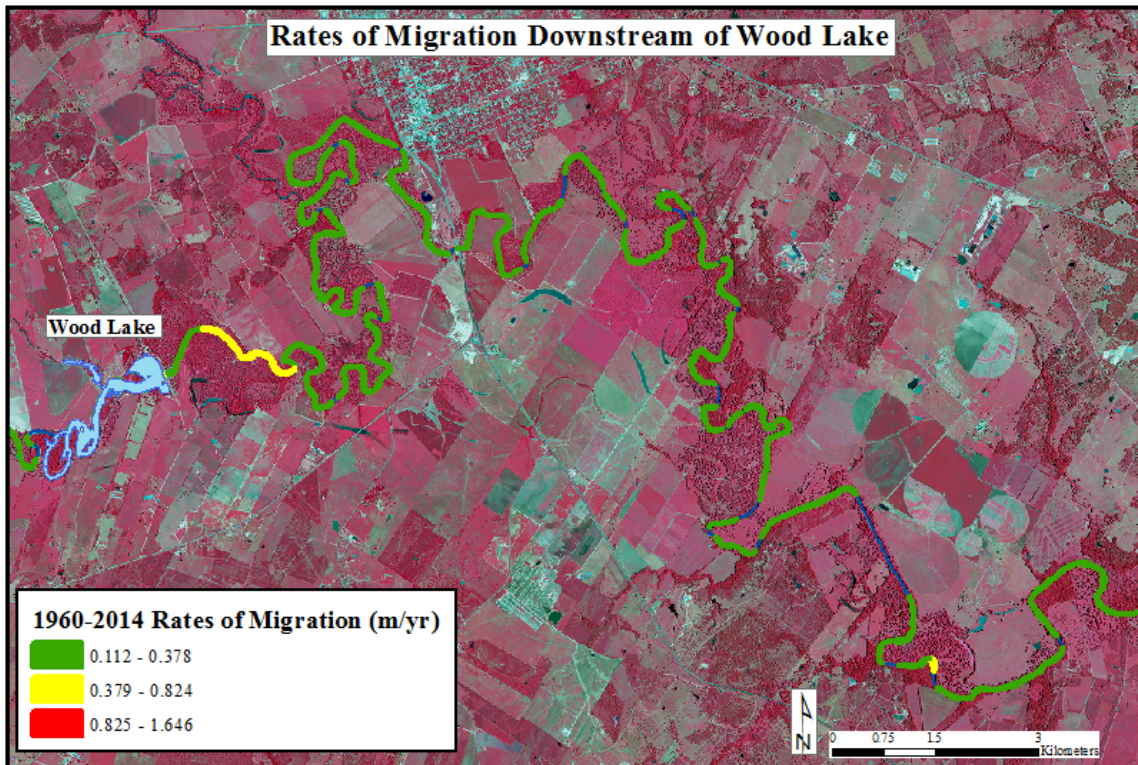


**Figure 42. Rates of migration on the Guadalupe River downstream of Wood Lake, TX. Wood Lake is a reservoir formed behind the second dam within the Upper Coastal Plain reach.**

Minor lateral adjustment is seen downstream of the dams. Philips (2007) suggested that it takes ~55 km for the river to regain the desired sediment load to minimize channel adjustment downstream of a dam. The two dams within the study reach are ~30 km apart. The close proximity to Wood Lake from Lake Gonzales might explain minimal changes downstream because the local base level is established relatively close. The relative stability below Wood Lake, however, cannot be explained by a local base-level effect.

The stability below Wood Lake can be linked to the altered flow regimes, which are controlled by dam releases. Dam releases dampen peak flows and increase base-flows creating a more moderate flow regime for the river. A hydrograph at Seguin, TX, upstream of the lake, shows flood-pulses which, might be the result of hydropeaking, shown in Figure 43.

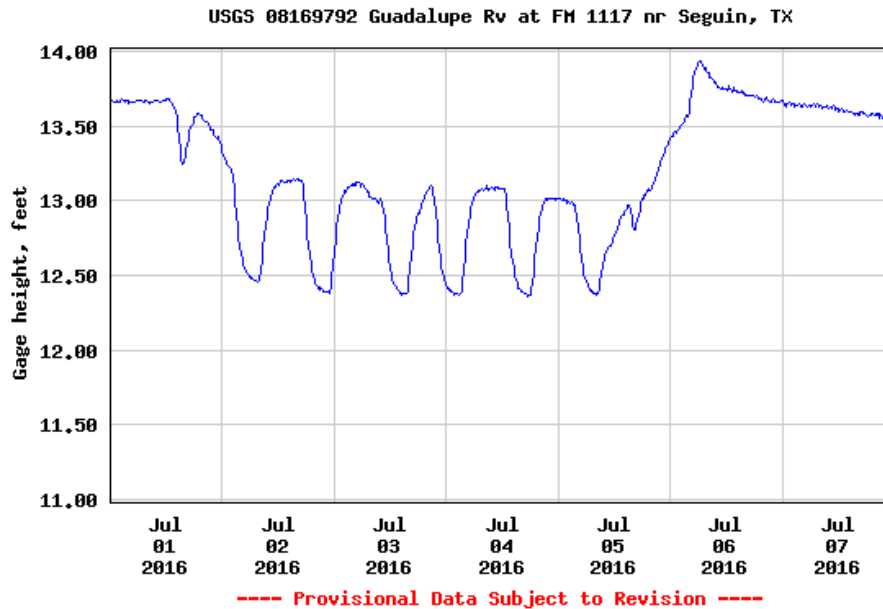


**Figure 43. Hydrograph of USGS gauge 08169792 Guadalupe River at FM 1117 near Seguin, TX, showing diurnal flood pulses from releases of upstream dams. (Data from waterdata.usgs.gov, 2016).**

Although peak flows are dampened, hydropeaking occurs as releases of water from the dams for hydropower generation. Hydropeaking creates daily pulses of increased flows that cause daily stage height changes. The effects of hydropeaking, however, depend on the volume of water being released. Because Wood Lake is relatively small, daily fluctuations are minimal, and a moderate flow regime dominates, which enhances channel stability.

The size of the dam must be considered when analyzing the effects of a dam on a river system. Lake Gonzales and Wood Lake are very small compared to the dam at Canyon Lake, which is ~150 km upstream. Canyon Lake has a storage capacity of 728,400 acre-feet compared to the capacity of Lake Gonzales at ~7,500 acre-feet and Wood Lake at ~4,000 acre-feet. According to Phillips (2011), ~ 20% of the flow that reaches the Gulf of Mexico is attributed to Canyon Lake releases. Phillips (2011) also suggested that it is difficult to attribute channel change to the dam because of the numerous geomorphic factors affecting the river. Thus, one must discount each of the geomorphic factors before taking the influence of the dam into consideration. Although it is difficult to quantify effects from dams within the study area, we think, nevertheless, that the artificial, moderate flow regimes contribute to channel stability on the lower Guadalupe River.

### 6.3 Meander Cut-Offs

Although meander cut-offs were not examined in the analysis of the rate of migration, the process of formation is important when considering the stability of a river system. Stølum (1996) suggests that meandering river systems develop through opposing processes where lateral migration increases sinuosity, and meander cut-offs decrease it. Stølum goes on to suggest that meander cut-offs create short periods of dampened rates of migration because the river straightens to the path it wants to take. The effect of a cut-off to the river system is dependent, however, on the state of the system itself. In a chaotic, unstable state, cut-offs bring the system toward a more stable state, whereas cut-offs that occur in a stable state tend toward instability. Stølum relates high sinuosities to an active system, so a system such as the lower Guadalupe River should be active and, therefore, unstable.

Hooke (2007) suggests that high sinuosity, however, does not necessarily relate to the level of activity and state of stability. The lower Guadalupe River is a good example of co-occurring activity and stability. The channel is tortuous in nature, but has had only six meander cut-offs in the last 54 years. Although geologically that is a short time period, the process of meander cut-offs does not follow what others have observed. Stølum (1996) suggests an avalanching effect once a cut-off has occurred. Bends around the initial cut-off will change drastically in a short time period. Rapid change does not seem to hold true for the lower Guadalupe River.

The Guadalupe River floodplain is scarred with oxbows and meander scrolls, which indicate a historically active channel. A future study focusing on dating the oxbows and meander scrolls would give insight into the temporal activity of the channel. Unfortunately, that objective was outside the scope of this project. Currently the channel of the Guadalupe River is focused on lateral migration. Some areas of the study area are very active, but the areas are increasing the size of the meander bend rather than termination of growth through a cutoff.

Throughout the study area, only six meander cut-offs and one avulsion have occurred. Four of the meander cut-offs occurred during the highly active flood period of 1995-2004. One can speculate that the cut-offs may have been the direct result of a high discharge. Chute cut-offs, the more immediate type, are typically the result of high discharges. Only one chute cut-off appears to have occurred during the active flood period of 1995-2004. The type of cut-off, however, is determined by observing temporal aerial imagery. Thus, a visually identified neck cut-off could have been accelerated as a result of chute development during or post-flood.

The avulsion that occurred during the 1995-2004 period was initially a result of the decommissioning of the hydropower plant in 1965 (Godfrey and Dowell, 1968). Turbines no longer facilitated the flow of water through the structure, so flow was inhibited, creating a backwater. The structure created an area of high pressure above the dam, initiating groundwater flow paths as water moved from high pressure to the lower pressure, below

and around the structure. A combination of flow path development, soil saturation, and high-flow events contributed to the channel avulsion around the flow structure. The channel now completely avoids the structure.

The two cut-offs and the avulsion occurred within the same sub-reach, the Middle Coastal Plain. The cut-offs occurred after the dam was decommissioned and the channel started to adjust. Proximity of the cut-offs to each other may have been a result of the channel adjusting to each major change. The fourth cut-off during the same time period occurred in the lower part of the Upper Delta reach. The upper part of the Upper Delta reach experienced another cut-off in the following study period, 2004-2010. In this sub-reach, both were neck cut-offs. A neck cut-off is more indicative of meander growth and termination. Because the Upper Delta is highly active, cut-offs of lateral meanders are expected as the sub-reach continues to adjust.

Another neck cut-off occurred in the lower part of the Belmont Fault Zone reach during the 2004-2010 study period. In the same study period, a neck cut-off occurred in the lower part of the Belmont Fault Zone reach. The cut-off occurred just below the areas of maximum migration. Because the zone is very active, the cut-off may be a result of channel adjustment. A flood also occurred in 2013 that could have contributed to the cut-off. The Belmont Fault Zone has the highest sinuosity by sub-reach at 3.07. Stølum's (1996) model finds that a bend will tend toward a steady-state value of 3.14. The author looks at an individual bend, however, rather than several in succession.

Sinuosity, along with other planform variables, is difficult to account for in a single bend because each bend is affected by adjacent meanders. It is thus important to use sinuosity as an indicator and view the river and each bend as a system. One must also understand the importance of the indicator and recognize the relation to and role within the system.

#### *6.4 Radius of Curvature*

Indicators of river stability and the consideration of factors affecting different sites are important. Nicoll and Hickin (2010) look at the difference in  $R_c/W$  measurements for confined and freely migrating meanders. Confined valleys dominate the Canadian prairie where the authors have study sites. Confined meanders have higher  $R_c/W$  ratios whereas freely meandering have lower, closer to the accepted ratio between two and three.

The lower Guadalupe River is a freely meandering system in the sense that the valley is wide enough so as not to confine the river. The river is under-fit for the valley which allows it to meander and migrate freely apart from dams and other channel obstructions. Although the river has free-meanders,  $R_c/W$  ratios are lower than what the authors found for Canadian Prairie rivers. Because the river is under-fit, having a larger valley than the current size of river needs, large meanders can develop which in turn develops compound bends. Compound bends form because flow velocities decline and reverse if the distance

is too large through a meander bend, resulting in the formation of another bend within the larger bend.

Numerous compound bends characterize the lower Guadalupe, resulting in a tortuous river with sinuosities above 2 for all sub-reaches. Sinuosities in Nicoll and Hickin's study area are closer to regular; between 1.1 and 1.8. The difference in average sinuosity influences Rc/W measurements and could account for the difference between the Canadian Prairie study site and the lower Guadalupe River.

Results for the lower Guadalupe River are also compared to results to a tortuous river system in Puerto Rico where highest rates of migration occur at an average Rc/W of 2.42 (Alvarez, 2005). Results of two different studies on the Brazos River, another Texas Coastal Plain river, present similar results. Gillespie and Giardino (1997) found rates of migration were highest for bends with a Rc/W ratio of 2.5-3.5. Giardino and Lee (2011) found similar results where ratios of 2-3 experienced the highest rates of migration.

Rates of migration were greatest with an Rc/W measurement of  $<2$  on the lower Guadalupe River. This can be attributed to an overall stable channel throughout the reach. Average rate of migration for a Rc/W value  $<2$  is 0.5 m/yr compared to 0.32 m/yr at a ratio of 2-3. Major changes can occur in one bend over 54 years, and that can bias the Rc/W ratio. Each bend is dependent on local factors, outside of channel planform. Vegetation and soil composition can control the migration of a meander bend more than the geometry of the channel itself. The ratio should be used as an indicator of the stability of the river, but each bend should also be observed independently. To better understand the relationship that the Rc/W ratio has on the lower Guadalupe River, each meander bend should be quantified. The ratios of a larger compound bend and single simple bends within the compound bend should also be analyzed to understand the compounding effect.

## 7. CONCLUSION

The purpose of this study was to analyze and understand the migration of meanders as a response to systematic changes along the lower Guadalupe River, TX. The study area extends from Seguin, TX, on the northern end, to the confluence with the San Antonio River, on the southern end, for a distance of ~380 km. To achieve this, rates of migration were calculated along the lower Guadalupe River over several temporal intervals. Rates were determined for the entire reach as well as for predetermined sub-reaches. Mechanisms of channel adjustment were also investigated to determine what the major controls of lateral migration are on the lower Guadalupe River. The objectives of this study were: (1) Calculate rates of meander migration along selected reaches of the Guadalupe River, and (2) Determine the driving mechanisms controlling channel migration. This project was in support of the Texas Instream Flow Program.

Our study and detailed analysis suggest that overall the channel is stable in the sense that it appears it can adjust well to dynamic discharges. Although a 54-year time period is limited, it does provide a temporal perspective on the stability of the channel. We use stable to refer to dynamic stability, so while one section of channel may be very active, the reach as a whole adjusts to keep the system relatively stable within itself. When examining the 380 km reach, it appears that the river experiences minimal rates of migration at an average of 0.36 m/yr over the 54-year period. Unstable areas are noticeable when observing the river at the individual reach scale.

The Belmont Fault Zone and Upper Delta are the most unstable reaches with average rates of migration at 0.53 and 0.47 m/yr, respectively. The most stable reaches are found in the Upper Coastal Plain and Middle Delta with average rates of migration at 0.22 and 0.2 m/yr, respectively.

Mechanisms contributing to the rates of lateral migration are the presence of vegetation on the outside banks and a high silt-clay content of the bank. Another mechanism that plays an important role is the influence of dams, especially in the Belmont Fault Zone and Upper Coastal Plain reaches. It is important to note that the influence of Canyon Lake, which is ~150 km outside the study area, is present throughout the 380 km reach. Moderate flows produced by releases at the dam contribute to the channel stability of this reach of the Guadalupe River. No channel change is present directly downstream of the two dams within the Upper Coastal Plain reach. This stable channel is a result of the artificial, moderate flow regimes, as well as the installation of the dam 85 years ago that has allowed time for the channel to equilibrate.

The zone of subsidence in the Upper Delta and Middle Delta is another mechanism affecting channel change. The flexure zone is active, so channel adjustment occurs in response to any disruptions. The effect of rising sea-level, also an active process, contributes to channel change in the lower reaches because relative base-level is changing.

Several factors are not accounted for in this study that may contribute to rates of lateral migration. First, we made assumptions that bank composition is homogeneous through a soil column. To better understand the relationship between soils and a meander bend, field sampling of soil type, pore-pressure, silt-clay content, and soil stratigraphy should be quantified in several locations along a meander bend to develop a site-specific understanding of the bend.

Another factor to account for is the channel hydraulics through a meander bend. The flow mechanisms through various shaped bends are generally understood; however, the flow patterns assume that the channel bottom follows a standard geometry. Sediment movement, type, and size vary throughout a meander bend and will affect the hydraulics within the bend. Documenting the bathymetry of a meander bend and several successive bends can lead to important geomorphic factors that have not been considered to effect lateral migration.

In conclusion, our study provides a broad overview of the stability of the lower Guadalupe River using rates of lateral migration. We used three different scales to gain insight into the relationship between a single meander bend, the individual reach it is in, and the entire 380 km reach. Each reach affects one another, so it is important to consider the mechanisms working at different scales. A future study should include the mechanisms we did not account for and should include a field-work component that will enhance and advance the work of this study.

To recap, the major findings of this study are:

- Rates of migration range from ~0.11 – 8.15 m/yr.
- The Belmont Fault Zone reach has the highest rates of migration with an average of 0.53 m/yr.
- The Middle Delta has the lowest rates of migration, with an average of 0.2 m/yr.
- Drought can accelerate rates of migration as a result of a low river stage and slumping of channel banks.
- Channel change below Lake Gonzales and Wood Lake is minimal compared to other locations in the study area.
- Individual variables do not control rates of migration.
- Geomorphic and watershed characteristics together control meander migration at multiple spatial scales.

## REFERENCES

- Ahnert, Frank. "Equilibrium, Scale and Inheritance in Geomorphology." *Geomorphology* 11, no. 2 (1994): 125-140.
- Alvarez, Aldo. "Channel Planform Dynamics of an Alluvial Tropical River." Dissertation, Texas A&M University, (2005): 1-98.
- Association, Texas State Historical. "Texas Almanac: Rivers." (2010).
- Bagnold, Ralph Alger. *Some Aspects of the Shape of River Meanders*. USGS, (1960): 135-144.
- Baker, Victor R. "Flood Hazards Along the Balcones Escarpment Incentral Texas Alternative Approaches to Their Recognition, Mapping, and Management." *Bureau of Economic Geology Circular* 75, no. 5 (1975): 1-20.
- Baker, Victor R. "Hydrogeomorphic Methods for the Regional Evaluation of Flood Hazards." *Environmental Geology* 1, no. 5 (1976): 261-281.
- Baker, Victor R. "Stream-Channel Response to Floods, with Examples from Central Texas." *Geological Society of America Bulletin* 88, no. 8 (1977): 1057-1071.
- Barnhardt, Walter A, Joseph T Kelley, Stephen M Dickson, and Daniel F Belknap. "Mapping the Gulf of Maine with Side-Scan Sonar: A New Bottom-Type Classification for Complex Seafloors." *Journal of Coastal Research*(1998): 646-659.
- Baz, Ibrahim, Abdurrahman Geymen and Semih Nogay Er. "Development and Application of Gis-Based Analysis/Synthesis Modeling Techniques for Urban Planning of Istanbul Metropolitan Area." *Advances in Engineering Software* 40, no. 2 (2009): 128-140.
- Bizzi, Simone and David N Lerner. "The Use of Stream Power as an Indicator of Channel Sensitivity to Erosion and Deposition Processes." *River Research and Applications* 31, no. 1 (2015): 16-27.
- Blondel, Philippe and Bramley J Murton. *Handbook of seafloor sonar imagery*. Chichester, UK: Wiley, 1997.
- Blum, Michael D and Andres Aslan. "Signatures of Climate Vs. Sea-Level Change within Incised Valley-Fill Successions: Quaternary Examples from the Texas Gulf Coast." *Sedimentary Geology* 190, no. 1 (2006): 177-211.

- Bracken, Louise J and John Wainwright. "Geomorphological Equilibrium: Myth and Metaphor?" *Transactions of the Institute of British Geographers* 31, no. 2 (2006): 167-178.
- Brewer, Cynthia A and Linda Pickle. "Evaluation of Methods for Classifying Epidemiological Data on Choropleth Maps in Series." *Annals of the Association of American Geographers* 92, no. 4 (2002): 662-681.
- Briaud, Jean-Louis, Hamn-Ching Chen and Siyoung Park. *Predicting Meander Migration: Evaluation of Some Existing Techniques*. (2001): 2-18.
- Brice, James C. "Evolution of Meander Loops." *Geological Society of America Bulletin* 85, no. 4 (1974): 581-586.
- Bridge, John S. *Rivers and Floodplains: Forms, Processes, and Sedimentary Record*: John Wiley & Sons, (2009).
- Brierley, Gary J and Kirstie Fryirs. "River Styles, a Geomorphic Approach to Catchment Characterization: Implications for River Rehabilitation in Bega Catchment, New South Wales, Australia." *Environmental Management* 25, no. 6 (2000): 661-679.
- Brierley, Gary J and Kirstie A Fryirs. *Geomorphology and River Management: Applications of the River Styles Framework*: John Wiley & Sons, (2013).
- Census.gov, "Quick Facts: Texas", 2014. <http://www.census.gov/quickfacts/table/SEX255214/4866644>.
- Church, Michael. "The Trajectory of Geomorphology." *Progress in Physical Geography* 34, no. 3 (2010): 265-286.
- Cyr, Andrew J and Darryl E Granger. "Dynamic Equilibrium among Erosion, River Incision, and Coastal Uplift in the Northern and Central Apennines, Italy." *Geology* 36, no. 2 (2008): 103-106.
- Darby, Stephen E, Andrei M Alabyan and Marco J. Van de Wiel. "Numerical Simulation of Bank Erosion and Channel Migration in Meandering Rivers." *Water Resources Research* 38, no. 9 (2002): 1-21.
- Data, US Climate, "Texas", 2016. <http://www.usclimatedata.com/climate/texas/united-states/3213>.
- Deussen, Alexander. *Geology of the Coastal Plain of Texas West of Brazos River*. Vol. 126. US Government Printing Office, (1924): 1-139.

- Donaldson, Alan C, Richard H Martin and William H Kanen. "Holocene Guadalupe Delta of Texas Gulf Coast." *Society of Economic Paleontologists and Mineralogists: Deltaic Sedimentation, Modern and Ancient*, no. SP15 (1970): 107-137.
- Dorroh, John H. "Certain Hydrologic and Climatic Characteristics of the Southwest." *University of New Mexico Publications in Engineering*. University of New Mexico Press, (1946).
- Fish, John P, and H Arnold Carr. *Sound underwater images: a guide to the generation and interpretation of side scan sonar data*. Lower Cape Pub Co, 1990.
- Frissell, Christopher A, William J Liss, Charles E Warren and Michael D Hurley. "A Hierarchical Framework for Stream Habitat Classification: Viewing Streams in a Watershed Context." *Environmental management* 10, no. 2 (1986): 199-214.
- Geist, David R. *Grays River Watershed Geomorphic Analysis*. Pacific Northwest National Laboratory (PNNL), Richland, WA, (2005): 77-83.
- Giardino, John R and Adam A Lee. "Rates of Channel Migration on the Brazos River." Austin, Texas: Texas Water Development Board, (2011): 1-41.
- Gillespie, Ben M and John R Giardino. "The Nature of Channel Planform Change: Brazos River, Texas." *Texas Journal of Science* 49, no. 2 (1997): 109-142.
- Godfrey, F.A. and C.L. Dowell. *Major Hydroelectric Powerplants in Texas*. Austin, Texas: Texas Water Development Board, (1968): 10.
- Graf, William L. "The Rate Law in Fluvial Geomorphology." *American Journal of Science* 277, no. 2 (1977): 178-191.
- Graf, William L. "Downstream Hydrologic and Geomorphic Effects of Large Dams on American Rivers." *Geomorphology* 79, no. 3 (2006): 336-360.
- Gurnell, Angela. "Plants as River System Engineers." *Earth Surface Processes and Landforms* 39, no. 1 (2014): 4-25.
- Hack, John T. "Dynamic Equilibrium and Landscape Evolution." *Theories of Landform Development* 1 (1975): 87-102.
- Hatch, Stephan L, Kancheepuram Natarajan Gandhi and Larry E Brown. "Checklist of the Vascular Plants of Texas." *College Station, Tex.: Texas Agricultural Experiment Station iv, En Maps Plant records. Geog* 3, (1990): 1-158.

- Hickin, Edward J and Gerald C Nanson. "Lateral Migration Rates of River Bends." *Journal of Hydraulic Engineering* 110, no. 11 (1984): 1557-1567.
- Holley, Edward R. "Sediment Transport in the Lower Guadalupe and San Antonio Rivers." Texas Water Resources Institute, (1992): 1-100.
- Hooke, Janet. "River Meander Behaviour and Instability: A Framework for Analysis." *Transactions of the Institute of British Geographers* 28, no. 2 (2003): 238-253.
- Hooke, Janet. "Complexity, Self-Organisation and Variation in Behaviour in Meandering Rivers." *Geomorphology* 91, no. 3 (2007): 236-258.
- Jiang, Bin. "Head/Tail Breaks: "A New Classification Scheme for Data with a Heavy-Tailed Distribution." *The Professional Geographer* 65, no. 3 (2013): 482-494.
- Kaesler, Adam J and Thomas L Litts. "A Novel Technique for Mapping Habitat in Navigable Streams Using Low-Cost Side Scan Sonar." *Fisheries* 35, no. 4 (2010): 163-174.
- Kaesler, Adam J., Thomas L. Litts, and T. Tracy. "Using Low-Cost Side-Scan Sonar for Benthic Mapping Throughout the Lower Flint River, Georgia, USA." *River Research and Applications* 29, no. 5 (2013): 634-644.
- Kidd, Robert B, Robert W Simm, and Roger C Searle. "Sonar Acoustic Facies and Sediment Distribution on an Area of the Deep Ocean Floor." *Marine and Petroleum Geology* 2, no. 3 (1985): 210-221.
- Knighton, David. *Fluvial Forms and Processes: A New Perspective*: Routledge, (2014): 1-52.
- Konsoer, Kory M, Bruce L Rhoads, Eddy J Langendoen, James L Best, Mick E Ursic, Jorge D Abad and Marcelo H Garcia. "Spatial Variability in Bank Resistance to Erosion on a Large Meandering, Mixed Bedrock-Alluvial River." *Geomorphology* 252, (2016): 80-97.
- Langbein, Walter B and Luna B Leopold. "Quasi-Equilibrium States in Channel Morphology." *American Journal of Science* 262, no. 6 (1964): 782-794.
- Leopold, Luna Bergere. *A View of the River*: Harvard University Press, (1994): 58.
- Leopold, Luna B and Markley G Wolman. "River Channel Patterns: Braided, Meandering, Straight." U.S. Geological Survey Professional Paper 282-B (1957): 39-73.

- Lewin, John. "The Lexicon of Geomorphology." *Earth Surface Processes and Landforms* 41, no. 1 (2016): 5-15.
- Magilligan, Francis J and Keith H Nislow. "Changes in Hydrologic Regime by Dams." *Geomorphology* 71, no. 1 (2005): 61-78.
- Montgomery, David R and John M Buffington. "Channel-Reach Morphology in Mountain Drainage Basins." *Geological Society of America Bulletin* 109, no. 5 (1997): 596-611.
- Nanson, Gerald C and Edward J Hickin. "Channel Migration and Incision on the Beatton River." *Journal of Hydraulic Engineering* 109, no. 3 (1983): 327-337.
- Nanson, Gerald C and Edward J Hickin. "Lateral Migration Rates of River Bends." *Journal of Hydraulic Engineering* 110, no. 11 (1984): 1557-1567.
- Nanson, Gerald C and Edward J Hickin. "A Statistical Analysis of Bank Erosion and Channel Migration in Western Canada." *Geological Society of America Bulletin* 97, no. 4 (1986): 497-504.
- Nicoll, Tami J and Edward J Hickin. "Planform Geometry and Channel Migration of Confined Meandering Rivers on the Canadian Prairies." *Geomorphology* 116, no. 1 (2010): 37-47.
- Nrcs.usda.gov, "Official Soil Series Descriptions (OSDs)", 2014.  
[http://www.nrcs.usda.gov/wps/portal/nrcs/detailfull/soils/home/?cid=nrcs142p2\\_053587](http://www.nrcs.usda.gov/wps/portal/nrcs/detailfull/soils/home/?cid=nrcs142p2_053587)
- Nws.gov, "Guadalupe River at Victoria", 2016.  
<http://water.weather.gov/ahps2/hydrograph.php?wfo=CRP&gage=VICT2>.
- Ouchi, Shunji. "Response of Alluvial Rivers to Slow Active Tectonic Movement." *Geological Society of America Bulletin* 96, no. 4 (1985): 504-515.
- Perkin, J. S. and T.H. Bonner. "Long-Term Changes in Flow Regime and Fish Assemblage Composition in the Guadalupe and San Marcos Rivers of Texas." *River Research and Applications* 27 no.5 (2005): 566-579.
- Phillips, Jonathan D. "Geomorphic Equilibrium in Southeast Texas Rivers." Texas Water Development Board, (2007): 6-103.
- Phillips, Jonathan D. "Geomorphic Processes, Controls, and Transition Zones in the Guadalupe River." Austin, Texas: Texas Water Development Board, (2011): 6-68.

- Phillips, Jonathan D. "Geomorphic Responses to Changes in Flow Regimes in Texas Rivers." Texas Water Development Board and Texas Instream Flow Program, (2012): 9-68.
- Phillips, Jonathan D and Michael C Slattery. "Downstream Trends in Discharge, Slope, and Stream Power in a Lower Coastal Plain River." *Journal of Hydrology* 334, no. 1 (2007): 290-303.
- Program, Texas Instream Flow. "Instream Flow Study of the Middle and Lower Brazos River." *Middle and Lower Brazos River Sub-Basin Study Design Workgroup*, (2010): 5-31.
- Richard, Gigi A, Pierre Y Julien and Drew C Baird. "Statistical Analysis of Lateral Migration of the Rio Grande, New Mexico." *Geomorphology* 71, no. 1 (2005): 139-155.
- Schumm, Stanley A. "Sinuosity of Alluvial Rivers on the Great Plains." *Geological Society of America Bulletin* 74, no. 9 (1963): 1089-1100.
- Schumm, Stanley A, Jean F Dumont and John M Holbrook. *Active Tectonics and Alluvial Rivers*: Cambridge University Press, (2002): 8-12.
- Solis, R F I, and F Raul. "Upper Tertiary and Quaternary Depositional Systems, Central Coastal Plain, Texas—Regional Geology of the Coastal Aquifer and Potential Liquidwaste Repositories." *Report of Investigations* 108 (1981): 89.
- Stølum, Hans Henrik. "River Meandering as a Self-Organization Process." *Science* 271, no. 5256 (1996): 1710.
- Tobler, Waldo R. "A Computer Movie Simulating Urban Growth in the Detroit Region." *Economic Geography* 46, (1970): 234-240.
- Tranmer, Andrew W, Daniele Tonina, Rohan Benjankar, Matthew Tiedemann, and Peter Goodwin. "Floodplain Persistence and Dynamic-Equilibrium Conditions in a Canyon Environment." *Geomorphology* 250 (2015): 147-158.
- Wallick, Jennifer Rose, Stephen T Lancaster and John P Bolte. "Determination of Bank Erodibility for Natural and Anthropogenic Bank Materials Using a Model of Lateral Migration and Observed Erosion Along the Willamette River, Oregon, USA." *River Research and Applications* 22, no. 6 (2006): 631-649.
- Waterdata.usgs.gov, "USGS Surface-Water Historical Instantaneous Data for the Nation: Build Time Series", 2016.  
[http://waterdata.usgs.gov/nwis/uv/?referred\\_module=sw](http://waterdata.usgs.gov/nwis/uv/?referred_module=sw)

Winterbottom, Sandra J and David J Gilvear. "A Gis-Based Approach to Mapping Probabilities of River Bank Erosion: Regulated River Tummel, Scotland." *Regulated Rivers: Research & Management* 16, no. 2 (2000): 127-140.

Wohl, Ellen. "Floodplains and Wood." *Earth-Science Reviews* 123, (2013): 194-212.

Wolman, M Gordon and John P Miller. "Magnitude and Frequency of Forces in Geomorphic Processes." *The Journal of Geology*, (1960): 54-74.

## APPENDIX A

### *A.1 Introduction to Side-Scan Sonar*

One of the parameters we wanted to examine in the project was the river at a fourth scale. We attempted to use a side-scan sonar to map the morphology and sediment of the river channel substrate. We used a Humminbird® 698ci HD SI Combo. Unfortunately, the unit did not operate as hoped. We had a problem with linking the Humminbird® with a GPS unit to georeferenced the can. However, because we think this unit has so much potential for mapping rivers in Texas, we have included an appendix to discuss our use of the unit and suggested uses in the future.

Sonar has been widely used in marine environments to gain a view of the bottom surface morphologies and substrates of the ocean or sea floor (Kidd et al., 1985; Fish and Carr, 1990; Blondel and Murton, 1997; Barnhardt et al., 2003). More recently, sonar has been used to study rivers for habitat mapping for aquatic life (Kaeser and Litts, 2010, Kaeser et al., 2013).

We acquired a Humminbird® 698ci HD SI Combo. This instrument is equipped with side-scan sonar that can image the channel bottom, from side to side. Acoustic signals are sent out, and the reflected backscatter intensity is used to produce an image. The more intense the backscatter is, the darker the pixel, and the less intense the backscatter is, the lighter the pixel is (Kaeser et al., 2013). A lighter pixel typically relates to finer sediment because absorbs the acoustic signal compared to coarser sediment, woody debris, or rip - rap that reflect the acoustic signal, resulting in a darker pixel. The unit is also able to work at three different frequencies; 83, 200, or 455 kHz. A higher frequency will produce an image with a higher resolution. It is important to consider the scope of the task when considering what frequency to operate the sonar at. A higher frequency may not obtain a full range as there is more signal scatter involved when operating at a high frequency.

To apply sonar to a river setting, the sonar unit was attached to a boat that follows the thalweg as it travels downstream. As the boat travels at a uniform speed, the sonar captures images of the substrate. A side-scan sonar is able to capture an image of the channel, from channel side to channel side, depending on the width of the river and signal frequency used on the sonar. The images attained from a survey can be seen in Figure 44.

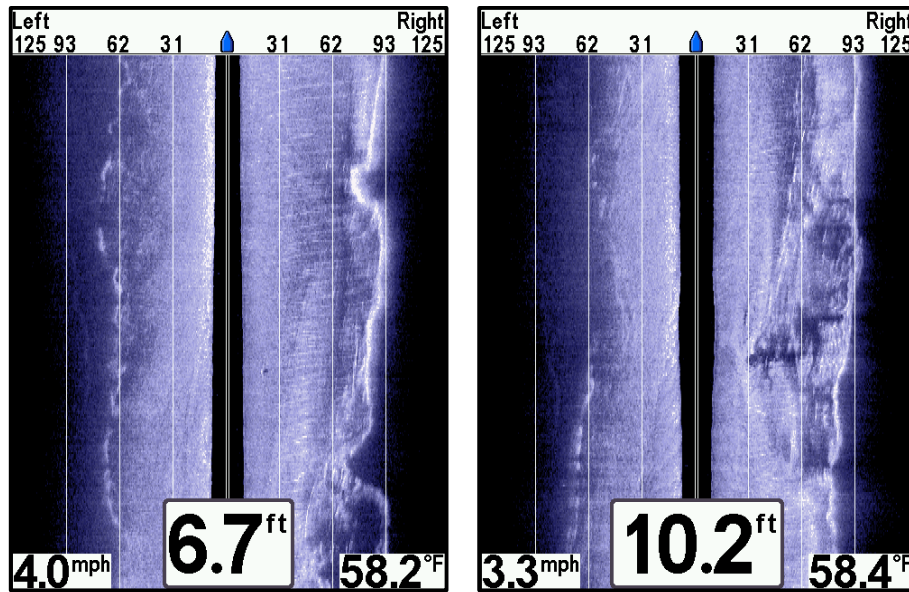


**Figure 44. Sonar image examples. The black line in the middle of both images represents the depth of the water column. A wider strip represents a deeper area whereas a narrower strip is more shallow. The lighter pixels typically represent finer materials including sands, silts and clays, whereas the darker pixels relate to denser material including cobbles, boulders and riprap. (Images captured on the Guadalupe River near Cuero, TX).**

### *A.2 Guidelines for Using Side-Scan Sonar*

The Humminbird® side-scan sonar is a relatively easy instrument to mount on a boat and use. It is a robust instrument that will tolerate relative rough handling. The instrument should be mounted on the back of the boat where the mount must be rigid and minimize any play, as the boat moves through the water. The side-scan sonar must be connected to a quality GPS to collect positional data simultaneously as side-scan data are collected. The positional data is required to georeference the side-scan data. In-situ sediment samples of the channel substrate should also be collected when performing a survey. All points should be documented with a GPS to georeference with the side-scan data.

Images and samples are continuously taken for the survey reach at intervals determined by the speed of the boat. Once collected, images are cropped and mosaicked together to create a continuous image of the channel substrate. Collected substrate samples can be compared to the images to bottom truth the substrate type.

### *A.3 Side-Scan Sonar Work*

The use of side-scan sonar was attempted on a 51 km segment of the lower Guadalupe River near Cuero, TX. This reach of river was selected to encompass a transition between

the Middle Coastal Plain and Coastal Plain Transition reaches, as well as having previously established river access points. The segment was sufficiently long for data collection, as well as allowing room for error.

This reach of the river was surveyed on two days, December 5<sup>th</sup> and 6<sup>th</sup>, 2015. This was our first time using the sonar, so the survey functioned as a learning experience and gathering of preliminary data. The survey was conducted from a canoe with two paddlers and one data collector. Unfortunately, the river had a higher than normal discharge for the time of year, so maintaining the velocity of the canoe was difficult. This also compromised the collection of in-situ substrate samples for comparison with the collected imagery.

Another major issue involved the continuous collection of GPS data, as the result of a faulty connection between the side-scan sonar and the GPS unit. The simultaneous collection of GPS data and side scan data is necessary to relate the collected image to the position on the river. Because no external GPS could be connected to the head-unit, so we relied on the internal GPS and two hand held units. The GPS in the sonar head-unit was very unreliable for this reach of river, so it limited the amount of data that could be collected. It goes without saying that in the future, a different set-up is necessary to collect usable data.

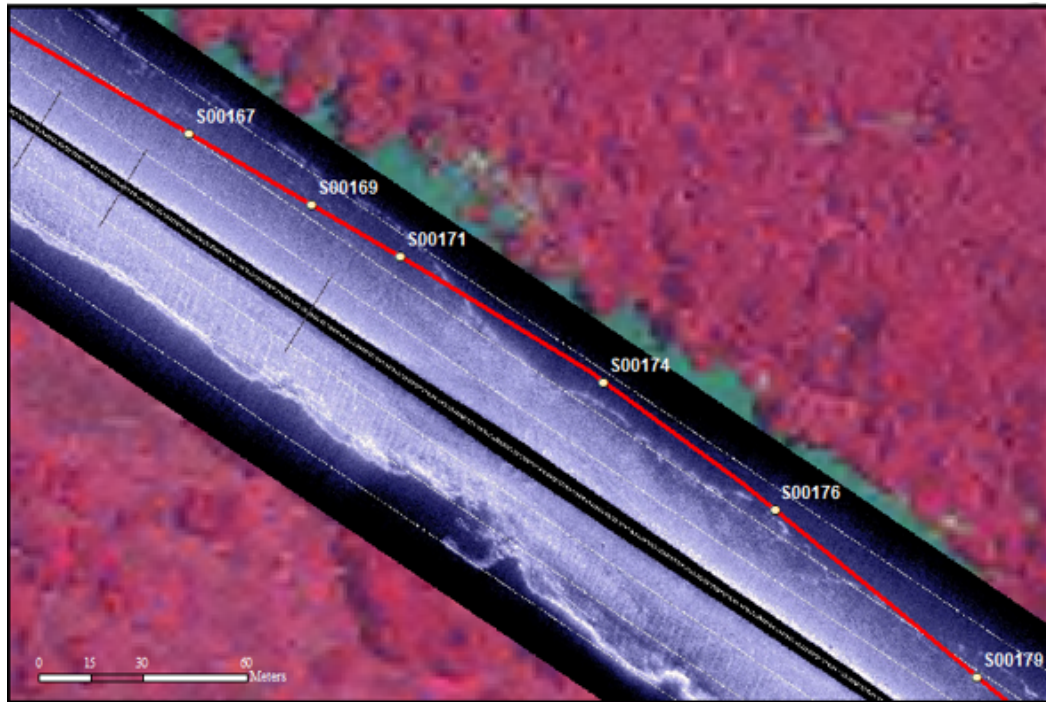
#### *A.4 Example from Preliminary Data*

A segment of river, which is ~1 km, demonstrates where continuous data were collected with a working GPS and is shown in Figure 45a. A close-up of several imagery points is shown in Figure 45b. The image consists of 18 images that were cropped and mosaicked to create a continuous image of the river substrate.



(a)

Figure 45. (a) Sonar image mosaic. The black box outlines a close-up of sonar waypoints S00167-S00176, and is shown in Figure 44b.



(b)

**Figure 45. Continued.**

Observing the segment of river and associate imagery, it is, unfortunately, difficult to identify substrate type through imagery alone. If sediment samples had been able to be collected, the images could have been calibrated to produce a map of channel substrate type.

Although the use of the side-scan sonar was not successful for this project, we strongly believe that the method has real promise in fluvial geomorphology studies. Thus, we will continue to test the technique and will continue to establish a working methodology, so the instrument can be used in the future to provide data fundamentally important to analyzing and understanding the spatial distribution and role of bottom sediment. Future work should include this type of survey to gain further insight into the dynamics of the river. Surveys can be implemented on a regular basis to monitor changes to the channel following extreme discharges. The methods can be implemented on a variety of reach sizes to target different areas of interest.

## APPENDIX B

This appendix includes photographs of meander bends taken along the ~50 km field surveyed portion of the river near Cuero, TX. A map of the reach is shown in Figure 46. Rates of migration in three classes, are shown on the map relative to the photograph location. A close-up of the “A” and “B” locations are shown in Figures 47 and 48, respectively. Photographs of each location follow in figures 49-79.

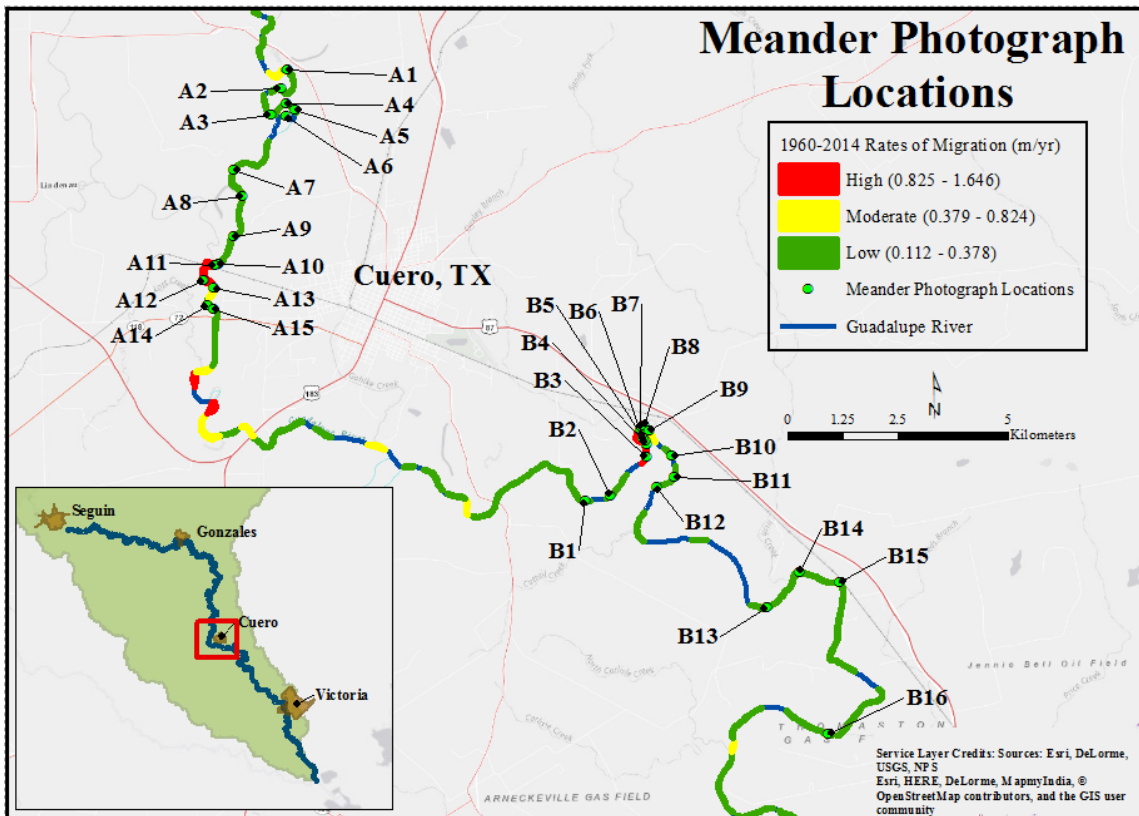
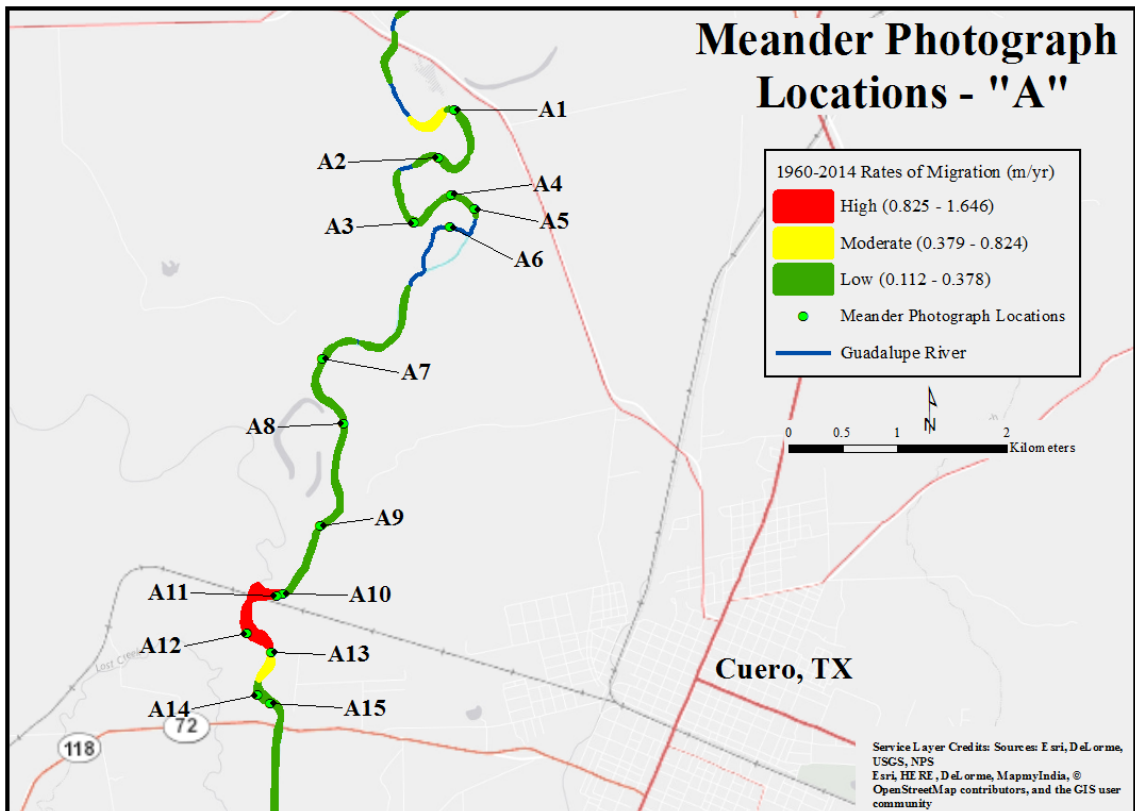


Figure 46. Map of all photograph locations of meanders during the field survey near Cuero, TX, of a ~50 km reach.



**Figure 47. Map of "A" photograph locations. Rates of migration are included, divided into three classes.**

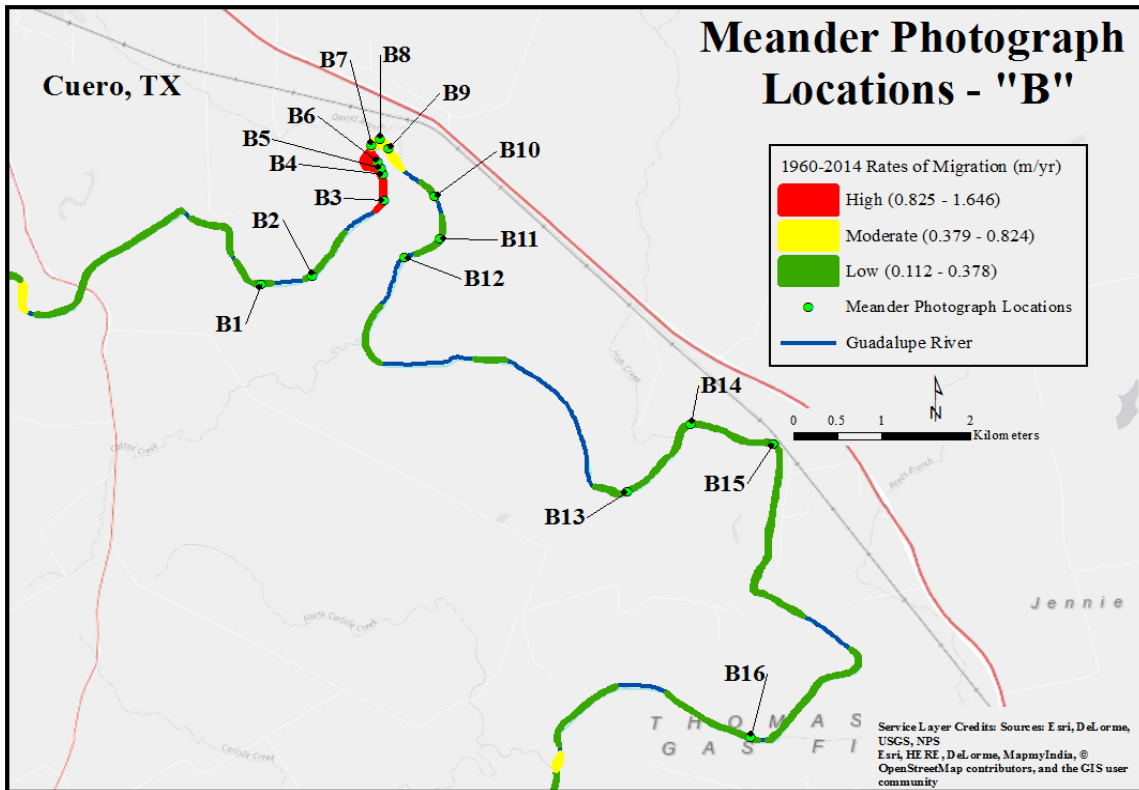


Figure 48. Map of "B" photograph locations. Rates of migration are included, divided into three classes.



Figure 49. Location of A1. Photograph taken near Cuero, TX, (December 5, 2016).



**Figure 50. Location of A2. Photograph taken near Cuero, TX, (December 5, 2016).**



**Figure 51. Location of A3. Photograph taken near Cuero, TX, (December 5, 2016).**



**Figure 52. Location of A4. Photograph taken near Cuero, TX, (December 5, 2016).**



**Figure 53. Location of A5. Photograph taken near Cuero, TX, (December 5, 2016).**



**Figure 54. Location of A6. Photograph taken near Cuero, TX, (December 5, 2016).**



**Figure 55. Location of A7. Photograph taken near Cuero, TX, (December 5, 2016).**



**Figure 56. Location of A8. Photograph taken near Cuero, TX, (December 5, 2016).**



**Figure 57. Location of A9. Photograph taken near Cuero, TX, (December 5, 2016).**



**Figure 58. Location of A10. Photograph taken near Cuero, TX, (December 5, 2016).**



**Figure 59. Location of A11. Photograph taken near Cuero, TX, (December 5, 2016).**



**Figure 60. Location of A12. Photograph taken near Cuero, TX, (December 5, 2016).**



**Figure 61. Location of A13. Photograph taken near Cuero, TX, (December 5, 2016).**



**Figure 62. Location of A14. Photograph taken near Cuero, TX, (December 5, 2016).**



**Figure 63. Location of A15. Photograph taken near Cuero, TX, (December 5, 2016).**



**Figure 64. Location of B1. Photograph taken near Cuero, TX, (December 6, 2016).**



**Figure 65. Location of B2. Photograph taken near Cuero, TX, (December 6, 2016).**



**Figure 66. Location of B3. Photograph taken near Cuero, TX, (December 6, 2016).**



**Figure 67. Location of B4. Photograph taken near Cuero, TX, (December 6, 2016).**



**Figure 68. Location of B5. Photograph taken near Cuero, TX, (December 6, 2016).**



**Figure 69. Location of B6. Photograph taken near Cuero, TX, (December 6, 2016).**



**Figure 70. Location of B7. Photograph taken near Cuero, TX, (December 6, 2016).**



**Figure 71. Location of B8. Photograph taken near Cuero, TX, (December 6, 2016).**



**Figure 72. Location of B9. Photograph taken near Cuero, TX, (December 6, 2016).**



**Figure 73. Location of B10. Photograph taken near Cuero, TX, (December 6, 2016).**



**Figure 74. Location of B11. Photograph taken near Cuero, TX, (December 6, 2016).**



**Figure 75. Location of B12. Photograph taken near Cuero, TX, (December 6, 2016).**



**Figure 76. Location of B13. Photograph taken near Cuero, TX, (December 6, 2016).**



**Figure 77. Location of B14. Photograph taken near Cuero, TX, (December 6, 2016).**



**Figure 78. Location of B15. Photograph taken near Cuero, TX, (December 6, 2016).**



**Figure 79. Location of B16. Photograph taken near Cuero, TX, (December 6, 2016).**

## APPENDIX C

This appendix includes the soil descriptions for the outside bank on the individual meander bends that were analyzed. Soil type was identified using a shapefile from the Natural Resources Conservation Service (NRCS) in a GIS. More detailed descriptions for the soil series were obtained from the United States Department of Agriculture (USDA) official series descriptions documents (Nrcs.usda.gov, 2014).

<b>Bend</b>	<b>Outside Bank Soil</b>	<b>Symbol</b>	<b>Soil Descriptions from USDA</b>
BFZ1	Seguin silty clay loam, flooded	Se	Seguin soils are deep and well drained soils that formed in alluvium adjacent to stream and river channels.
BFZ2	Bosque and Seguin soils, frequently flooded	Bo	Bosque soils are very deep and well drained that formed in loamy, calcareous alluvial sediments.
BFZ3	Bosque and Seguin soils, frequently flooded	Bo	Bosque soils are very deep and well drained that formed in loamy, calcareous alluvial sediments.
BFZ4	Bosque and Seguin soils, frequently flooded	Bo	Bosque soils are very deep and well drained that formed in loamy, calcareous alluvial sediments.
BFZ5	Seguin silty caly loam, flooded	Se	Seguin soils are deep and well drained soils that formed in alluvium adjacent to stream and river channels.
BFZ6	Sunev loam, 0-1 percent slopes	SuA	Sunev soils are very deep and well drained soils that formed in a loamy alluvium.
BFZ7	Meguín silty clay loam, 0-1 percent slopes, frequently flooded	MfA	Meguín soils consist of deep, well drained soils that form in calcareous loamy alluvium (Qt-aged)
BFZ8	Luckenbach sandy clay loam, 0-1 percent slopes	LkA	Luckenbach soils are very deep and well drained soils that formed in ancient loamy/clayey alluvium.
BFZ9	Sunev loam, 3-5 percent slopes	SyC	Sunev soils are very deep and well drained soils that formed in a loamy alluvium.
BFZ10	Meguín silt clay loam, 0-1 percent slopes, occasionally flooded	MeA	Meguín soils consist of deep, well drained soils that form in calcareous loamy alluvium (Qt-aged)
UCP1	Meguín silty clay loam, 0-1 percent slopes, frequently flooded	MfA	Meguín soils consist of deep, well drained soils that form in calcareous loamy alluvium (Qt-aged)

<b>Bend</b>	<b>Outside Bank Soil</b>	<b>Symbol</b>	<b>Soil Descriptions from USDA</b>
UCP2	Meguín silt clay loam, 0-1 percent slopes, occasionally flooded	MeA	Meguín soils consist of deep, well drained soils that form in calcareous loamy alluvium (Qt-aged)
UCP3	Meguín silty clay loam, 0-1 percent slopes, frequently flooded	MfA	Meguín soils consist of deep, well drained soils that form in calcareous loamy alluvium (Qt-aged)
UCP4	Meguín silt clay loam, 0-1 percent slopes, occasionally flooded	MeA	Meguín soils consist of deep, well drained soils that form in calcareous loamy alluvium (Qt-aged)
UCP5	Jedd gravelly fine sandy loam, 5-15 percent slopes	JsE	Jedd soils are moderately deep and well drained soils that formed in stratified sandstone and shale.
UCP6	Buchel clay, 0-1 percent slopes, frequently flooded	BvA	Buchel soils are very deep, moderately well drained soils that formed in calcareous clayey alluvium.
UCP7	Meguín silty clay loam, 0-1 percent slopes, frequently flooded	MfA	Meguín soils consist of deep, well drained soils that form in calcareous loamy alluvium (Qt-aged)
UCP8	Meguín silty clay loam, 0-1 percent slopes, frequently flooded	MfA	Meguín soils consist of deep, well drained soils that form in calcareous loamy alluvium (Qt-aged)
UCP9	Meguín silt clay loam, 0-1 percent slopes, occasionally flooded	MeA	Meguín soils consist of deep, well drained soils that form in calcareous loamy alluvium (Qt-aged)
UCP10	Meguín silty clay loam, 0-1 percent slopes, frequently flooded	MfA	Meguín soils consist of deep, well drained soils that form in calcareous loamy alluvium (Qt-aged)
MCP1	Bosque-Tinn complex, 0-1 percent slopes, frequently flooded	BpA	Bosque soils are very deep and well drained that formed in loamy, calcareous alluvial sediments.
MCP2	Meguín silty clay loam, 0-1 percent slopes, frequently flooded	MfA	Meguín soils consist of deep, well drained soils that form in calcareous loamy alluvium (Qt-aged)
MCP3	Meguín silty clay loam, 0-1 percent slopes, frequently flooded	MfA	Meguín soils consist of deep, well drained soils that form in calcareous loamy alluvium (Qt-aged)
MCP4	Meguín silty clay loam, 0-1 percent slopes, frequently flooded	MfA	Meguín soils consist of deep, well drained soils that form in calcareous loamy alluvium (Qt-aged)
MCP5	Meguín silty clay loam, 0-1 percent slopes, frequently flooded	MfA	Meguín soils consist of deep, well drained soils that form in calcareous loamy alluvium (Qt-aged)
MCP6	Trinity clay, occasionally flooded	To	Trinity soils are very deep and moderately well drained soils that formed in calcareous clayey alluvium derived from mudstone.

<b>Bend</b>	<b>Outside Bank Soil</b>	<b>Symbol</b>	<b>Soil Descriptions from USDA</b>
MCP7	Meguín soils, frequently flooded	Mf	Meguín soils consist of deep, well drained soils that form in calcareous loamy alluvium (Qt-aged)
MCP8	Meguín soils, frequently flooded	Mf	Meguín soils consist of deep, well drained soils that form in calcareous loamy alluvium (Qt-aged)
MCP9	Meguín soils, frequently flooded	Mf	Meguín soils consist of deep, well drained soils that form in calcareous loamy alluvium (Qt-aged)
MCP10	Trinity clay, occasionally flooded	To	Trinity soils are very deep and moderately well drained soils that formed in calcareous clayey alluvium derived from mudstone.
CPT1	Meguín silty clay loam, frequently flooded	Me	Meguín soils consist of deep, well drained soils that form in calcareous loamy alluvium (Qt-aged)
CPT2	Sarnosa fine sandy loam, 5-8 percent slopes	SaD	Sarnosa soils are very deep and well drained soils that formed in calcareous sandstone and loamy soil materials, typically found in the Oakville sandstone and sandstone members of the Goliad Formation.
CPT3	Sarnosa fine sandy loam, 5-8 percent slopes	SaD	Sarnosa soils are very deep and well drained soils that formed in calcareous sandstone and loamy soil materials, typically found in the Oakville sandstone and sandstone members of the Goliad Formation.
CPT4	Shiner fine sandy loam, 5-8 percent slopes	ShD	Shiner soils are shallow and well drained soils that formed in residuum from calcareous sandstone.
CPT5	Sinton loam	Sn	Sinton soils are very deep and well drained soils that formed in a loamy alluvium.
CPT6	Sarnosa fine sandy loam, 5-8 percent slopes	SaD	Sarnosa soils are very deep and well drained soils that formed in calcareous sandstone and loamy soil materials, typically found in the Oakville sandstone and sandstone members of the Goliad Formation.
CPT7	Meguín silty clay loam, frequently flooded	Me	Meguín soils consist of deep, well drained soils that form in calcareous loamy alluvium (Qt-aged)
CPT8	Sinton loam	Sn	Sinton soils are very deep and well drained soils that formed in a loamy alluvium.
CPT9	Meguín silty clay loam, frequently flooded	Me	Meguín soils consist of deep, well drained soils that form in calcareous loamy alluvium (Qt-aged)

<b>Bend</b>	<b>Outside Bank Soil</b>	<b>Symbol</b>	<b>Soil Descriptions from USDA</b>
CPT10	Meguín silty clay loam, frequently flooded	Me	Meguín soils consist of deep, well drained soils that form in calcareous loamy alluvium (Qt-aged)
LCP1	Meguín silty clay loam, frequently flooded	Me	Meguín soils consist of deep, well drained soils that form in calcareous loamy alluvium (Qt-aged)
LCP2	Sinton loam	Sn	Sinton soils are very deep and well drained soils that formed in a loamy alluvium.
LCP3	Meguín silty clay loam, frequently flooded	Me	Meguín soils consist of deep, well drained soils that form in calcareous loamy alluvium (Qt-aged)
LCP4	Meguín silty clay loam, frequently flooded	Me	Meguín soils consist of deep, well drained soils that form in calcareous loamy alluvium (Qt-aged)
LCP5	Meguín silty clay loam, frequently flooded	Me	Meguín soils consist of deep, well drained soils that form in calcareous loamy alluvium (Qt-aged)
LCP6	Meguín soils, frequently flooded	Mf	Meguín soils consist of deep, well drained soils that form in calcareous loamy alluvium (Qt-aged)
LCP7	Meguín soils, frequently flooded	Mf	Meguín soils consist of deep, well drained soils that form in calcareous loamy alluvium (Qt-aged)
LCP8	Meguín soils, frequently flooded	Mf	Meguín soils consist of deep, well drained soils that form in calcareous loamy alluvium (Qt-aged)
LCP9	Trinity clay, frequently flooded	Tr	Trinity soils are very deep and moderately well drained soils that formed in calcareous clayey alluvium derived from mudstone.
LCP10	Trinity clay, frequently flooded	Tr	Trinity soils are very deep and moderately well drained soils that formed in calcareous clayey alluvium derived from mudstone.
UD1	Meguín soils, frequently flooded	Mf	Meguín soils consist of deep, well drained soils that form in calcareous loamy alluvium (Qt-aged)
UD2	Meguín soils, frequently flooded	Mf	Meguín soils consist of deep, well drained soils that form in calcareous loamy alluvium (Qt-aged)
UD3	Meguín soils, frequently flooded	Mf	Meguín soils consist of deep, well drained soils that form in calcareous loamy alluvium (Qt-aged)
UD4	Trinity clay, frequently flooded	Tr	Trinity soils are very deep and moderately well drained soils that formed in calcareous clayey alluvium derived from mudstone.

<b>Bend</b>	<b>Outside Bank Soil</b>	<b>Symbol</b>	<b>Soil Descriptions from USDA</b>
UD5	Trinity clay, frequently flooded	Tr	Trinity soils are very deep and moderately well drained soils that formed in calcareous clayey alluvium derived from mudstone.
UD6	Trinity clay, frequently flooded	Tr	Trinity soils are very deep and moderately well drained soils that formed in calcareous clayey alluvium derived from mudstone.
UD7	Rydolph silty clay, 0-1 percent slopes, frequently flooded	Rf	Rydolph soils are deep and poorly drained soils that formed in clayey and loamy alluvium.
UD8	Rydolph silty clay, 0-1 percent slopes, frequently flooded	Rf	Rydolph soils are deep and poorly drained soils that formed in clayey and loamy alluvium.
UD9	Rydolph silty clay, 0-1 percent slopes, frequently flooded	Rf	Rydolph soils are deep and poorly drained soils that formed in clayey and loamy alluvium.
UD10	Trinity clay, frequently flooded	Tr	Trinity soils are very deep and moderately well drained soils that formed in calcareous clayey alluvium derived from mudstone.
MD1	Trinity clay, frequently flooded	Tr	Trinity soils are very deep and moderately well drained soils that formed in calcareous clayey alluvium derived from mudstone.
MD2	Aransas clay	Ar	Aransas soils are very deep and poorly drained. Formed in clayey alluvial sediments.
MD3	Aransas clay	Ar	Aransas soils are very deep and poorly drained. Formed in clayey alluvial sediments.
MD4	Aransas clay	Ar	Aransas soils are very deep and poorly drained. Formed in clayey alluvial sediments.
MD5	Aransas clay, high bottom	As	Aransas soils are very deep and poorly drained. Formed in clayey alluvial sediments.
MD6	Aransas clay	Ar	Aransas soils are very deep and poorly drained. Formed in clayey alluvial sediments.
MD7	Aransas clay	Ar	Aransas soils are very deep and poorly drained. Formed in clayey alluvial sediments.
MD8	Aransas clay	Ar	Aransas soils are very deep and poorly drained. Formed in clayey alluvial sediments.
MD9	Aransas clay	Ar	Aransas soils are very deep and poorly drained. Formed in clayey alluvial sediments.
MD10	Aransas clay	Ar	Aransas soils are very deep and poorly drained. Formed in clayey alluvial sediments.